Analytical Solutions of Unsteady Thin Film Flow with Internal Heating and Thermal Radiation

Author

Ahsan Ali Naseer

Reg. # 318229

Supervisor

Dr. Muhammad Safdar

DEPARTMENT OF MECHANICAL ENGINEERING

SCHOOL OF MECHANICAL & MANUFACTURING ENGINEERING

NATIONAL UNIVERSITY OF SCIENCES AND TECHNOLOGY

ISLAMABAD

JUNE 2023

Analytical Solutions of Unsteady Thin Film Flow with Internal Heating and Thermal Radiation

Author

Ahsan Ali Naseer

Reg. # 318229

A thesis submitted in partial fulfillment of the requirements for the degree of

MS Mechanical Engineering

Thesis Supervisor:

Dr. Muhammad Safdar

Thesis Supervisor's Signature: _____

DEPARTMENT OF MECHANICAL ENGINEERING

SCHOOL OF MECHANICAL & MANUFACTURING ENGINEERING

NATIONAL UNIVERSITY OF SCIENCES AND TECHNOLOGY,

ISLAMABAD

JUNE 2023

THESIS ACCEPTANCE CERTIFICATE

Certified that final copy of MS thesis written by Mr. Ahsan Ali Naseer, Registration No.318229 of SMME has been vetted by undersigned, found complete in all aspects as per NUST Statutes/Regulations, is free of plagiarism, errors, and mistakes and is accepted as partial fulfillment for award of MS/MPhil degree. It is further certified that necessary amendments as pointed out by GEC members of the scholar have also been incorporated in the said thesis.

Signature with stamp: _____

Name of Supervisor: Dr. Muhammad Safdar

Date: _____

Signature of HoD with stamp: _____

Date: _____

Countersign by

Signature (Dean/Principal): _____

Date: _____

Declaration

I certify that this research work titled "*Analytical Solutions of Unsteady Thin Film Flow with Internal Heating and Thermal Radiation*" is my own work. The work has not been presented elsewhere for assessment. The material that has been used from other sources it has been properly acknowledged / referred.

Signature of Student

Ahsan Ali Naseer

2019-NUST-MS-Mech-318229

Plagiarism Certificate (Turnitin Report)

This thesis has been checked for Plagiarism. Turnitin report endorsed by Supervisor is attached.

Signature of Student
Ahsan Ali Naseer
318229

Signature of Supervisor
Dr. Muhammad Safdar

Copyright Statement

Acknowledgements

I am thankful to my Creator Allah Subhana-Watala to have guided me throughout this work at every step and for every new thought which You setup in my mind to improve it. Indeed, I could have done nothing without Your priceless help and guidance. Whosever helped me throughout the course of my thesis, whether my parents or any other individual was Your will, so indeed none be worthy of praise but You.

I am profusely thankful to my beloved parents who raised me when I was not capable of walking and continued to support me throughout in every department of my life.

I would also like to express special thanks to my supervisor **Dr. Muhammad Safdar** for his help throughout my thesis and also for **Optimization** course which he has taught me. I can safely say that I have not learned any other engineering subject in such depth than the one which he has taught.

I would also like to thank **Dr. Adnan Munir**, **Dr. Usman Bhutta** and **Dr. Riaz Ahmad** for being on my thesis guidance and evaluation committee. I am also thankful to **Mr. Zeeshan Bhatti** for his support and cooperation.

Finally, I would like to express my gratitude to all the individuals who have rendered valuable assistance to my study.

Dedicated to my exceptional parents and adored siblings whose tremendous support and cooperation led me to this wonderful accomplishment.

Abstract

The formation of boundary layer takes place whenever an object is placed in the path of flowing fluid. This phenomenon of formation of hydrodynamic and thermal boundary layer is used in various engineering processes. This type of fluid flow can be expressed mathematically in terms of Navier-Stokes equations. The solution of the Navier-Stokes equations may help in creating better understanding of the said phenomenon and may also help in the creation of better and improved engineering processes. However, the exact solution of the Navier-Stokes equations for all fluid flow types do not exist yet, but the approximate solutions may be obtained using different numerical and analytical techniques.

In this research, a system of partial differential equations (PDEs) of an unsteady film flow over a stretching surface with internal source of heat generation and thermal radiation is considered. An algebraic technique, Lie symmetry is used to obtain the Lie point symmetries of system of partial differential equations for constructing invariants and reductions. Multiple reductions are obtained to solve the fluid flow for different physical conditions. Then the deduced reductions are used to transform a system of partial differential equations into various systems of ordinary differential equations in order to apply homotopy analysis method, which solves the system of ordinary differential equations analytically.

In this study, all systems of ordinary differential equations are solved analytically to investigate the impact of unsteadiness parameter, Prandtl number, internal heat generation parameter, and thermal radiation parameter on flow velocity, temperature and heat transfer rate. The study then presents the results of this analysis using both graphical and tabular formats. The study of thin film flows under different physical conditions can provide valuable insights into dynamics of fluid flows, and how they can be controlled and optimized for better performance. By understanding the impact of various parameters on the velocity and heat transfer rate, engineers can design and improve various engineering processes.

Key Words: *Homotopy analysis method, Lie point symmetries, Similarity transformations, Thermal boundary layer, Thermal radiation*

Table of Contents

List of Figures

List of Tables

CHAPTER 1: INTRODUCTION

Fluid is a form of matter that acts as a working substance in numerous engineering processes. Each fluid behaves uniquely under same conditions due to the difference in their macroscopic properties, as a result of which some fluids perform better than the others in a specific application. All types of fluid flows can be expressed in the form of Navier-Stokes equations. Solution to the Navier-Stokes equations may help in creating better understating of various phenomena. Hence, improving the overall functioning of a system. However, the exact solution of Navier-Stokes equations does not exist yet, but different techniques may be employed to solve the fluid flow.

1.1 Background:

Numerous industrial machines, household products and engineering systems utilize fluids as a working substance. Fluids serve different purposes in different applications, which depend on the type of machine and its use. In some applications fluids are used to transfer heat energy from one place to another, while a few require fluid to produce lift force, some applications require fluids to do some work on rotating objects to produce electricity. Besides the mentioned there are many other ways in which fluids can be used for our benefit. Common thing in all of these applications is the generation of boundary layer on the surface of an object.

1.1.1 Boundary layer theory:

The concept of boundary layer was first suggested by L. Prandtl in 1904 [1]. He considered two flow regions inside the whole flow field: one region contains the boundary layer where the viscosity dominates, and the second region is the area outside the boundary layer where viscosity can be neglected due to its negligible effect on flow solution. This results in the simplification of Navier-Stokes equations. In boundary layer theory, boundary layer is a thin layer of fluid formed over the solid surface (external flow) or inside the channels (internal flow) due to the viscosity of fluid.

A boundary layer is a thin layer of viscous fluid close to the solid surface of a wall, which comes in contact with a moving stream of fluid. Flow velocity inside the boundary layer varies with the distance from the wall. Figure 1.1 shows the generation of a boundary layer on the surface of a flat plate as flow passes over it. Velocity gradient inside the boundary layer can also be visualized through Figure 1.1.

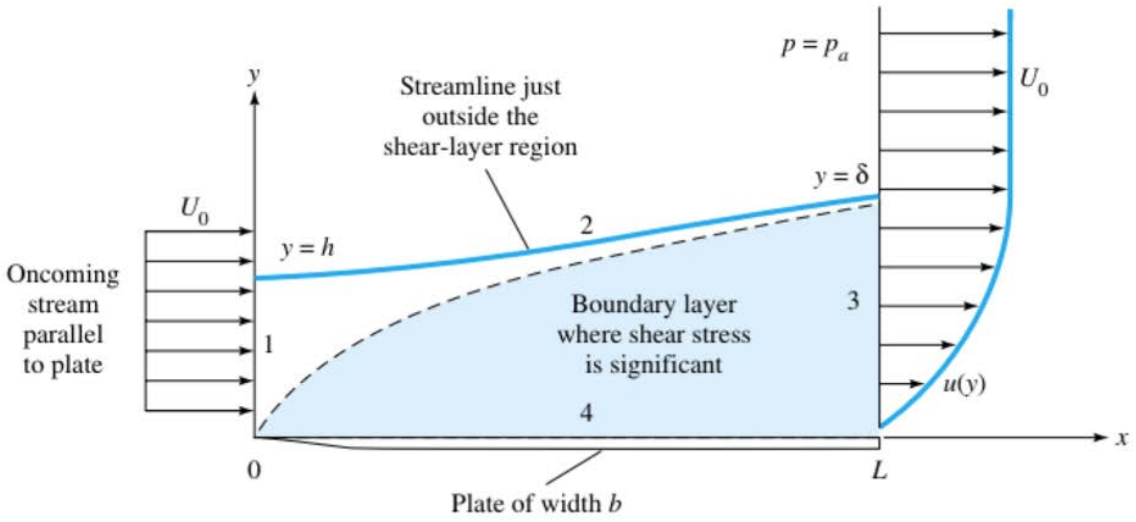

Figure 1.1: Hydrodynamic boundary layer on flat plate

In Figure 1.1 , fluid is flowing parallel to the surface of flat plate with U_0 velocity. As the fluid comes in contact with the surface of flat plate it induces a no-slip boundary condition (zero velocity at wall). Shear forces between the adjacent layers of fluid causes the flow to slow down, which results in the generation of boundary layer. The velocity of fluid increases from zero (at wall) to free stream velocity U_0 (away from wall). The vertical distance from the wall to the point where fluid moves with $0.99U_0$ is termed as boundary layer thickness.

Both velocity and thermal boundary layers generate if a temperature difference exists between the fluid and the surface of an object and the majority of heat transfer to and from the body takes place inside the vicinity of velocity boundary layer.

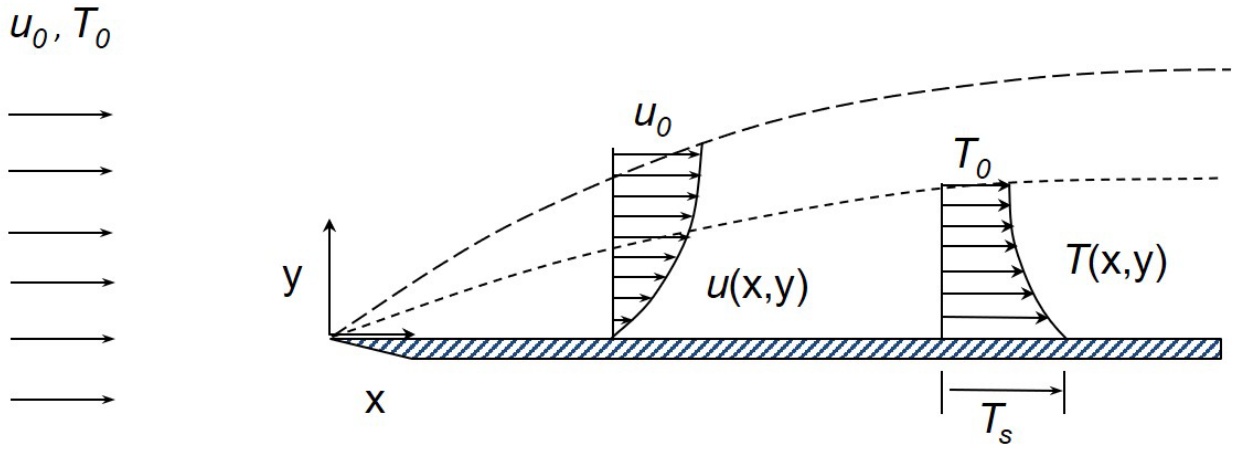

Figure 1.2: Thermal boundary layer for external flow

Now a days, researchers use wind tunnel machines, special equipment and test benches to simulate the fluid flow and commercially available simulation softwares can also be used for the same purpose. However, the fluid flows which can be simulated using these techniques are limited and performing the wind tunnel testing require a lot of time and resources.

Moreover, the flow simulating softwares offer solutions for the limited and specific fluid flow types, so the researchers and engineers rely on other techniques for improving the processes.

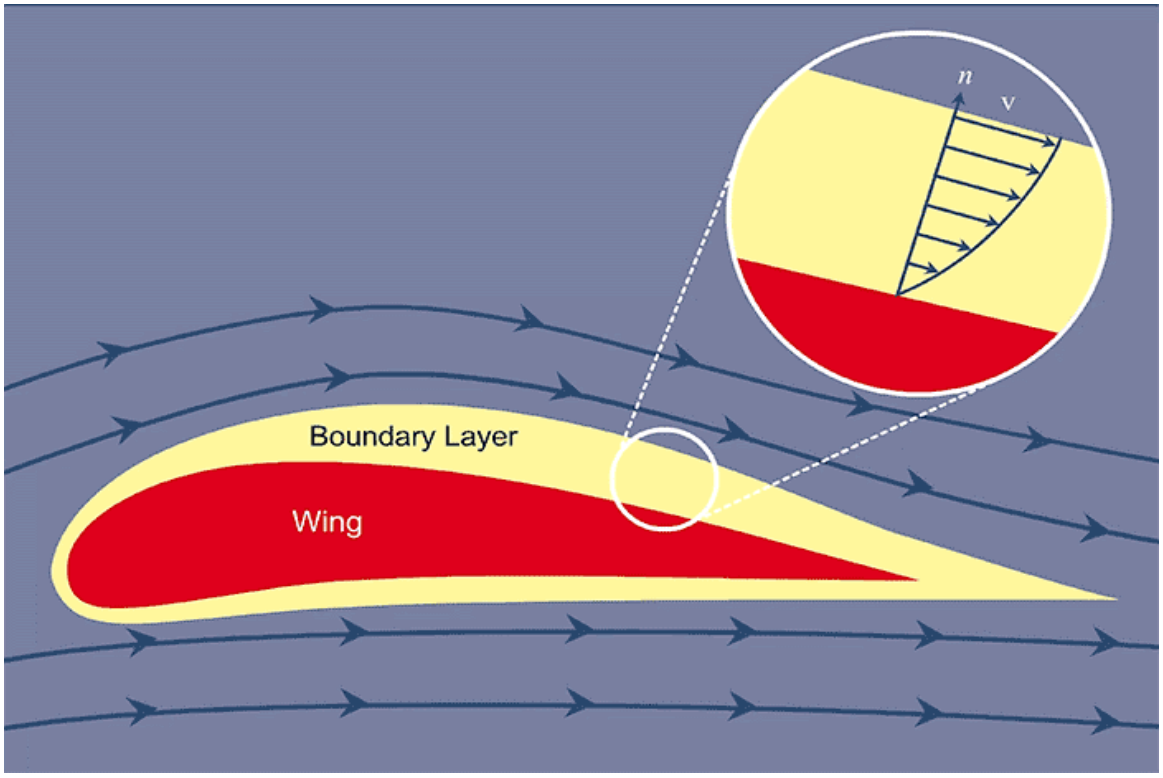

Figure 1.3: Boundary layer around an airfoil

1.2 Applications:

Concept of generation of boundary layers in steady and unsteady flows are widely used in industrial engineering processes. These processes include cooling of metallic plates, wire and fiber coating, metal and polymer extrusion, drawing of plastic sheets, continuous casting etc. The schematics of few of these processes can be seen in the following pictures:

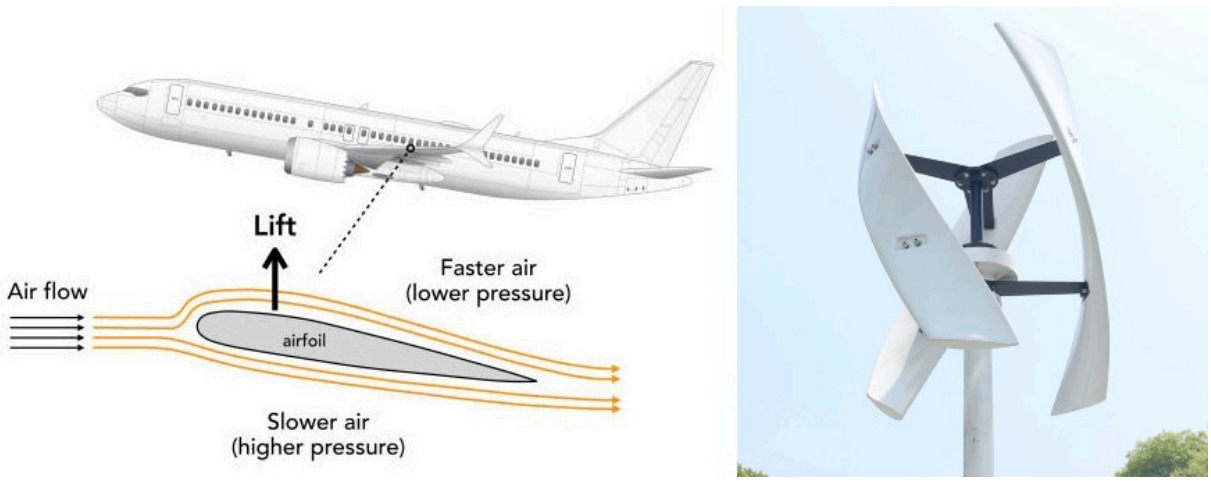

Figure 1.4: Importance of hydrodynamic boundary layer

Whenever the fluid flows over an aerodynamic shape like an airfoil, generation of boundary layer occurs around that object. Flow passes faster on one side than the other, which generates the lift force. This force is responsible for the flying of an airplane, rotation of wind and water turbines. Lift force increases with the increase in angle of attack of an airfoil, but it can also be increased by improving the shape of an object and it is only possible by analyzing its boundary layer.

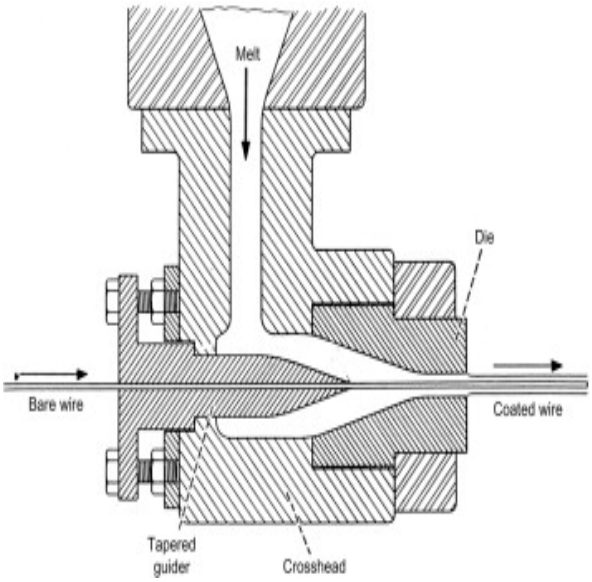

Figure 1.5: Wire coating process

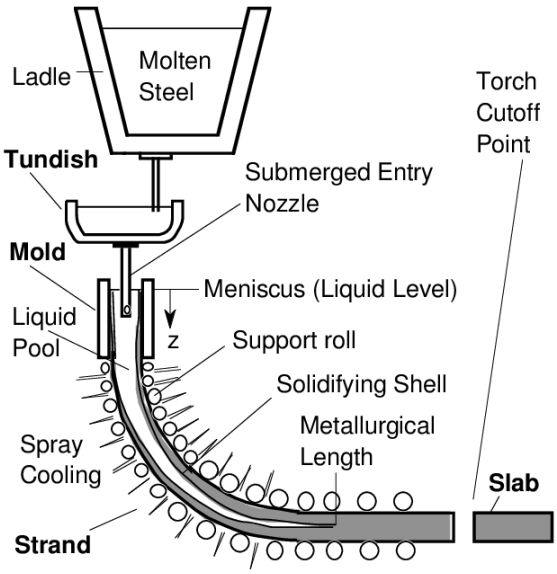

Figure 1.6: Continuous casting process

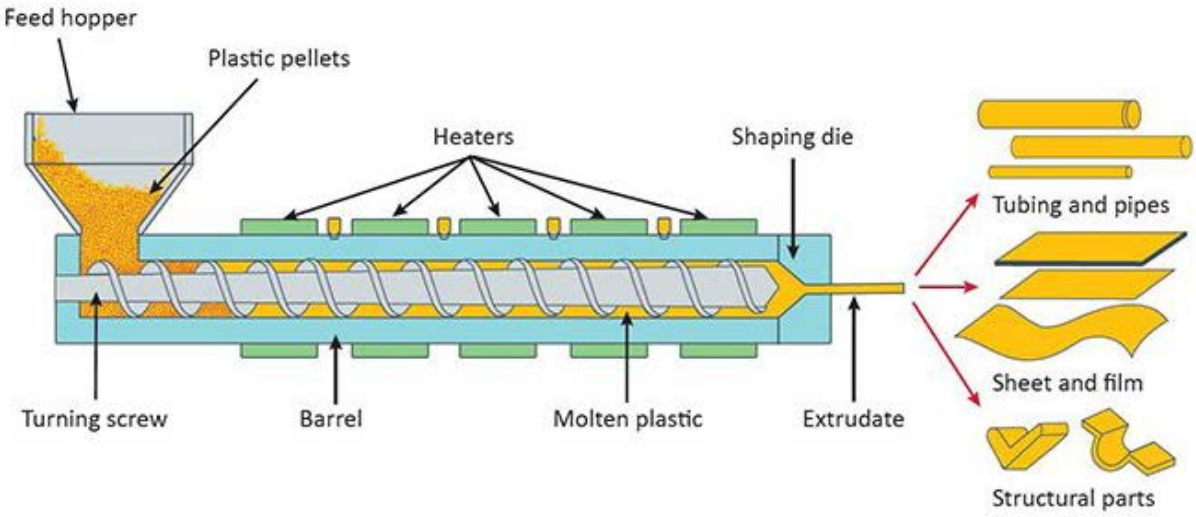

Figure 1.7: Polymer extrusion process

Studies of the formation of hydrodynamic and thermal boundary layers over the solid surface have shown a relationship between fluid flow's frictional resistance and heat transfer

characteristics, so the solution to the boundary layer flows is required to improve the processes and designs of industrial equipment.

1.3 Motivation:

Researchers have done extensive studies to solve various steady and unsteady fluid flows using different techniques including homotopy analysis method (HAM). This research is conducted to solve unsteady fluid flow with internal heat generation and thermal radiation. A few solutions of said flow exist in the literature which were found using a class of similarity transformation. However, this research aims at finding more than one type of solution for the unsteady fluid flow with internal heat generation and thermal radiation, due to which solving the unsteady fluid flows under different physical conditions will become possible.

Unsteady thin film flows are of great importance in many industrial processes, such as coating and drying operations, microfabrication, and the manufacturing of electronic devices. Developing a better understanding of these flows can help improve the efficiency and reliability of these processes, leading to lower costs and better performance.

1.4 Solution procedure:

In this research, Lie symmetry method is used to map one solution of a system to another solution of the system. It helps in solving the system for different physical conditions. Transformations deduced using the Lie symmetry method is employed to convert two-dimensional mass, momentum and energy equations of flow into ODEs and then the HAM is applied onto the transformed ODEs to solve the fluid flow analytically.

1.5 Objectives:

Construction and solution of new solvable classes of ordinary differential equations (ODEs) of unsteady thin film flow over stretching surface with internal heating and thermal generation are the primary objectives of this research.

CHAPTER 2: PRELIMINARY AND BASIC DEFINITIONS

Fluid is a state of matter which undergoes a continuous deformation when they are subjected to shearing stress. All liquids and gases are the example of fluids. Fluids are divided into two categories on the basis of the reaction of fluids when they are subjected to shear force.

2.1 Newton's law of viscosity:

Newton's law of viscosity states that velocity gradient $\left({}^{\partial u}/_{\partial y}\right)$ is directly proportional to shear stress (τ). The shear stress between the two adjacent layers of the fluid is directly proportional to the negative value of the velocity gradient between the same two adjacent layers of the fluid. Mathematically, this law can be represented as

$$\tau = \mu \frac{du}{dy} \tag{2.1}$$

where μ is constant of proportionality which represents **dynamic viscosity**. It is a fluid's property, and it can be defined as a measure of fluid's resistance to flow under an action of external force and its unit is $\boldsymbol{Ns/m^2}$.

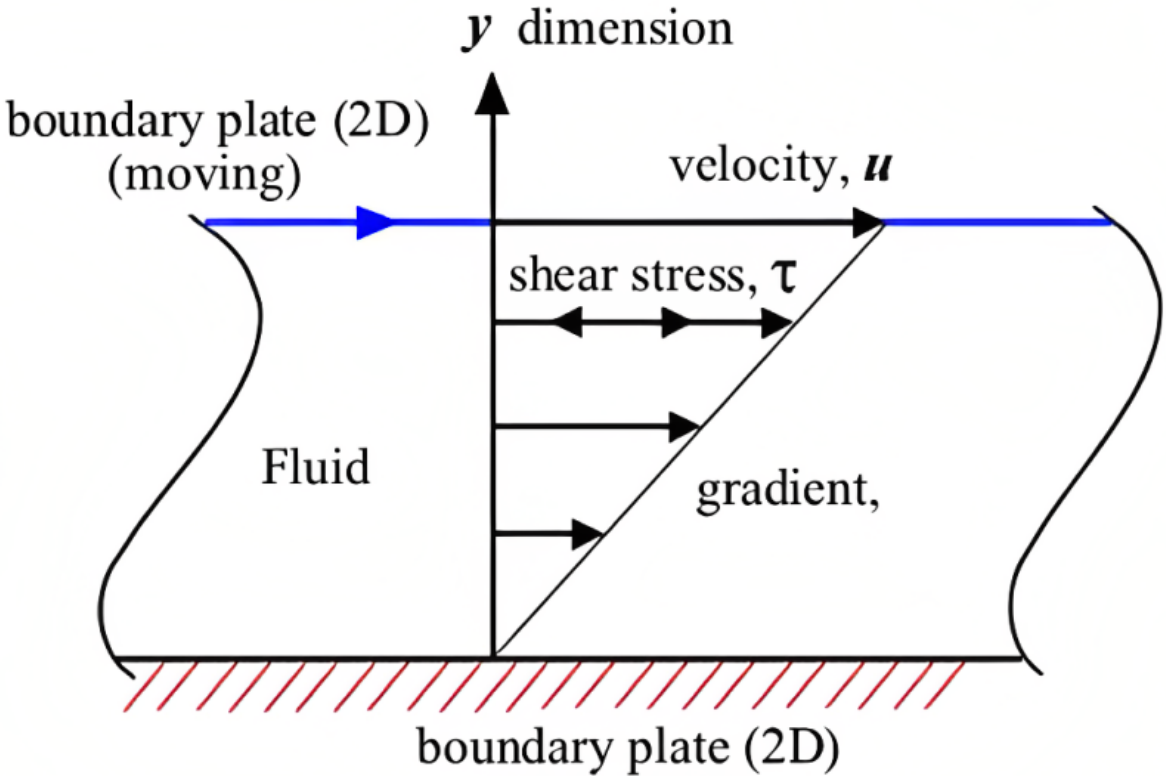

Figure 2.1: Fluid between stationary and moving plates.

2.2 Newtonian and non-Newtonian fluids:

Those fluids which obey newton's law of viscosity are known as Newtonian fluids.

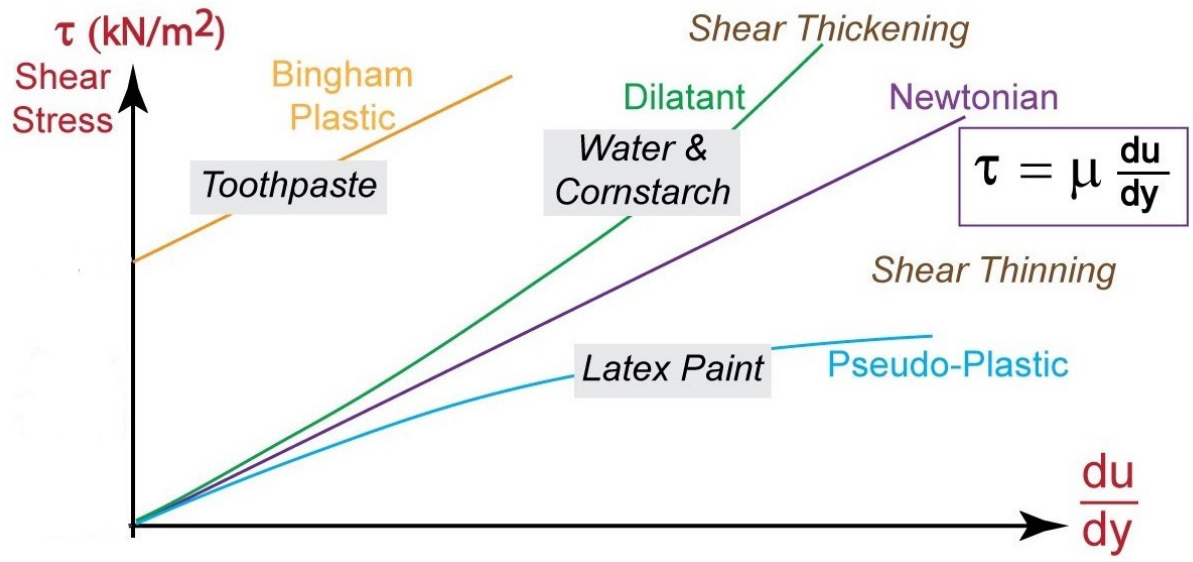

Figure 2.2: Relation between shear stress and velocity gradient for several types of fluids

In other words, all those fluids for which the shear stress between the two adjacent layers is directly proportional to the negative value of the velocity gradient between the same two adjacent layers are Newtonian fluids. For these types of fluids, a linear relation exists between deformation and shear stress, and deformation or velocity gradient of fluid increases with an increase in shear stress. Water, honey, gasoline, alcohol are the few examples of Newtonian fluids. However, all those fluids which do not obey newton's law of viscosity are known as non-Newtonian fluids. The viscosity of non-Newtonian fluids depends on shear rate. Blood, ketchup, quicksand, oobleck etc. are the examples of non-Newtonian fluids.

2.3 Types of fluid flow:

Various types of fluid flow exist as fluids behave and move uniquely under different boundary conditions. The type of fluid flow depends upon the manner in which the particles move. Few of them are:

2.3.1 Uniform and non-uniform flow:

Uniform flow is a type of flow in which the velocity of liquid particles at every point within a pipe or a channel remains same whereas in non-uniform flow the fluid particles at different sections of a pipe or channel move with different velocity. Inviscid fluid must be flowing through a channel of uniform cross-sectional area for uniform flow.

2.3.2 Laminar and turbulent flow:

Laminar flow is also known as streamline flow, in this type of flow each liquid particle has a definite path and the paths of individual particles do not cross each other. At low velocity,

fluid flow occurs in parallel layers with no disruption between the layers. Whereas in turbulent flow each liquid particle does not have a definite path and the paths of individual particles cross each other. Fluids do not move in parallel layers and mixing of layers takes place in turbulent flow.

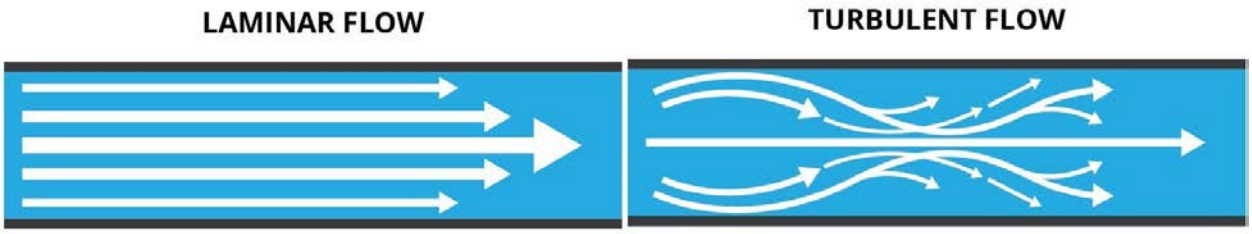

Figure 2.3: Laminar and turbulent flow

2.3.3 Steady and unsteady flow:

The flow in which the characteristics of fluid do not change at any point with time is known as **steady flow**. The fluid flow properties may change from point to point but do not change with time. Constant fluid flow rate is a characteristic of a steady flow. However, in an **unsteady flow** the characteristics like velocity, temperature, pressure, density etc. change with time and flow rate does not remain constant all the time.

2.3.4 Compressible and incompressible flow:

Compressible flow is a type of flow in which the volume and density of a fluid change. However, a flow in which the volume and density of a fluid do not change is called incompressible flow. All gases and liquids are considered to generate compressible and incompressible flow, respectively.

2.4 Bernoulli's equation:

According to Bernoulli's principal, the total energy of the fluid flowing between two points on a streamline remains constant. Total energy of a fluid at a point is the sum of potential energy, kinetic energy and static pressure of fluid. Mathematical expression of this principal is known as Bernoulli's equation.

$$P + \frac{1}{2}\rho v^2 + \rho g h = constant \tag{2.2}$$

For two points on a streamline,

$$P_1 + \frac{1}{2}\rho {v_1}^2 + \rho g h_1 = P_2 + \frac{1}{2}\rho {v_2}^2 + \rho g h_2 \tag{2.3}$$

2.4.1 Assumptions:

Bernoulli's equation can be applied to a specific type of fluid flow and some conditions must be met for the correct use of this principal. The flow must be steady, which means that the fluid flow properties like velocity, pressure and density must not change at any point with time. The flow must be incompressible, even with the change in pressure the density of fluid must remain constant throughout the flow field. The fluid must be inviscid or the shear stress between the adjacent layers of flowing fluid must be minimal. So, the Bernoulli's equation will not provide a correct solution of flow if the fluid flow properties change with time or the flow is compressible, or the fluid is highly viscous. The gases moving at less than 0.3 Ma number are considered to form an incompressible flow.

2.5 Navier-Stokes equation:

Navier-Stokes equations are partial differential equations (PDEs), which were developed over the several decades. They are based on the theories that were proposed by Claude-Louis Navier and George G. Stokes during the 19^{th} century. Navier-Stokes equations mathematically express the conservation of mass and momentum for Newtonian fluids. Navier-Stokes equations arise from applying the Newton's second law of motion to fluid, with the assumption that stress in the fluid generates due to viscosity of fluid and pressure.

N-S equations take viscous effects into account and are capable of providing the solution for viscous fluid flows while Euler equations or Bernoulli's equation model only inviscid flow. Steady or unsteady, compressible or incompressible, all types of Newtonians' flows can be mathematically expressed in terms of N-S equations. N-S equations are sometimes accompanied by an equation of state relating pressure, temperature and density.

2.6 Dimensionless numbers:

Dimensionless number represents a property of a system without measuring it on a scale of physical units. Dimensionless number has no dimension or a unit. Dimensionless numbers are a ratio of two physical quantities that reduces the number of variables to describe a system and provide an order-of-magnitude estimate about the behavior of a system. Different dimensionless numbers are used to represent different properties of a system and helps in analyzing the behavior of fluids.

2.6.1 Reynolds number:

Reynolds number is a ratio of **inertial forces** and **viscous forces**. R_e predicts the flow pattern in different fluid flow situation. R_e helps in determining whether the flow is laminar or turbulent. Low quantitative ratio of inertial and viscous forces implies that the flow is laminar while high value of Re suggests that the flow has been transformed from laminar to turbulent. The mathematical expression of R_e is

$$R_e = \frac{\rho v D}{\mu} \tag{2.4}$$

In the above mathematical expression of R_e, ρ and μ are temperature-dependent fluid properties. ρ is the density of fluid, D represents the hydraulic diameter of a pipe, v is the velocity of fluid and μ represents dynamic viscosity of fluid.

2.6.2 Nusselt number:

Nusselt number is a ratio of **convective heat transfer** to **conductive heat transfer** across a boundary. Convective heat transfer or convection represents the process in which heat energy transfer from one place to another due to the movement of fluid while conductive heat transfer represents a process in which heat energy transfer due to the collision of atoms or molecules with each other. Large ratio of convective to conductive heat transfer means that the more heat energy is flowing across a boundary through convection than conduction. Formula of Nusselt number is

$$Nu_L = \frac{hL}{k} \tag{2.5}$$

where h is convective heat transfer coefficient, L is the characteristic length and k is the thermal conductivity of fluid that describe fluid's ability to conduct heat. Thus, these three quantities are important in determining the rate of heat transfer between a fluid and a solid surface.

2.6.3 Prandtl number:

Prandtl number is the ratio of momentum diffusivity to thermal diffusivity. **Momentum diffusivity** can be defined as a phenomenon of diffusion of momentum of fluid particles within a flow, and this diffusion or transport of momentum can occur in any direction. Thermal diffusivity is the measure of rate of heat transfer from the hot end to cold end. Prandtl number tells us how fast or slow thermal diffusion will occur in comparison to momentum diffusion in fluids. In heat transfer problem, the value of Prandtl number tells us about the relative thickness of velocity and thermal boundary layers. For $Pr \ll 1$, the thermal boundary layer thickness

will be greater than the momentum boundary layer thickness and for $Pr \gg 1$, the momentum boundary layer thickness will be greater than thermal boundary layer thickness.

$$Pr = \frac{\nu}{\alpha} = \frac{{}^{\mu}/_{\rho}}{{}^{k}/_{C_p/\rho}}$$

$$Pr = \frac{\mu . C_p}{k} \tag{2.6}$$

Dynamic viscosity μ refers to the resistance of a fluid to flow, specific heat at constant pressure Cp is the amount of heat energy required to raise the temperature of a unit mass of the fluid by one degree celsius at constant pressure, and thermal conductivity k is a measure of a fluid's ability to conduct heat. These three parameters are important in determining the transport of heat and momentum in fluid flows.

2.6.4 Eckert number:

Eckert number is a dimensionless number which is a ratio of advective mass transfer and heat dissipation potential, it expresses the relationship between flow's kinetic energy and boundary layer enthalpy difference. Eckert number is used to characterize the heat dissipation in high-speed flows where viscous dissipation is significant. In other words, it is used to characterize the self-heating of a fluid as a consequence of dissipation effects. The numerical value of Eckert number helps in making the decision whether the effect of self-heating can be neglected or not.

$$Ec = \frac{advective\ mass\ transport}{heat\ dissipation\ potential}$$

$$Ec = \frac{u^2}{C_p \Delta T} \tag{2.7}$$

where, u is the local flow velocity, C_p represents the value of specific heat at constant pressure and ΔT represents the temperature difference between the wall and local temperature.

2.6.5 Hartmann number:

Hartmann number is a dimensionless number, it is a ratio of electromagnetic force to viscous force. This dimensionless number becomes important in the flow cases where fluid passes through magnetic field, it gives a measure of the relative importance of drag forces resulting from the magnetic field and viscous forces. The mathematical expression for calculating Hartmann number is

$$Ha = BL\sqrt{\frac{\sigma}{\mu}} \tag{2.8}$$

where, B is the magnetic field intensity, L is the characteristic length scale, σ is the electrical conductivity and μ is the dynamic viscosity of fluid.

CHAPTER 3: LITERATURE REVIEW

Unsteady thin film flows are an important area of study in fluid mechanics that involve the behavior of thin fluid layers that are in motion. Such flows are characterized by their dynamics and time-varying nature, and they occur in a wide range of physical and engineering systems, such as coating and drying processes, lubrication of mechanical components, and the formation of thin films in microelectronics. Understanding the fundamental principles that govern unsteady thin film flows is important in order to design and optimize these processes, as well as to develop the accurate mathematical models for simulating and predicting their behavior. This requires a combination of theoretical and experimental approaches, as well as the use of advanced computational tools to analyze and simulate the complex fluid dynamics involved.

3.1 Unsteady film flow over stretching surface:

Wang considered the thin film of Newtonian fluid on an unsteady stretching surface and solved the hydrodynamics of the said flow numerically [2]. He considered a film of fluid on a surface which moves along the x-axis of cartesian coordinate system with velocity that changes with time. This type of fluid flow resembles with the fresh paint and protective coating which has been applied to the extrudate. The schematic diagram of flow is shown in Figure 3.1.

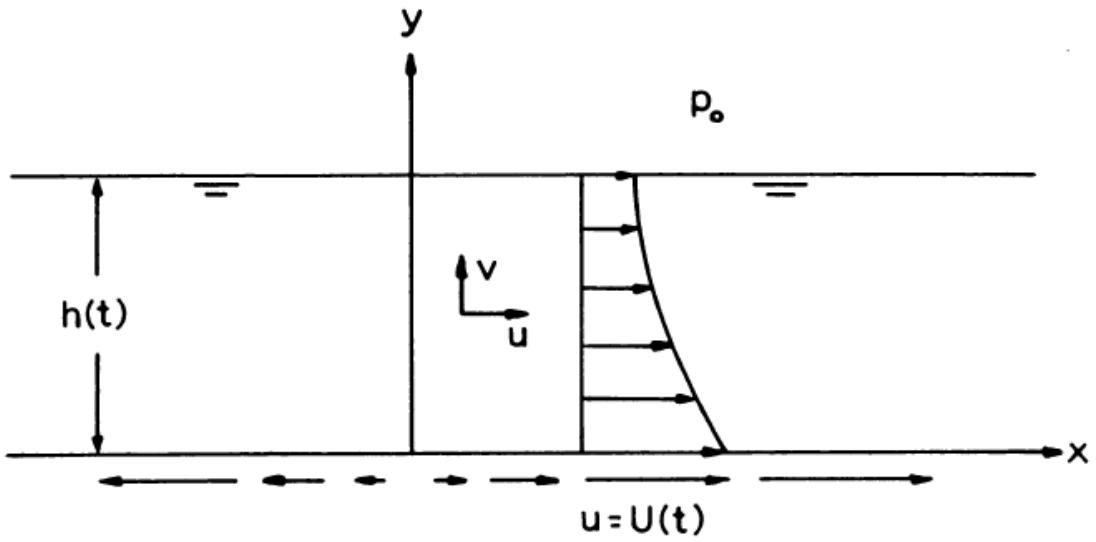

Figure 3.1: Film flow on an unsteady stretching surface

$U(t, x)$ is time-dependent stretching velocity of surface and velocity of fluid along x and y axis are u and v respectively. $h(t)$ is boundary layer thickness and it is a function of time.

$$U(t,x) = \frac{bx}{1-\alpha t} \tag{3.1}$$

In above expression of stretching velocity $U(t)$, b and $b/(1-\alpha t)$ represent initial stretching rate and effective stretching rate, respectively. The similarity transformation used by the author is,

$$\eta = \frac{\sqrt{\frac{b}{\nu}}}{\sqrt{(1-\alpha t)}} y, \quad u = \frac{bx}{(1-\alpha t)} f'(\eta), \quad v = -\sqrt{\frac{\nu b}{(1-\alpha t)}} f(\eta) \tag{3.2}$$

Wang considered the Navier-Stokes equations of the flow, and he transformed the PDEs into ODEs using the similarity transformation. Then he solved the obtained ODEs numerically, which is given below.

$$f''' = S\left(f' + \frac{\eta}{2} f''\right) + f'^2 - f f'' \tag{3.3}$$

The unsteadiness in stretching velocity of surface is controlled by the unsteadiness parameters S, which appeared in ordinary differential equation (3.3) due to the transformation of PDEs into ODEs. Unsteadiness parameter S is the ratio of α to b.

He concluded in [2] that the range of unsteadiness parameter for valid solution of flow is [0,2). However, the flow transforms into steady flow when the unsteadiness parameter is considered as zero. He also concluded that the unsteadiness parameter governs the value of dimensionless boundary layer thickness, the value of dimensionless boundary layer thickness decreases when S is increased from 0 to 2.

3.2 Heat transfer in an unsteady film flow over stretching surface:

Wang solved the hydrodynamics of a film flow over an unsteady stretching surface in [2]. The solution did not give any insight on heat transfer in a liquid film as wang only considered the conservation of momentum. Anderson in [3] considered equations for conservation of mass, momentum and heat energy for the same flow. Anderson considered a thin elastic sheet of fluid that emerge from a narrow slit at the origin of cartesian coordinate system. The elastic sheet at $y = 0$ is along the x-axis which moves with velocity $u(t,x)$, which is the function of time. Similarly, the surface temperature T_s of the stretching sheet varies with the distance x from the slit as:

$$U(t,x) = \frac{bx}{1-\alpha t} \tag{3.4}$$

$$T_s(t,x) = T_0 - T_{ref}\frac{bx^2}{2v}(1-\alpha t)^{-3/2} \tag{3.5}$$

The two-dimensional conservation of mass, momentum and energy equations for boundary layer flow problem are,

$$\begin{gathered}\frac{\partial u}{\partial x}+\frac{\partial v}{\partial y}=0\\ \frac{\partial u}{\partial t}+u\frac{\partial u}{\partial x}+v\frac{\partial u}{\partial y}=\nu\frac{\partial^2 u}{\partial y^2}\\ \frac{\partial T}{\partial t}+u\frac{\partial T}{\partial x}+v\frac{\partial T}{\partial y}=\kappa\frac{\partial^2 T}{\partial y^2}\end{gathered} \tag{3.6}$$

The boundary conditions which govern the fluid flow and heat transfer are shown below

$$\begin{gathered}y=0,\ \ u=U(x,t),\ \ v=0,\ \ T=T_s(t,x)\\ y=h(t),\ \ u_y=T_y=0,\ \ v=h_t=\frac{dh}{dt}\end{gathered} \tag{3.7}$$

Anderson showed in his study that the same exact similarity which wang used in his research can also be achieved for the temperature field. The similarity transformation used by Anderson in his study [3] is

$$\begin{gathered}\eta=\frac{\sqrt{\frac{b}{\nu}}}{\sqrt{(1-\alpha t)}}y\\ u=\frac{bx}{(1-\alpha t)}f'(\eta)\\ v=-\sqrt{\frac{\nu b}{(1-\alpha t)}}f(\eta)\\ T_s=T_0-T_{ref}\frac{bx^2}{2v}(1-\alpha t)^{-3/2}\theta(\eta)\end{gathered} \tag{3.8}$$

Then he transformed system of PDEs and the associated boundary conditions into non-linear system of ODEs using the above transformation. The transformed system of ODEs and their associated boundary conditions are:

$$\begin{gathered}f'''=S\left(f'+\frac{\eta}{2}f''\right)+f'^2-ff''\\ \theta''=Pr\left(\frac{3S}{2}\theta+\frac{\eta S}{2}\theta'+2\theta f'-f\theta'\right)\end{gathered} \tag{3.9}$$

$$f'(0) = 1, \qquad f(0) = 0, \qquad f''(\beta) = 0$$
$$\theta(0) = 1, \qquad \theta'(\beta) = 0, \qquad f(\beta) = S\beta/2 \tag{3.10}$$

where, β denotes the value of the similarity variable η at the free surface.

Then he applied multiple shooting subroutine (MUSN) method to solve the system of ODEs. He conducted this research to explore the heat transfer characteristics of fluid flow which was solved by wang. He provided an accurate solution of heat flow problem for two characteristic values of unsteadiness parameter, covering the range of Prandtl number from 0.001 to 1000.

He observed that temperature increases from the elastic sheet to the free surface except when the Prandtl number approaches to 0, he also observed that the effect of unsteadiness parameter on heat transfer rate from film of fluid to stretching sheet is more pronounced at low Prandtl number than for $Pr \geq 1$.

However, wang published an article on an analytical solution of thin film flow over a stretching surface [4]. Wang solved the system of ODEs for the same thin film flow using HAM whereas Anderson used multiple shooting subroutine (MUSN) method. Later Anderson solved the same problem for the various special cases using fifth order Runge-Kutta scheme [5].

3.3 Effect of fluid properties and thermocapillarity:

B. S. Dandapat considered an emergence of thin elastic sheet of fluid from the small opening at the origin of cartesian coordinate [6]. The motion within the fluid arises due to the stretching of sheet, at which the thin film of fluid exists. This is the same flow which was considered by the previous researchers. However, B. S. Dandapat conducted this research to explore the effect of viscosity, thermal conductivity and thermocapillarity on flow and heat transfer rate. This research helps in understanding the flow and heat transfer characteristics for the fluids with different values of viscosity and thermal conductivity. The velocity and temperature field in an unsteady thin film flow over a stretching surface are governed by the following equations.

$$\frac{\partial u}{\partial x} + \frac{\partial v}{\partial y} = 0$$
$$\frac{\partial u}{\partial t} + u\frac{\partial u}{\partial x} + v\frac{\partial u}{\partial y} = \frac{1}{\rho_0}\frac{\partial}{\partial y}\left(\mu\frac{\partial u}{\partial y}\right) \tag{3.11}$$
$$\frac{\partial T}{\partial t} + u\frac{\partial T}{\partial x} + v\frac{\partial T}{\partial y} = \frac{1}{\rho_0 C_p}\frac{\partial}{\partial y}\left(\kappa\frac{\partial T}{\partial y}\right)$$

The associated boundary conditions for the two-dimensional boundary layer equations for mass, momentum and thermal energy are:

$$\begin{aligned} &at\ y = 0, \qquad u = U(x,t), \qquad v = 0, \qquad T = T_s(t,x) \\ &at\ y = h(t), \qquad \mu\frac{\partial u}{\partial y} = \frac{\partial \sigma}{\partial x}, \qquad \frac{\partial T}{\partial y} = 0, \qquad v = \frac{dh}{dt} \end{aligned} \tag{3.12}$$

B. S. Dandapat transformed above system of PDEs and the associated boundary conditions using the following transformation equations.

$$\begin{aligned} \eta &= \frac{\sqrt{\frac{b}{\nu_0}}}{\sqrt{(1-\alpha t)}} y \\ u &= \frac{bx}{(1-\alpha t)} f'(\eta) \\ v &= -\sqrt{\frac{\nu_0 b}{(1-\alpha t)}} f(\eta) \\ T &= T_0 - T_{ref}\frac{bx^2}{2\nu_0}(1-\alpha t)^{-3/2}\theta(\eta) \end{aligned} \tag{3.13}$$

The deduced system of ODEs and associated boundary conditions using the above transformations are,

$$\begin{aligned} e^{A\theta}(f''' + Af''\theta') &= S\left(f' + \frac{\eta}{2}f''\right) + f'^2 - ff'' \\ -\delta(\theta')^2 + (1-\delta\theta)\theta'' &= Pr\,(\frac{3S}{2}\theta + \frac{\eta S}{2}\theta' + 2\theta f' - f\theta') \end{aligned} \tag{3.14}$$

$$\begin{aligned} &f'(0) = 1, \qquad f(0) = 0, \qquad f''(\beta) = M.\theta(\beta)e^{-A\theta(\beta)} \\ &\theta(0) = 1, \qquad \theta'(\beta) = 0, \qquad f(\beta) = S\beta/2 \end{aligned} \tag{3.15}$$

A, δ and M are viscosity variation parameter, thermal conductivity variation parameter and thermocapillarity number, respectively.

ODEs and the associated boundary conditions are solved numerically using the method of adjoints. The author observed that the dimensionless boundary layer thickness increases with the increase in viscosity of fluid while the free surface velocity decreases due to the thickening of liquid layer. At the sheet ($y = 0$), local heat transfer coefficient increases with the increase

in viscosity of fluid. He also observed that the variation in thermal conductivity does not change the velocity profile much.

3.4 Effect of viscous dissipation on surface temperature:

Viscous dissipation is the process which involves generation of heat due to the shear forces between adjacent layers of viscous fluid. The effects of this phenomenon of heat generation at the cost of momentum loss of viscous flow on the temperature of fluid is studied numerically by the R. C. Aziz [7]. Author considered the same flow problem which had been explored by the previous mentioned researchers but with an addition of viscous dissipation. The two-dimensional boundary layer equations for mass, momentum and heat energy for the flow with viscous dissipation are,

$$\frac{\partial u}{\partial x}+\frac{\partial v}{\partial y}=0$$

$$\frac{\partial u}{\partial t}+u\frac{\partial u}{\partial x}+v\frac{\partial u}{\partial y}=\nu\frac{\partial^2 u}{\partial y^2} \tag{3.16}$$

$$\rho C_p\left(\frac{\partial T}{\partial t}+u\frac{\partial T}{\partial x}+v\frac{\partial T}{\partial y}\right)=\kappa\frac{\partial^2 T}{\partial y^2}+\mu\left(\frac{\partial u}{\partial y}\right)^2$$

subject to

$$y=0,\ \ u=U(x,t),\ \ v=0,\ \ T=T_s(t,x)$$

$$y=h(t),\ \ u_y=T_y=0,\ \ v=h_t=\frac{dh}{dt} \tag{3.17}$$

R.C. Aziz transformed above system of ODEs and the associated boundary conditions using the following transformations.

$$\eta=\frac{1}{\beta}\frac{\sqrt{\frac{b}{\nu}}}{\sqrt{(1-\alpha t)}}y$$

$$u=\frac{bx}{(1-\alpha t)}f'(\eta)$$

$$v=-\sqrt{\frac{\nu b}{(1-\alpha t)}}\beta f(\eta) \tag{3.18}$$

$$T=T_0-T_{ref}\frac{dx^{r_1}}{\nu(1-\alpha t)^{r_2}}\theta(\eta)$$

The deduced system of ODEs and associated boundary conditions using the above transformations are:

$$f''' + \gamma\left(ff'' - \frac{1}{2}S\eta f'' - (f')^2 - Sf'\right) = 0$$
$$\frac{1}{Pr}\theta'' + \gamma\left(f\theta' - r_1 f'\theta - \frac{1}{2}S\eta\theta' - r_2 S\theta - Ec(f'')^2\right) = 0 \tag{3.19}$$

$$f'(0) = 1, \quad f(0) = 0, \quad f''(1) = 0$$
$$\theta(0) = 1, \quad \theta'(1) = 0, \quad f(1) = S/2 \tag{3.20}$$

R. C. Aziz conducted this problem to investigate the effects of viscous dissipation on free surface temperature of fluid [7]. He followed the same scheme to transform PDEs to ODEs which was used by many researchers stated earlier and then used the 10th order HAM to investigate the effect of Eckert number on free surface temperature at different unsteadiness parameter and Prandtl number. He observed that increasing the value of Eckert number reduces free surface temperature and improves the heat transfer rate. He also observed that heat transfer rate can be improved by increasing the Prandtl number for the cases: Ec= -1 (fluid cooling case), Ec= 0 (no viscous dissipation) and Ec= 1 (fluid heating case).

3.5 Effect of magnetic field and thermocapillarity on unsteady film flow:

N.F.M Noor and I. Hashim conducted a research to analyze the effects of thermocapillarity and magnetic field on unsteady thin film flow over the stretching surface [8]. They considered magnetic field $B = B_0/(1-\alpha t)^{1/2}$ normal to stretching sheet. The time-dependent two-dimensional conservation equations for mass, momentum and energy of the boundary layer flow with magnetic effect are:

$$\frac{\partial u}{\partial x} + \frac{\partial v}{\partial y} = 0$$
$$\frac{\partial u}{\partial t} + u\frac{\partial u}{\partial x} + v\frac{\partial u}{\partial y} = \nu\frac{\partial^2 u}{\partial y^2} - \frac{\sigma B^2}{\rho}u \tag{3.21}$$
$$\frac{\partial T}{\partial t} + u\frac{\partial T}{\partial x} + v\frac{\partial T}{\partial y} = \kappa\frac{\partial^2 T}{\partial y^2}$$

subject to following boundary conditions

$$at\ y = 0, \quad u = U(x,t), \quad v = 0, \quad T = T_s(t,x)$$
$$at\ y = h(t), \quad \mu\frac{\partial u}{\partial y} = \frac{\partial \sigma}{\partial x}, \quad \frac{\partial T}{\partial y} = 0, \quad v = \frac{dh}{dt} \tag{3.22}$$

They were able to transform the system of PDEs into ODEs using the same similarity transformation as used by B.S. Dandapat [6]. The transformed ODEs with the subject boundary conditions are:

$$f''' + \gamma\left(ff'' - \frac{1}{2}S\eta f'' - (f')^2 - (S + Ma)f'\right) = 0$$
$$\frac{\theta''}{Pr} = \gamma\left(-\frac{3S}{2}\theta - \frac{\eta S}{2}\theta' - 2\theta f' + f\theta'\right) \tag{3.23}$$

$$f'(0) = 1, \qquad f(0) = 0, \qquad f''(1) = M\theta(1) \tag{3.24}$$
$$\theta(0) = 1, \qquad \theta'(1) = 0, \qquad f(1) = S/2$$

M and Ma are thermocapillarity parameter and Marangoni number, respectively. The mathematical expression of M and Ma are

$$M = \frac{\gamma\sigma_0 T_{ref}}{\mu_0 (b\nu_0)^{1/2}} \tag{3.25}$$

$$Ma = \frac{\gamma\sigma_0 T_{ref}\sqrt{\nu_0/b}\,\rho_0 C_p}{\mu_0 k_0} = Pr.M \tag{3.26}$$

The transformed ODEs were analytically solved using the HAM. They observed that when thermocapillarity number is increased in the absence of magnetic field the fluid speeds up after a slight deceleration while the fluid's temperature decreases regularly. Furthermore, flow velocity and temperature rise with an increment in unsteadiness parameter. However, increasing the magnetic field parameter effected the flow velocity and temperature differently. Temperature rises while velocity reduces with an increase in Hartmann number.

3.6 Effect of internal heating on an unsteady film flow:

R.C. Aziz observed an unsteady film flow over the stretching surface with internal heating [9]. The motion within the fluid and heat transfer arises solely due to the stretching of surface. He investigated the effects of heat generation due to an internal source on flow velocity and temperature. He analyzed the effect of heat generation and absorption on the flow and heat transfer first by converting PDEs into ODEs and then by solving the transformed ODEs using HAM.

He concluded that the heat generation/absorption had no effect on velocity due to the absence of this parameter in conservation of momentum equation. However, heat

generation/absorption parameter effects the temperature of fluid significantly. Dimensionless temperature increases while heat transfer rate decreases with the increase in internal heating.

Similarly, M. Megahed used homotopy perturbation method to observe the effects of slip velocity and variable heat flux on the velocity, temperature, heat transfer rate and skin friction coefficient in an unsteady boundary layer flow [10]. Later, I-C Liu along with A.M. Megahed investigated how thermal radiation and variable fluid properties impact the flow and heat transfer [11]. Then they numerically solved the boundary layer fluid flow problem with internal heat generation, variable heat flux and thermal radiation [12].

Different researchers investigated the time dependent film flow over the stretching surface with distinct attributes, see e.g., [13-15]. Each of these researches helped in creating better understanding of various phenomena with their work.

3.7 Construction of similarity transformation using Lie point symmetries:

M. Safdar published an article on the use of Lie point symmetries for constructing similarity transformations for thin film flow over an unsteady stretching sheet [16]. The Lie point symmetries had already been employed to study the motion of one-dimensional harmonic oscillator [17], hyperbolic shallow water equations and green Naghdi model [18]. Lie symmetry method is an algebraic technique that provides invariants for the differential equations, see e.g., [19-23] . Use of this technique give more than one set of similarity transformation equations, which help in mapping the differential equations of the flow and heat transfer to multiple types of systems of ODEs involving different physical parameters.

M. Safdar constructed invariants by obtaining the Lie point symmetries for the mass, momentum and heat energy equations for the thin film flow over an unsteady stretching sheet, written in terms of the following

$$\frac{\partial u}{\partial x}+\frac{\partial v}{\partial y}=0$$
$$\frac{\partial u}{\partial t}+u\frac{\partial u}{\partial x}+v\frac{\partial u}{\partial y}=\frac{1}{\rho_0}\frac{\partial}{\partial y}(\mu\frac{\partial u}{\partial y}) \qquad (3.27)$$
$$\frac{\partial T}{\partial t}+u\frac{\partial T}{\partial x}+v\frac{\partial T}{\partial y}=\frac{1}{\rho_0 C_p}\frac{\partial}{\partial y}(\kappa\frac{\partial T}{\partial y})$$

This is the same flow model which was considered by the wang and Anderson in their respective studies. Moreover, the associated boundary conditions are also same. However, in [16] various different and new similarity transformations are constructed for reducing a system

of PDEs into ODEs. He used Lie point symmetries for the construction of similarity transformations. He found following Lie symmetry generators for the considered flow

$$\boldsymbol{X_1} = \frac{\partial}{\partial t},\ \ \boldsymbol{X_2} = \frac{\partial}{\partial x},\ \ \boldsymbol{X_3} = t\frac{\partial}{\partial x} + \frac{\partial}{\partial u},\ \ \boldsymbol{X_4} = T\frac{\partial}{\partial T}$$
$$\boldsymbol{X_5} = x\frac{\partial}{\partial x} + u\frac{\partial}{\partial u},\ \ \boldsymbol{X_6} = t\frac{\partial}{\partial t} + \frac{y}{2}\frac{\partial}{\partial y} - u\frac{\partial}{\partial u} - \frac{v}{2}\frac{\partial}{\partial v} \qquad (3.28)$$
$$\boldsymbol{X_7} = \frac{\partial}{\partial T}$$

The original system of PDEs and associated boundary conditions remain invariant for these symmetry generators. However, it is found that the boundary conditions remain invariant for all the symmetry generators except X_7. The authors performed double reductions and found invariants which gave six different sets of similarity transformations. These similarity transformations are used to reduce the system of PDEs to systems of ODEs. Six systems of ODEs are obtained and the solution of each of these systems reflect the solution of original flow model. The solution of all six systems of ODEs are presented using HAM.

CHAPTER 4: METHODOLOGY

The process for achieving the objectives mentioned in section 1.5 begins with the mathematical formulation of fluid flow. Then, the procedure to solve the flow model for different physical conditions involve the use of different techniques and methods. The steps involved in the solution procedure can be visualized through Figure 4.1.

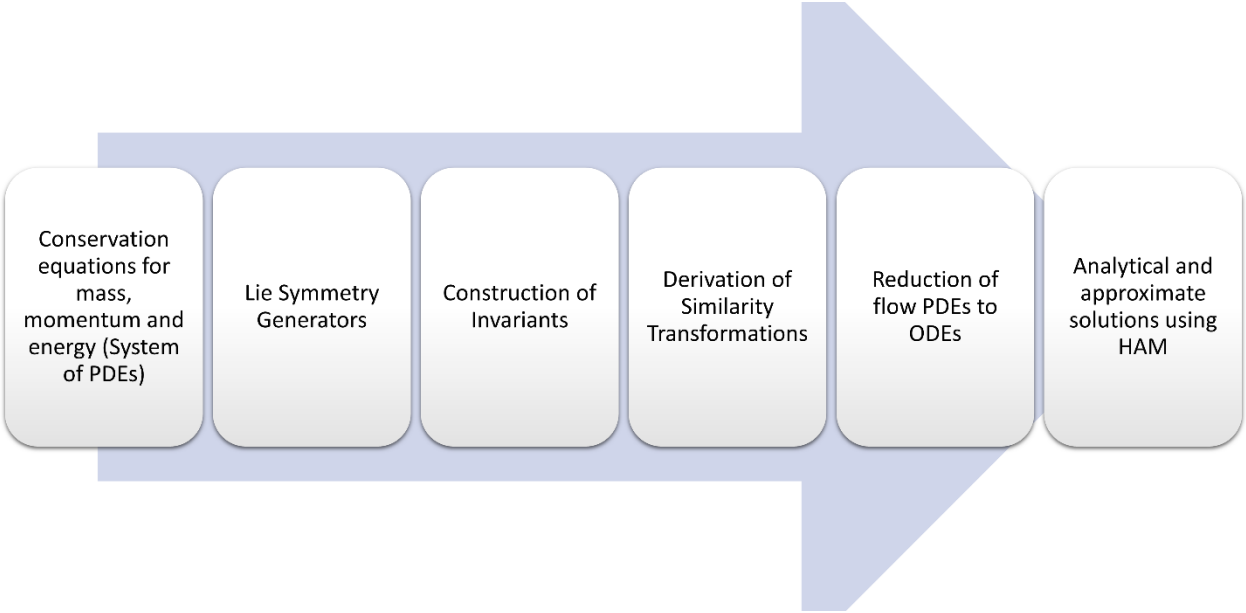

Figure 4.1: Solution procedure

4.1 Governing equations:

Consider a thermally radiating Newtonian fluid with an internal source of heating is emerging from a small opening that exists at origin of cartesian coordinate system. The motion within the fluid arises due to the unsteady stretching of surface aligned with x-axis at $y = 0$. The unsteady stretching of surface makes the fluid flow properties to change with time. The two-dimensional conservation equations for mass, momentum and energy for unsteady thin film flow over stretching surface with internal heating and thermal radiation are:[12]

$$\frac{\partial u}{\partial x} + \frac{\partial v}{\partial y} = 0$$

$$\frac{\partial u}{\partial t} + u\frac{\partial u}{\partial x} + v\frac{\partial u}{\partial y} = \frac{\mu}{\rho}\frac{\partial^2 u}{\partial y^2} \tag{4.1}$$

$$\frac{\partial T}{\partial t} + u\frac{\partial T}{\partial x} + v\frac{\partial T}{\partial y} = \frac{\kappa}{\rho C_p}\frac{\partial^2 T}{\partial y^2} - \frac{1}{\rho C_p}\frac{\partial q_r}{\partial y} + \frac{Q}{\rho C_p}$$

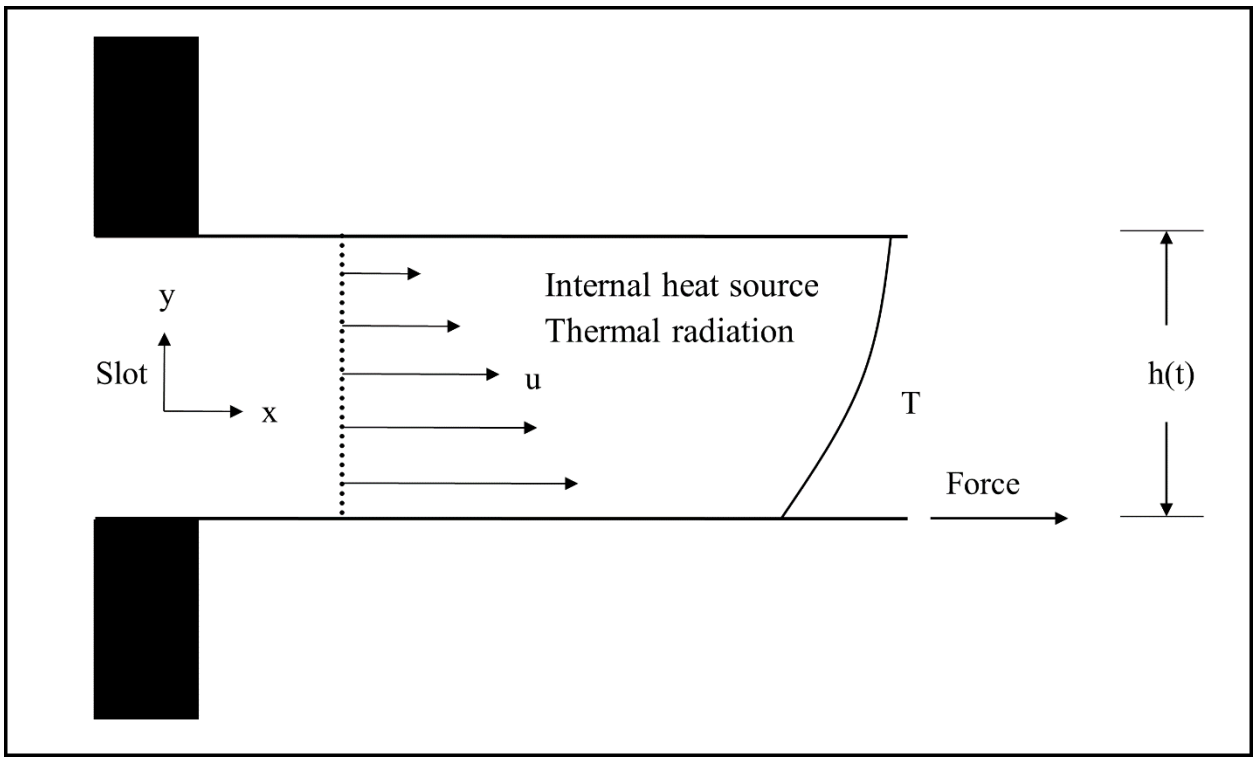

Figure 4.2: Schematic of unsteady film flow over stretching surface.

In the above system of PDEs, *u* and *v* are the velocity components along the *x* and *y* directions, respectively. t is time and the existence of derivative of dependent variables with respect to 't' implies that this mathematical model is for unsteady fluid flow. T is temperature of fluid, μ is dynamic viscosity of fluid, κ is thermal conductivity of fluid, ρ is density of fluid and C_p is specific heat at constant pressure. The term Q represents the heat generation/absorption per unit volume and its mathematical expression is:

$$Q = \frac{\kappa \rho U}{\mu x} B^{\star}(T - T_0) \tag{4.2}$$

$B^{\star}$ is temperature-dependent heat generation/absorption parameter. Positive value of $B^{\star}$ represent the heat generation process. However, the value of $B^{\star}$ for heat absorption process will be negative. The term q_r in energy equation represent radiative heat flux and it is employed according to the Rosseland approximation [24] such that

$$q_r = -\frac{4\sigma^*}{3k^*}\frac{\partial T^4}{\partial y} \tag{4.3}$$

$$T^4 \cong 4T_0^3 T - 3T_0^4 \tag{4.4}$$

The boundary conditions which govern the velocity and temperature are

$$y = 0,\ \ u = U(x,t),\ \ v = 0,\ \ T = T_s(x,t)$$
$$y = h(t),\ \ u_y = T_y = 0,\ \ v = h_t = \frac{dh}{dt} \tag{4.5}$$

In this research, a multi-paradigm programming tool **MAPLE** is used to perform the complex mathematical operations. It covers several areas of technical computing, such as symbolic mathematics, numerical analysis, data processing, visualization, and others.

4.2 Lie symmetry:

A Norwegian mathematician, Sophus Lie introduced the concept of **Lie groups** in late 19th century. He proposed that Lie groups can be used to study the solution of ODEs. He showed that the order of ODEs can be reduced by one if it is invariant under one-parameter Lie group of transformations. Lie's infinitesimal transformation method provides a widely applicable technique to find closed-form similarity solutions for ODEs.

Lie point symmetry maps the solution set of the system of differential equations to itself. In simple words, a Lie point symmetry of a system is a local group of transformations that maps every solution of the system to another solution of the same system.

The Lie point symmetries for an unsteady thin film flow over the stretching surface with internal heating and thermal radiation can be found using the **infinitesimals command** in Maple package "**PDEtools**". The maple code for finding Lie point symmetries of considered flow model can be found in Appendix A. Reader may consult to [16, 18, 19, 22, 23, 25] for detailed algebraic method for finding Lie point symmetries. Following are the Lie point symmetries for the considered flow model:

$$\boldsymbol{X_1} = \frac{\partial}{\partial x},\ \ \boldsymbol{X_2} = t\frac{\partial}{\partial x} + \frac{\partial}{\partial u},\ \ \boldsymbol{X_3} = x\frac{\partial}{\partial x} + u\frac{\partial}{\partial u},\ \ \boldsymbol{X_4} = (T - T_0)\frac{\partial}{\partial T}$$
$$\boldsymbol{X_5} = t^{\frac{B\kappa}{\mu C_p}}\frac{\partial}{\partial T},\ \ \boldsymbol{X_6} = t\frac{\partial}{\partial t} + \frac{y}{2}\frac{\partial}{\partial y} - u\frac{\partial}{\partial u} - \frac{v}{2}\frac{\partial}{\partial v} \tag{4.6}$$
$$\boldsymbol{X_7} = \frac{\partial}{\partial t} + \frac{\kappa B(T - T_0)}{\mu t C_p}\frac{\partial}{\partial T}$$

System of PDEs along with the associated boundary conditions must remain form invariant under these Lie point symmetry generators. Lie point generators and respective transformations are shown in table 4-1.

Table 4-1: Lie symmetry generators and Lie symmetry transformations.

Generators	Transformations
X_1	$t=\bar{t}, x=\bar{x}+\epsilon, y=\bar{y}, u=\bar{u}, v=\bar{v}, T=\bar{T}$
X_2	$t=\bar{t}, x=\bar{x}+\epsilon\bar{t}, y=\bar{y}, u=\bar{u}+\epsilon, v=\bar{v}, T=\bar{T}$
X_3	$t=\bar{t}, x=\bar{x}e^{\epsilon}, y=\bar{y}, u=\bar{u}e^{\epsilon}, v=\bar{v}, T=\bar{T}$
X_4	$t=\bar{t}, x=\bar{x}, y=\bar{y}, u=\bar{u}, v=\bar{v}, T=(\bar{T}-T_0)e^{\epsilon}$
X_5	$t=\bar{t}, x=\bar{x}, y=\bar{y}, u=\bar{u}, v=\bar{v}, T=\bar{T}+\epsilon\bar{t}^{\frac{B\kappa}{\mu C_p}}$
X_6	$t=\bar{t}e^{\epsilon}, x=\bar{x}, y=\bar{y}\sqrt{e^{\epsilon}}, u=\bar{u}e^{-\epsilon}, v=\frac{\bar{v}}{\sqrt{e^{\epsilon}}}, T=\bar{T}$
X_7	$t=\bar{t}+\epsilon, x=\bar{x}, y=\bar{y}, u=\bar{u}, v=\bar{v}, T=\bar{t}^{-\frac{B\kappa}{\mu C_p}}(\bar{T}-T_0)(\bar{t}+\epsilon)^{\frac{B\kappa}{\mu C_p}}$

Table 4-2: Symmetry generators and respective reduced equations

Case	Symmetry generators	Reduction equations
1 (a,b)	$\boldsymbol{X_2+X_6}$	$\eta=\frac{1}{\beta}\sqrt{\frac{b\rho}{\mu at}}y, u=1\pm\frac{b(x-t)}{at}f'$ $v=\mp\beta\sqrt{\frac{b\mu}{a\rho t}}f, T=T_0+\frac{\sqrt{\frac{\mu}{b\rho}}}{k(x-t)}\theta$
2 (a,b)	$\boldsymbol{X_3+X_4}$	$\eta=\frac{1}{\beta}\sqrt{\frac{b\rho}{\mu at}}y, u=\pm\frac{bx}{at}f'$ $v=\mp\beta\sqrt{\frac{b\mu}{a\rho t}}f, T=T_0+\frac{1}{\kappa}\sqrt{\frac{\mu}{\rho b}}\theta tx$
3 (a,b)	$\boldsymbol{X_3+X_5}$	$\eta=\frac{1}{\beta}\sqrt{\frac{b\rho}{\mu at}}y, u=\pm\frac{bx}{at}f'$ $v=\mp\beta\sqrt{\frac{b\mu}{a\rho t}}f, T=T_0+\theta t^{\frac{\beta k}{\mu C_p}}+ln(x)t^{\frac{\beta k}{\mu C_p}}$
4 (a,b)	$\boldsymbol{X_3+X_6}$	$\eta=\frac{1}{\beta}\sqrt{\frac{b\rho}{\mu at}}y, u=\pm\frac{bx}{at}f'$ $v=\mp\beta\sqrt{\frac{b\mu}{a\rho t}}f, T=T_0+\frac{1}{\kappa}\sqrt{\frac{\mu}{\rho b}}\frac{t\theta}{x}$
5 (a,b)	$\boldsymbol{X_5+X_6}$	$\eta=\frac{1}{\beta}\sqrt{\frac{b\rho}{\mu at}}y, u=\pm\frac{bx}{at}f'$ $v=\mp\beta\sqrt{\frac{b\mu}{a\rho t}}f, T=T_0+\frac{1}{\kappa}\sqrt{\frac{\mu}{\rho b}}\frac{\theta}{x}+\frac{\mu C_p}{\kappa\beta}t^{\frac{\kappa\beta}{\mu C_p}}$
6 (a,b)	$\boldsymbol{X_6+X_7}$	$\eta=\frac{1}{\beta}\sqrt{\frac{b\rho}{\mu a(1+t)}}y, u=\pm\frac{bx}{a(1+t)}f'$ $v=\mp\beta\sqrt{\frac{b\mu}{a\rho(1+t)}}f, T=T_0+\frac{x}{\kappa}\sqrt{\frac{\mu}{\rho b}}(1+t)^{\frac{-k\beta}{\mu C_p}}\frac{\kappa\beta}{t^{\mu C_p}}\theta$

4.3 Similarity transformation:

Similarity transformations map system of PDEs and associated boundary conditions to system of ODEs and its respective boundary conditions.

Now, this is done using the chain rule, e.g., Consider case 1a of Table 4-2 this reads as

$$\eta = \frac{1}{\beta}\sqrt{\frac{b\rho}{\mu a t}}y, \quad u = 1 + \frac{b(x-t)}{at}f'$$
$$v = -\beta\sqrt{\frac{b\mu}{a\rho t}}f, \quad T = T_0 + \frac{\sqrt{\frac{\mu}{b\rho}}}{k(x-t)}\theta \tag{4.7}$$

Applying these transformations on system of PDEs (4.1) require the following derivatives

$$\boldsymbol{\frac{\partial u}{\partial x}} = \frac{\partial}{\partial x}\left(1 + \frac{b(x-t)}{at}f'(\eta)\right) = \frac{bf'(\eta)}{\alpha t}$$

$$\boldsymbol{\frac{\partial v}{\partial y}} = \frac{\partial}{\partial y}\left(-\beta\sqrt{\frac{b\mu}{a\rho t}}f(\eta)\right) = -\sqrt{\frac{b\mu}{\alpha\rho t}}f'(\eta)\sqrt{\frac{b\rho}{\alpha\mu t}} = -\frac{bf'(\eta)}{\alpha t}$$

With these, the continuity equation $\boldsymbol{\frac{\partial u}{\partial x} + \frac{\partial v}{\partial y} = 0}$ becomes.

$$\boldsymbol{\frac{\partial u}{\partial x} + \frac{\partial v}{\partial y}} = \frac{bf'(\eta)}{\alpha t} - \frac{bf'(\eta)}{\alpha t} = 0 \qquad (satisfied)$$

Likewise,

$$\boldsymbol{\frac{\partial u}{\partial t} + u\frac{\partial u}{\partial x} + v\frac{\partial u}{\partial y} - \frac{\mu}{\rho}\frac{\partial^2 u}{\partial y^2} = 0}$$

$$\boldsymbol{\frac{\partial u}{\partial t}} = \frac{bf'(\eta)}{\alpha t} - \frac{b(x-t)f'(\eta)}{\alpha t^2} - \frac{b^2(x-t)f''}{2\alpha^2 t^3\beta\sqrt{\frac{b\rho}{\mu\alpha t}}\,\mu}y\rho$$

$$\boldsymbol{u\frac{\partial u}{\partial x}} = \frac{\left(1 + \frac{b(x-t)f'(\eta)}{\alpha t}\right)}{\alpha t}\,bf'(\eta)$$

$$\boldsymbol{v\frac{\partial u}{\partial y}} = \frac{b^2(x-t)}{\alpha^2 t^2}ff''$$

$$\frac{\boldsymbol{\mu}}{\boldsymbol{\rho}}\frac{\boldsymbol{\partial^2 u}}{\boldsymbol{\partial y^2}} = \frac{b^2(x-t)f'''}{\alpha^2 t^2 \beta^2}$$

As unsteadiness parameter (S) is ratio of α to b. So, simplifying the above partial differential equation will give following ordinary differential equation.

$$f''' + \gamma\left(Sf' + \frac{S\eta}{2}f'' - f'^2 + ff''\right) = 0 \tag{4.8}$$

$$\boldsymbol{\frac{\partial T}{\partial t} + u\frac{\partial T}{\partial x} + v\frac{\partial T}{\partial y} - \frac{\kappa}{\rho C_p}\frac{\partial^2 T}{\partial y^2} + \frac{1}{\rho C_p}\frac{\partial q_r}{\partial y} - \frac{Q}{\rho C_p} = 0}$$

$$\frac{\boldsymbol{\partial T}}{\boldsymbol{\partial t}} = \frac{\sqrt{\frac{\mu}{b\rho}}\theta}{\kappa(x-t)^2} - \frac{\sqrt{\frac{\mu}{b\rho}}\, yb\rho\theta'}{2\kappa(x-t)\beta\sqrt{\frac{b\rho}{\mu\alpha t}}\mu\alpha t^2}$$

$$\boldsymbol{u\frac{\partial T}{\partial x}} = -\frac{\left(1 + \frac{b(x-t)f'(\eta)}{\alpha t}\right)\sqrt{\frac{\mu}{b\rho}}\,\theta}{\kappa(x-t)^2}$$

$$\boldsymbol{v\frac{\partial T}{\partial y}} = -\frac{b\sqrt{\frac{\mu}{b\rho}}f\theta'}{\alpha t\kappa(x-t)}$$

$$\boldsymbol{\frac{\kappa}{\rho C_p}\frac{\partial^2 T}{\partial y^2}} = \frac{b\sqrt{\frac{\mu}{b\rho}}\theta''}{C_p(x-t)\beta^2\mu\alpha t}$$

$$\boldsymbol{\frac{1}{\rho C_p}\frac{\partial q_r}{\partial y}} = -\frac{16\sigma\sqrt{\frac{\mu}{b\rho}}\theta'' T_0^3}{3C_p k\kappa(x-t)\beta^2\mu\alpha t}$$

$$\boldsymbol{\frac{Q}{\rho C_p}} = \frac{\left(1 + \frac{b(x-t)}{\alpha t}\right)B\sqrt{\frac{\mu}{b\rho}}\,\theta}{\mu x(x-t)C_p}$$

As we know that,

$$Pr = \frac{\mu C_p}{\kappa}, \quad \gamma = \beta^2, \quad R = \frac{16\sigma T_0^3}{3k * \kappa}$$

So, the energy equation changes to

$$\left(\frac{1+R}{Pr}\right)\theta'' + \gamma\left(\frac{S\eta}{2}\theta' + f'\theta + f\theta' + Pr^{-1}B^* S\theta\right) = 0 \tag{4.9}$$

Similarly, boundary conditions also change to

$$f'(0) = 1, \qquad f(0) = 0, \qquad f''(1) = 0 \tag{4.10}$$
$$\theta(0) = 1, \qquad \theta'(1) = 0, \qquad f(1) = S/2$$

The same procedure can be employed for transforming PDEs into ODEs using the remaining similarity transformations, in Table 4-2. From the Table 4-2, it can be observed that two types of stretching velocity exist: positive and negative. So, the system of ODEs due to reductions with positive u and negative u are given in Table 4-3 and Table 4-4 respectively.

Table 4-3: Similarity transformations and system of ODEs due to positive stretching

Case	Similarity Transformation	System of ODEs
1a	$\eta = \frac{1}{\beta}\sqrt{\frac{b\rho}{\mu at}}y, u = 1 + \frac{b(x-t)}{at}f'$ $v = -\beta\sqrt{\frac{b\mu}{a\rho t}}f, T = T_0 + \frac{\sqrt{\frac{\mu}{b\rho}}}{k(x-t)}\theta$	$f''' + \gamma\left(Sf' + \frac{S\eta}{2}f'' - f'^2 + ff''\right) = 0$ $\left(\frac{1+R}{Pr}\right)\theta'' + \gamma\left(\frac{S\eta}{2}\theta' + f'\theta + f\theta' + Pr^{-1}B^*S\theta\right) = 0$
2a	$\eta = \frac{1}{\beta}\sqrt{\frac{b\rho}{\mu at}}y, u = \frac{bx}{at}f'$ $v = -\beta\sqrt{\frac{b\mu}{a\rho t}}f, T = T_0 + \frac{1}{\kappa}\sqrt{\frac{\mu}{\rho b}}\theta tx$	$f''' + \gamma\left(Sf' + \frac{S\eta}{2}f'' - f'^2 + ff''\right) = 0$ $\left(\frac{1+R}{Pr}\right)\theta'' + \gamma\left(-S\theta + \frac{S\eta}{2}\theta' - f'\theta - f\theta' + Pr^{-1}B^*S\theta\right) = 0$
3a	$\eta = \frac{1}{\beta}\sqrt{\frac{b\rho}{\mu at}}y, u = \frac{bx}{at}f'$ $v = -\beta\sqrt{\frac{b\mu}{a\rho t}}f, T = T_0 + \theta t^{\frac{\beta k}{\mu C_p}} + ln(x)t^{\frac{\beta k}{\mu C_p}}$	$f''' + \gamma\left(Sf' + \frac{S\eta}{2}f'' - f'^2 + ff''\right) = 0$ $\left(\frac{1+R}{Pr}\right)\theta'' + \gamma\left(\frac{S\eta}{2}\theta' - f' + f\theta'\right) = 0$
4a	$\eta = \frac{1}{\beta}\sqrt{\frac{b\rho}{\mu at}}y, u = \frac{bx}{at}f'$ $v = -\beta\sqrt{\frac{b\mu}{a\rho t}}f, T = T_0 + \frac{1}{\kappa}\sqrt{\frac{\mu}{\rho b}}\frac{t\theta}{x}$	$f''' + \gamma\left(Sf' + \frac{S\eta}{2}f'' - f'^2 + ff''\right) = 0$ $\left(\frac{1+R}{Pr}\right)\theta'' + \gamma\left(-S\theta + \frac{S\eta}{2}\theta' + f'\theta + f\theta' + Pr^{-1}B^*S\theta\right) = 0$
5a	$\eta = \frac{1}{\beta}\sqrt{\frac{b\rho}{\mu at}}y, u = \frac{bx}{at}f'$ $v = -\beta\sqrt{\frac{b\mu}{a\rho t}}f, T = T_0 + \frac{1}{\kappa}\sqrt{\frac{\mu}{\rho b}}\frac{\theta}{x} + \frac{\mu C_p}{\kappa\beta}t^{\frac{\kappa\beta}{\mu C_p}}$	$f''' + \gamma\left(Sf' + \frac{S\eta}{2}f'' - f'^2 + ff''\right) = 0$ $\left(\frac{1+R}{Pr}\right)\theta'' + \gamma\left(\frac{S\eta}{2}\theta' + f'\theta + f\theta' + Pr^{-1}B^*S\theta\right) = 0$
6a	$\eta = \frac{1}{\beta}\sqrt{\frac{b\rho}{\mu a(1+t)}}y, u = \frac{bx}{a(1+t)}f'$ $v = -\beta\sqrt{\frac{b\mu}{a\rho(1+t)}}f, \quad T = T_0 + \frac{x}{\kappa}\sqrt{\frac{\mu}{\rho b}}(1+t)^{\frac{-\kappa\beta}{\mu C_p}}\frac{\kappa\beta}{t^{\mu C_p}}\theta$	$f''' + \gamma\left(Sf' + \frac{S\eta}{2}f'' - f'^2 + ff''\right) = 0$ $\left(\frac{1+R}{Pr}\right)\theta'' + \gamma\left(\frac{S\eta}{2}\theta' - f'\theta + f\theta' + Pr^{-1}B^*S\theta\right) = 0$

Table 4-4: Similarity transformation and system of ODEs due to negative stretching

Case	Similarity Transformation	System of ODEs
1b	$\eta = \frac{1}{\beta}\sqrt{\frac{b\rho}{\mu a t}}y, u = 1 - \frac{b(x-t)}{at}f'$ $v = +\beta\sqrt{\frac{b\mu}{a\rho t}}f, T = T_0 + \frac{\sqrt{\frac{\mu}{b\rho}}}{k(x-t)}\theta$	$f''' + \gamma\left(Sf' + \frac{S\eta}{2}f'' + f'^2 - ff''\right) = 0$ $\left(\frac{1+R}{Pr}\right)\theta'' + \gamma\left(\frac{S\eta}{2}\theta' - f'\theta - f\theta' + Pr^{-1}B^*S\theta\right) = 0$
2b	$\eta = \frac{1}{\beta}\sqrt{\frac{b\rho}{\mu a t}}y, u = -\frac{bx}{at}f'$ $v = +\beta\sqrt{\frac{b\mu}{a\rho t}}f, T = T_0 + \frac{1}{\kappa}\sqrt{\frac{\mu}{\rho b}}\theta t x$	$f''' + \gamma\left(Sf' + \frac{S\eta}{2}f'' + f'^2 - ff''\right) = 0$ $\left(\frac{1+R}{Pr}\right)\theta'' + \gamma\left(-S\theta + \frac{S\eta}{2}\theta' + f'\theta - f\theta' + Pr^{-1}B^*S\theta\right) = 0$
3b	$\eta = \frac{1}{\beta}\sqrt{\frac{b\rho}{\mu a t}}y, u = -\frac{bx}{at}f'$ $v = +\beta\sqrt{\frac{b\mu}{a\rho t}}f, T = T_0 + \theta t^{\frac{\beta k}{\mu C_p}} + ln(x)t^{\frac{\beta k}{\mu C_p}}$	$f''' + \gamma\left(Sf' + \frac{S\eta}{2}f'' + f'^2 - ff''\right) = 0$ $\left(\frac{1+R}{Pr}\right)\theta'' + \gamma\left(\frac{S\eta}{2}\theta' + f' - f\theta'\right) = 0$
4b	$\eta = \frac{1}{\beta}\sqrt{\frac{b\rho}{\mu a t}}y, u = -\frac{bx}{at}f'$ $v = +\beta\sqrt{\frac{b\mu}{a\rho t}}f, T = T_0 + \frac{1}{\kappa}\sqrt{\frac{\mu}{\rho b}}\frac{t\theta}{x}$	$f''' + \gamma\left(Sf' + \frac{S\eta}{2}f'' + f'^2 - ff''\right) = 0$ $\left(\frac{1+R}{Pr}\right)\theta'' + \gamma\left(-S\theta + \frac{S\eta}{2}\theta' - f'\theta - f\theta' + Pr^{-1}B^*S\theta\right) = 0$
5b	$\eta = \frac{1}{\beta}\sqrt{\frac{b\rho}{\mu a t}}y, u = -\frac{bx}{at}f'$ $v = +\beta\sqrt{\frac{b\mu}{a\rho t}}f, T = T_0 + \frac{1}{\kappa}\sqrt{\frac{\mu}{\rho b}}\frac{\theta}{x} + \frac{\mu C_p}{\kappa\beta}t^{\frac{\kappa\beta}{\mu C_p}}$	$f''' + \gamma\left(Sf' + \frac{S\eta}{2}f'' + f'^2 - ff''\right) = 0$ $\left(\frac{1+R}{Pr}\right)\theta'' + \gamma\left(\frac{S\eta}{2}\theta' - f'\theta - f\theta' + Pr^{-1}B^*S\theta\right) = 0$
6b	$\eta = \frac{1}{\beta}\sqrt{\frac{b\rho}{\mu a(1+t)}}y, u = -\frac{bx}{a(1+t)}f'$ $v = +\beta\sqrt{\frac{b\mu}{a\rho(1+t)}}f, \quad T = T_0 + \frac{x}{\kappa}\sqrt{\frac{\mu}{\rho b}}(1+t)^{\frac{-\kappa\beta}{\mu C_p}}\frac{\kappa\beta}{t^{\mu C_p}}\theta$	$f''' + \gamma\left(Sf' + \frac{S\eta}{2}f'' + f'^2 - ff''\right) = 0$ $\left(\frac{1+R}{Pr}\right)\theta'' + \gamma\left(\frac{S\eta}{2}\theta' + f'\theta - f\theta' + Pr^{-1}B^*S\theta\right) = 0$

Despite of different transformation equations, system of ODEs mentioned against case 1a and 5a in Table 4-3 and case 1b and 5b in Table 4-4 are same. Hence, solution of 1a and 5a will be same. Similarly, 1b and 5b will give same results.

4.4 Homotopy analysis method:

HAM is a semi-analytical method of solving nonlinear ODEs. The HAM creates a convergent series solution for nonlinear systems by employing the idea of the homotopy from topology. Liao Shijun devised HAM in 1992 and he further modified this method in 1997 by introducing a non-zero non-physical auxiliary parameter [26-29]. This auxiliary parameter is also known as convergence-control parameter, it offers an uncomplicated way to verify and enforce a convergence of the solution. It is a series expansion technique independent of the size

of the physical factors. As a result, it is suitable for both weak and strong nonlinear problems, overcoming some fundamental drawbacks of conventional perturbation methods.

The systems of ODEs mentioned in Table 4-3 and Table 4-4 are solved using the HAM. However, the detailed solution using the HAM is provided for a particular case. Consider a system of ODEs written against case 1a in Table 4-3

$$f''' + \gamma\left(Sf' + \frac{S\eta}{2}f'' - f'^2 + ff''\right) = 0 \tag{4.11}$$

$$\left(\frac{1+R}{Pr}\right)\theta'' + \gamma\left(\frac{S\eta}{2}\theta' + f'\theta + f\theta' + Pr^{-1}B^*S\theta\right) = 0 \tag{4.12}$$

and the associated boundary conditions are:

$$\begin{aligned} &f'(0) = 1, \quad f(0) = 0, \quad f''(1) = 0 \\ &\theta(0) = 1, \quad \theta'(1) = 0, \quad f(1) = S/2 \end{aligned} \tag{4.13}$$

Initial guesses of $f(\eta)$ and $\theta(\eta)$ are required for the initiation of HAM solution procedure. The initial guesses of $f(\eta)$ and $\theta(\eta)$ for the system of ODEs mentioned in Table 4-3 are:

$$f_0(\eta) = \eta - \frac{3S+6}{4}\eta^2 + \frac{2+S}{4}\eta^3 \tag{4.14}$$

$$\theta_0(\eta) = 1 \tag{4.15}$$

and initial guesses for the solution of system of ODEs given in Table 4-4 are:

$$f_0(\eta) = \eta + \frac{3S-6}{4}\eta^2 - \frac{2-S}{4}\eta^3 \tag{4.16}$$

$$\theta_0(\eta) = 1 \tag{4.17}$$

Both these sets of $f_0(\eta)$ and $\theta_0(\eta)$ are derived by applying respective boundary conditions on

$$f_0(\eta) = \alpha_1 + \alpha_2\eta + \alpha_3\eta^2 + \alpha_4\eta^3 \tag{4.18}$$

$$\theta_0(\eta) = \beta_1 + \beta_2\eta \tag{4.19}$$

The auxiliary linear operators for equations (4.14) and (4.15) are $L_f = \partial^3/\partial\eta^3$ and $L_\theta = \partial^2/\partial\eta^2$, respectively with the characteristics

$$L_f[C_1 + C_2\eta + C_3\eta^2 + C_4\eta^3] = 0 \tag{4.20}$$

$$L_\theta[C_1 + C_2\eta] = 0 \tag{4.21}$$

C_1, C_2, C_3 and C_4 are constants. Equations (4.11) and (4.12) can be written in terms of unknown functions F, Θ and Γ. F and Θ are functions of η and q while Γ is only a function of q. Deformation equations for zeroth-order in terms of F, Θ and Γ can be written as

$$(1-q)L_f[F(\eta,q) - f_0(\eta)] = qh_f H_f(\eta)\aleph_f[F(\eta,q), \Theta(\eta,q), \Gamma(q)] \tag{4.22}$$

$$(1-q)L_\theta[\Theta(\eta,q) - \theta_0(\eta)] = qh_\theta H_\theta(\eta)\aleph_\theta[F(\eta,q), \Theta(\eta,q), \Gamma(q)] \tag{4.23}$$

Where q is an embedding parameter. H_f, H_θ, h_f and h_θ are auxiliary functions and parameters. The value of H_f and H_θ are usually taken as 1. h_f and h_θ are also known as convergence-control parameters. They must carry an identical sign to enforce the convergence of the solution series. The range of q can be from 0 to 1. It is observed that when q is taken as 0, equations (4.22) and (4.23) give initial guesses (4.14) and (4.15) respectively, as result. Similarly, for $q = 1$, h_f, $h_\theta \neq 0$ and H_f, $H_\theta = 1$, equations (4.22) and (4.23) leads to $f(\eta)$ and $\theta(\eta)$, i.e., the approximate solution converges to exact solution when q is increased from 0 to 1. $\aleph_f$ and $\aleph_\theta$ are transformed versions of equations (4.11) and (4.12), written in terms of F, Θ and Γ,

$$\aleph_f = F''' + \Gamma\left[SF' + \frac{S\eta}{2}F'' - F'^2 + FF''\right] \tag{4.24}$$

$$\aleph_\theta = \left(\frac{1+R}{Pr}\right)\Theta'' + \gamma\left(\frac{S\eta}{2}\Theta' + F'\Theta + F\Theta' + Pr^{-1}B^*S\Theta\right) \tag{4.25}$$

Simplifying the equations (4.21) and (4.22) generates

$$(1-q)L_f[F(\eta,q) - f_0(\eta)] = qh_f\left[F''' + \Gamma\left(SF' + \frac{S\eta}{2}F'' - F'^2 + FF''\right)\right] \tag{4.26}$$

$$\begin{aligned}(1-q)L_\theta[\Theta(\eta,q) - \theta_0(\eta)] \\ = qh_\theta\left[\left(\frac{1+R}{Pr}\right)\Theta'' + \gamma\left(\frac{S\eta}{2}\Theta' + F'\Theta + F\Theta' + Pr^{-1}B^*S\Theta\right)\right]\end{aligned} \tag{4.27}$$

Differentiating equations (4.26) and (4.27) m-times with respect to q and then putting q=0 and dividing both sides by m! will generate m^{th}-order deformation equations of the form

$$L_f[f_m(\eta) - x_m f_{m-1}(\eta)] = h_f R_{f,m}(\eta) \tag{4.28}$$

$$L_\theta[\theta_m(\eta) - x_m \theta_{m-1}(\eta)] = h_\theta R_{\theta,m}(\eta) \tag{4.29}$$

Now, the transformation of boundary conditions is done in two steps. The boundary conditions (4.13) are only a function of η, first step consist of writing the boundary conditions in terms of $F(\eta, q)$ and $\Theta(\eta, q)$.

$$F(0;q) = 0, F'(0;q) = 1, \Theta(0;q) = 1, F(1;q) = \frac{S}{2}, F''(1;q) = 0, \Theta'(1;q) = 0 \tag{4.30}$$

Now, the second step involves writing of above boundary condition equations in terms of original variables using following equations

$$f_m(\eta) = \frac{1}{m!}\left[\frac{\partial^m F(\eta;q)}{\partial q^m}\right]_{q=0} \qquad \theta_m(\eta) = \frac{1}{m!}\left[\frac{\partial^m \Theta(\eta;q)}{\partial q^m}\right]_{q=0} \tag{4.31}$$

Following all these steps in right order will change the equations (4.11)-(4.13) to

$$L_f[f_m(\eta) - x_m f_{m-1}(\eta)] = h_f R_{f,m}(\eta) \tag{4.32}$$

$$L_\theta[\theta_m(\eta) - x_m \theta_{m-1}(\eta)] = h_\theta R_{\theta,m}(\eta) \tag{4.33}$$

with the boundary conditions

$$f_m(0) = 0, f_m(1) = 0, f_m'(0) = 0, f_m''(1) = 0, \theta_m(0) = 0, \theta_m'(1) = 0 \tag{4.34}$$

where,

$$\begin{aligned} R_{f,m}(\eta) = f_{m-1}''' + \sum_{n=0}^{m-1} \gamma_{m-1-n} \sum_{i=0}^{n} f_i f_{n-i}'' - f_i' f_{n-i}'' + \frac{\eta S}{2} \sum_{n=0}^{m-1} \gamma_n f_{m-1-n}'' \\ + S \sum_{n=0}^{m-1} \gamma_n f_{m-1-n}' \end{aligned} \tag{4.35}$$

$$R_{\theta,m}(\eta) = \left(\frac{1+R}{Pr}\right)\theta''_{m-1} + \sum_{n=0}^{m-1}\gamma_{m-1-n}\sum_{i=0}^{n} f_i\theta'_{n-i} + \theta_i f'_{n-i} + \frac{\eta S}{2}\sum_{n=0}^{m-1}\gamma_n\theta'_{m-1-n} + S\sum_{n=0}^{m-1}\gamma_n\frac{B\theta_{m-1-n}}{Pr} \tag{4.36}$$

The m^{th}-order approximation of $f(\eta), \theta(\eta)$ and γ are expressed as

$$f(\eta) \approx \sum_{n=0}^{m} f_n(\eta)\,, \quad \theta(\eta) \approx \sum_{n=0}^{m}\theta_n(\eta)\,, \quad \gamma \approx \sum_{n=0}^{m-1}\gamma_n \tag{4.37}$$

Applying the same procedure on all system of odes mentioned in Table 4-3 and Table 4-4 we obtain the same type of equations as (4.32)-(4.36). Then these equations are solved using Maple and it will give the result for (4.37). The maple code is given in Appendix A section.

4.4.1 Solution using MAPLE:

The solution procedure using (4.14), (4.15) and (4.32)-(4.36) using MAPLE is given in detail. This section explains the necessary steps which must be taken to plot the graphs for dimensionless velocity f' and temperature θ. All the results are generated using the 10th order HAM.

The convergence control parameters h_f and h_θ are essential for ensuring that the solution of the governing equations converge to a stable and accurate solution. The convergence control parameters, h_f and h_θ appear in equations (4.31) and (4.32), respectively. Equation (4.34) only contain $f(\eta)$ and its derivatives, and therefore, only requires the value of h_f to solve $f(\eta)$. On the other hand, equation (4.35) is a coupled equation that involve $f(\eta)$, $\theta(\eta)$, and their derivatives. As a result, the values of both h_f and h_θ are necessary to solve $\theta(\eta)$. In equation (4.36), the parameter $\theta(\eta)$ refers to the dimensionless temperature parameter, and its solution depends on both the momentum and energy equations. The momentum equation affects the velocity distribution, which in turn affects the temperature distribution through the energy equation. Therefore, finding the correct range of values for both h_f and h_θ are critical for solving the temperature distribution in the fluid accurately.

In order to determine the range of convergence control parameters, it is common practice to plot graphs between the convergence control parameters (h_f and h_θ), and γ. The range of convergence control parameters is then identified as the region of the curve where the value of γ remains constant. In other words, the convergence control parameters can be adjusted within this range without affecting the value of γ, which is the square of dimensionless boundary layer thickness β.

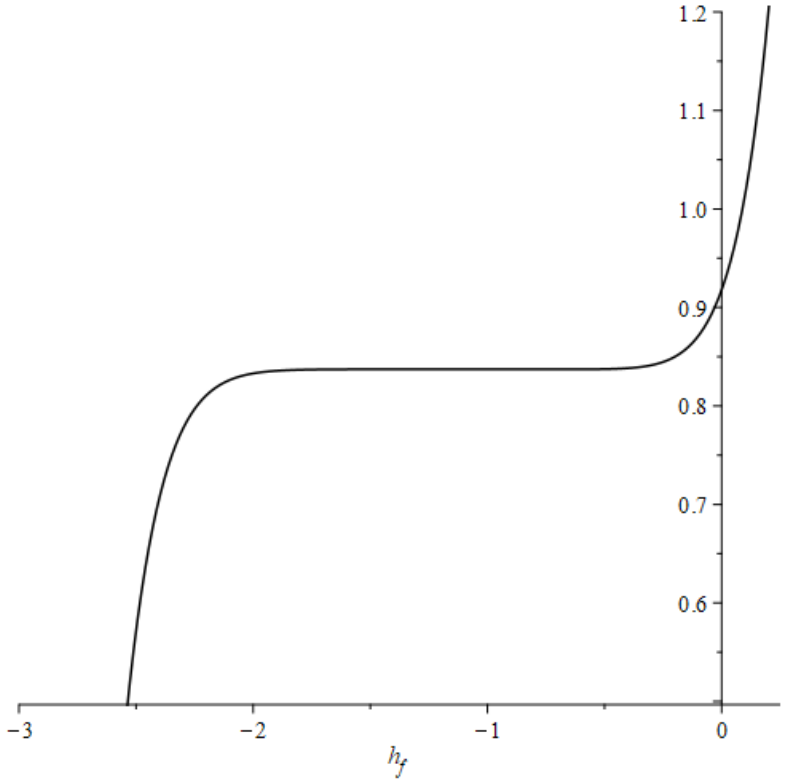

Figure 4.3: h_f curve

Figure 4.3 shows a graph between h_f and γ. h_f is on horizontal axis while γ is on vertical axis. The purpose of this graph is to help finding the feasible range of convergence control parameter h_f. This h_f curve is generated for 2.2, numerical value of unsteadiness parameter. The feasible range of h_f include all the points on horizontal axis for which the value of γ remain same. In other words, the region of h_f curve which is parallel to horizontal axis is considered as the feasible range of h_f parameter. From the above graph, it can be concluded that any value of h_f from the range [-1.6,-0.6] will generate comparable results. So, -1.25 is considered value of h_f for further calculations.

Similarly, the next step is to find the range of h_θ, which is another convergence-control parameter. The range of h_f may change with the change in unsteadiness parameter, while the range of h_θ is usually different for different set of values of S, B, Pr and R. It means that changing the value of any of the mentioned parameters may change the range of h_θ. The h_θ-curve for $S = 2.2, Pr = 1, B = 0.5, R = 0.5$ and $h_f = -1.25$ is shown in Figure 4.4.

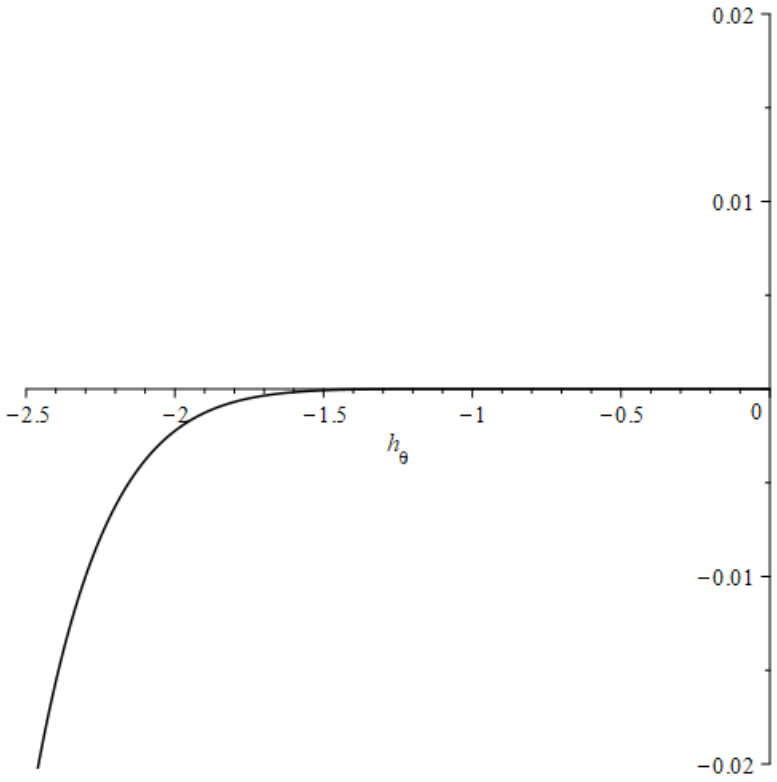

Figure 4.4: h_θ curve

From the above figure, it is obvious that the range of h_θ is (0,-1.4]. Moreover, -0.75 is considered value of h_θ for further calculations.

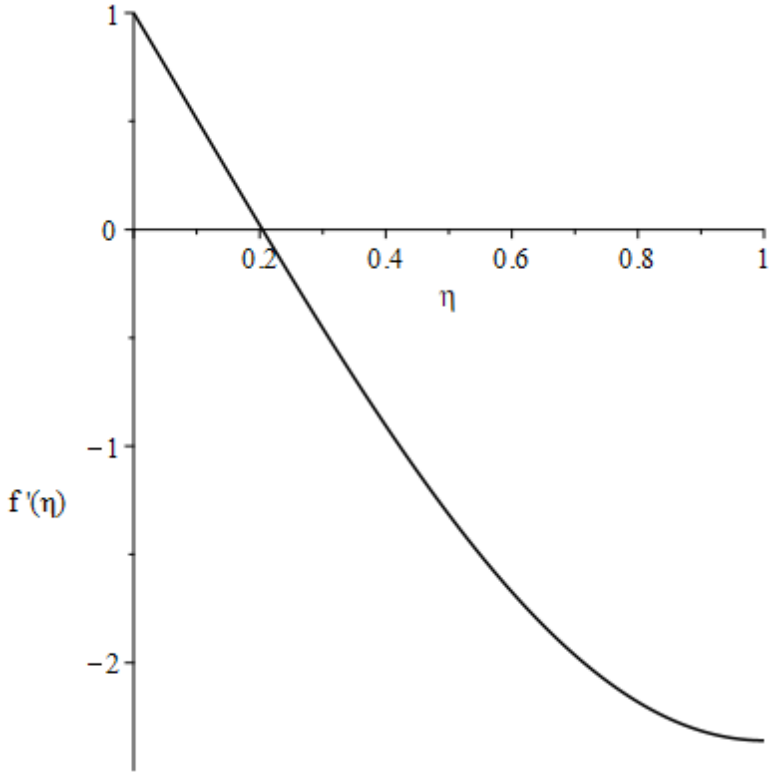

Figure 4.5: $f'(\eta)$ curve for S=2.2

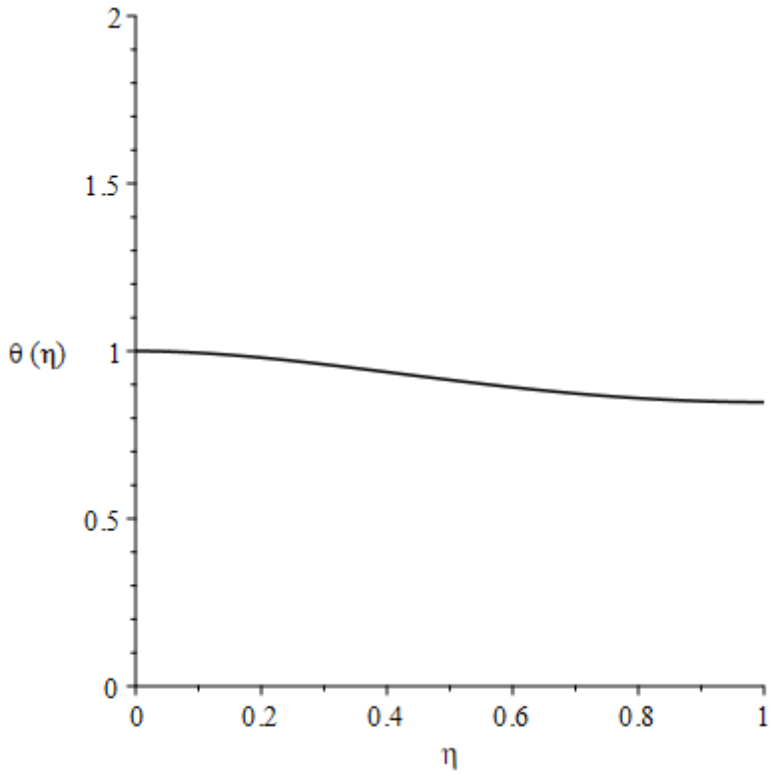

Figure 4.6: $\theta(\eta)$ curve for S=2.2, Pr=1, B=0.5 and R=0.5

Figures 4.5 and 4.6 show the relationship between the dimensionless velocity $f'(\eta)$ and η, and the dimensionless temperature $\theta(\eta)$ and η respectively. All the relevant MAPLE codes are given in Appendix A section.

CHAPTER 5: RESULTS AND DISCUSSION:

Systems of ODEs due to the positive stretching velocity are mentioned in Table 4-3. Total six systems of ODEs are written there. Similarly, six different cases are mentioned in Table 4-4, and all these cases contain system of ODEs due to the negative stretching velocity. Similarity transformations written against case 1a and case 5a generate same system of ODEs. Moreover, this observation is also true for systems due to negative stretching velocity. So, it is safe to say that solution of system of ODEs mentioned against case 1a and 5a will exactly be the same. Similarly, case 1b and case 5b will also give same results.

All the system of ODEs mentioned in Tables 4-3 and 4-4 are solved by writing code for HAM on MAPLE. All 12 Systems of ODEs are solved by applying 10^{th} order HAM. However, the MAPLE code is composed in such a way that the order of solution could be increased or decreased by simply changing the value of 'm' in the program.

The system of ODEs given in Tables 4-3 and 4-4 are solved for different values of unsteadiness parameter, prandtl number, radiative heat flux parameter and internal heat generation parameter to individually study the impact of all these parameters on velocity, temperature and heat flux through the boundary. The graphs for convergence-control parameter h_f are

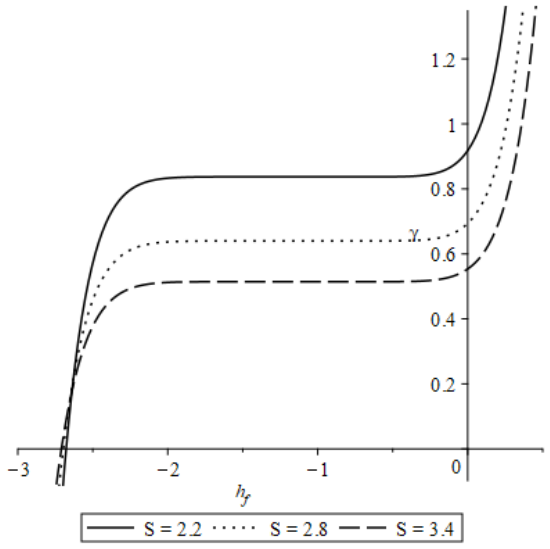

Figure 5.1: h_f curves for cases (1-6)a

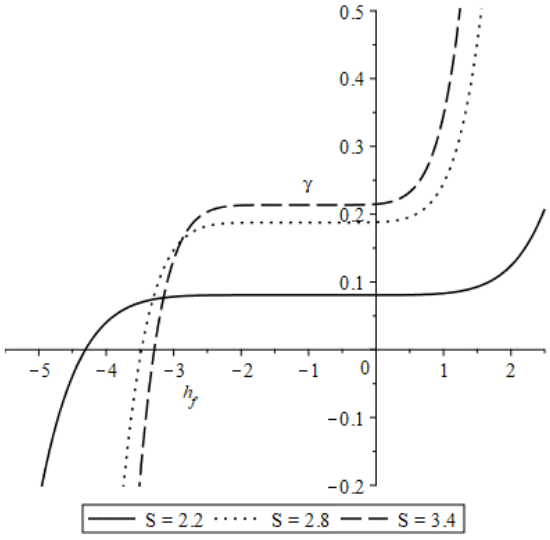

Figure 5.2: h_f curves for cases (1-6)b

The h_f-curves for cases (1-6)a are shown in Figure 5.1, and the h_f-curves for cases (1-6)b are shown in Figure 5.2. The value of h_f must be selected from the region parallel to horizontal axis. The value of unsteadiness parameter for cases (1-6)b must be greater than 2.0 for the

correct solution of flow equations. For $S \leq 2.0$, the method gives complex number as a result of dimensionless boundary layer thickness which is physically impossible. However, the value of unsteadiness parameter for the cases (1-6)a can be as low as 0, as they do not produce physically impossible results.

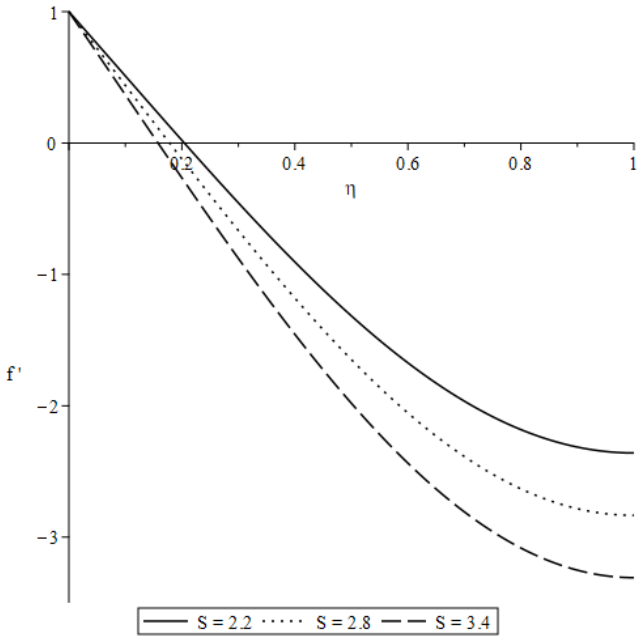

Figure 5.3: f' curves for cases (1-6)a for *S* (2.2, 2.8, 3.4)

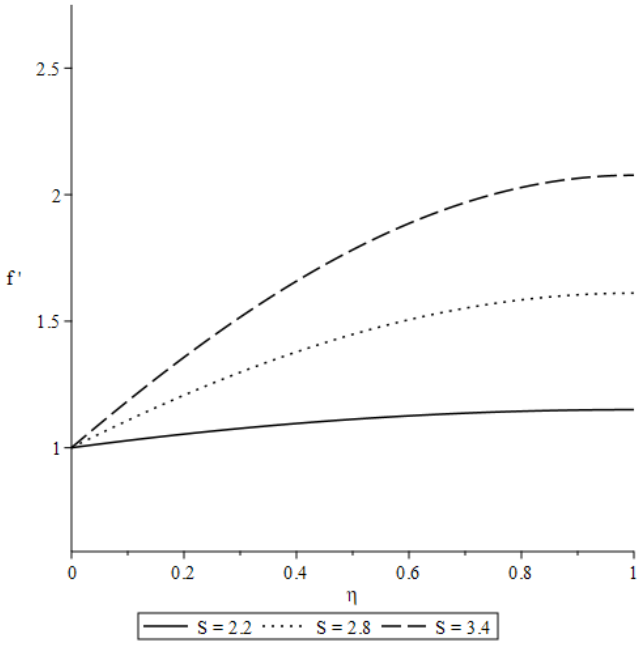

Figure 5.4: f' curves for cases (1-6)b for *S* (2.2, 2.8, 3.4)

Figures 5.3 and 5.4 show $f'(\eta)$ curves for systems of ODEs due to positive and negative stretching velocities, respectively. η is on the horizontal axis, while $f'(\eta)$ is on the vertical axis in both figures. Figure 5.3 shows that the value of $f'(1)$ decreases with an increase in the

unsteadiness parameter, and it also shows that the starting points of $f'(\eta)$ curves exist in 1st quadrant while they end in 4th quadrant. The existence of $f'(\eta)$ curves in two quadrants implies that the fluid changes its direction within the flow region. This type of phenomenon usually occurs around the separation point in the boundary layer. Moreover, the greater negative value of $f'(1)$ represent the fast-flowing fluid but in opposite direction. However, Figure 5.4 shows that the value of $f'(1)$ increases with an increase in unsteadiness parameter S. In other words, the value of $f'(1)$ is directly proportional to the value of the unsteadiness parameter for cases (1-6)b.

Table 5-1: Variation of dimensionless film thickness and reduced skin friction coefficient with respect to S for cases (1-6)a

S	h_f	β	$-f''(0)$	S	h_f	β	$-f''(0)$
2.2	-1.25	0.915105	-4.863915	3.2	-1.25	0.742151	-6.057596
2.4	-1.25	0.871935	-5.099799	3.4	-1.25	0.717272	-6.299162
2.6	-1.25	0.833843	-5.337495	3.6	-1.0	0.694575	-6.541234
2.8	-1.25	0.799948	-5.576559	3.8	-1.0	0.673771	-6.783714
3.0	-1.25	0.769564	-5.816671	4.0	-1.0	0.654620	-7.026524

Table 5-2: Variation of dimensionless film thickness and reduced skin friction coefficient with respect to S for cases (1-6)b

S	h_f	β	$-f''(0)$	S	h_f	β	$-f''(0)$
2.2	-2.0	0.283871	0.298758	3.2	-1.0	0.457383	1.639228
2.4	-1.5	0.363986	0.574556	3.4	-1.0	0.462066	1.896652
2.6	-1.25	0.407488	0.848143	3.6	-1.0	0.463893	2.152044
2.8	-1.25	0.433132	1.115873	3.8	-1.0	0.463748	2.405816
3.0	-1.0	0.448477	1.379219	4.0	-1.0	0.462222	2.658279

The ordinary differential equation that governs the flow velocity is same for all cases with the same type of stretching velocity. Tables 5-1 and 5-2 show the variation of dimensionless film thickness β and reduced skin-friction coefficient $-f''(0)$ with respect to the unsteadiness parameter S for cases (1-6)a and (1-6)b, respectively. Table 5-1 shows that the value of dimensionless film thickness parameter decreases with an increase in the unsteadiness parameter for cases (1-6)a, and the value of reduced skin friction coefficient remains negative for all values of unsteadiness parameter. However, Table 5-2 depicts an increase in dimensionless film thickness β and reduced skin friction coefficient $-f''(0)$ due to the increase in unsteadiness parameter. However, the increase in the value of dimensionless film thickness parameter slows when an unsteadiness parameter is increased beyond 3.0, and this observation is valid for cases (1-6)b . Furthermore, the reduced skin friction coefficient increases more rapidly for fluid flows with positive stretching velocities as compared to the

negative velocities. The effect of varying the unsteadiness parameter on the θ(η) curve is analyzed for internal heating, radiation, and Prandtl number, with the parameter values of 0.5, 0.5, and 1.0, respectively. The same values are used to analyze the effect of other parameters on the θ(η) curve.

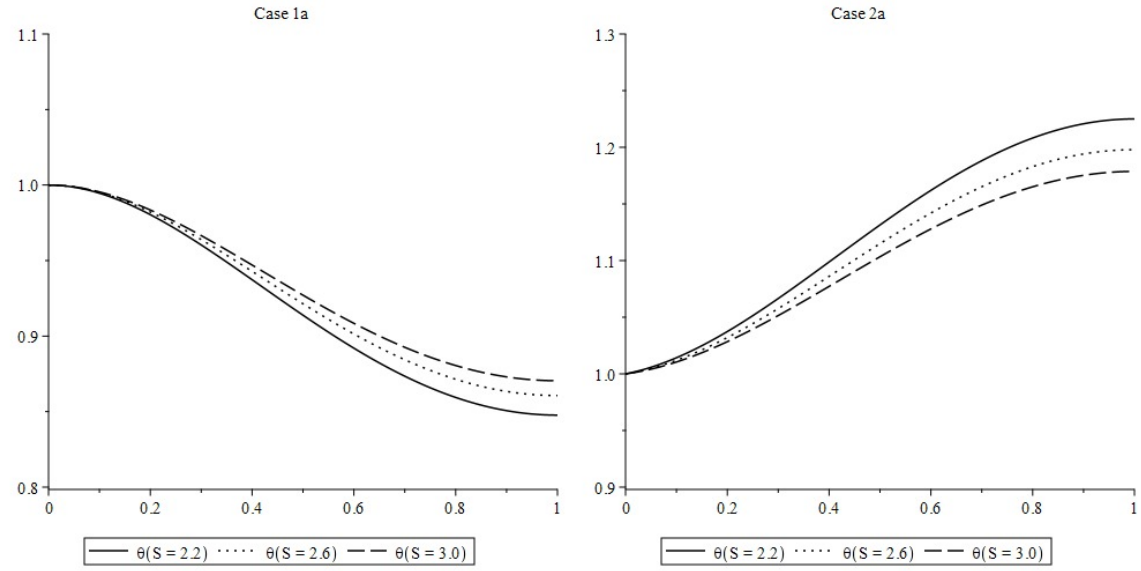

Figure 5.5: Case (1,2)a plots of θ(η) for S (2.2,2.6,3.0) at Pr=1, B=0.5, R=0.5

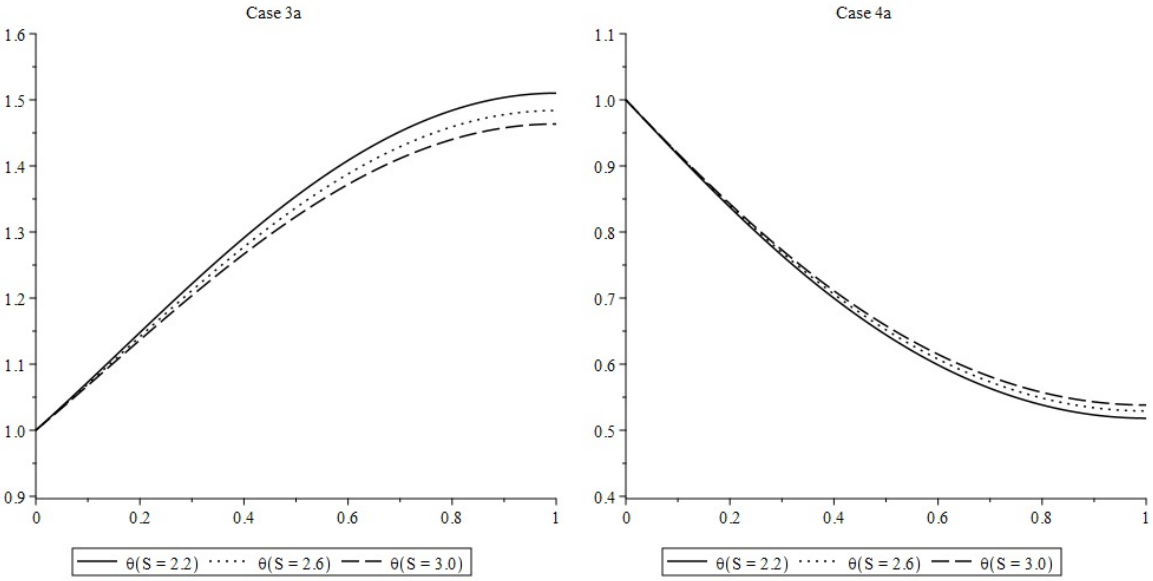

Figure 5.6: Case (3,4)a plots of θ(η) for S (2.2,2.6,3.0) at Pr=1, B=0.5, R=0.5

The $\theta(\eta)$ curves for cases 1a and 2a are shown in Figure 5.5, where η is on the horizontal axis and $\theta(\eta)$ is on the vertical axis. The above graphs show the impact of varying the unsteadiness parameter S on $\theta(\eta)$ for cases 1a and 2a. From the above graphs, it is obvious that the value of $\theta(1)$ is directly proportional to the unsteadiness parameter for the case 1a.

However, the value of $\theta(1)$ is inversely proportional to the value of the unsteadiness parameter for case 2a. Whereas, Figure 5.6 shows the impact of varying the unsteadiness parameter S on $\theta(\eta)$ for cases 3a and 4a. From the above figures, it is obvious that the value of $\theta(1)$ is inversely proportional to the value of the unsteadiness parameter for case 3a. However, the value of $\theta(1)$ is directly proportional to the value of the unsteadiness parameter for case 4a.

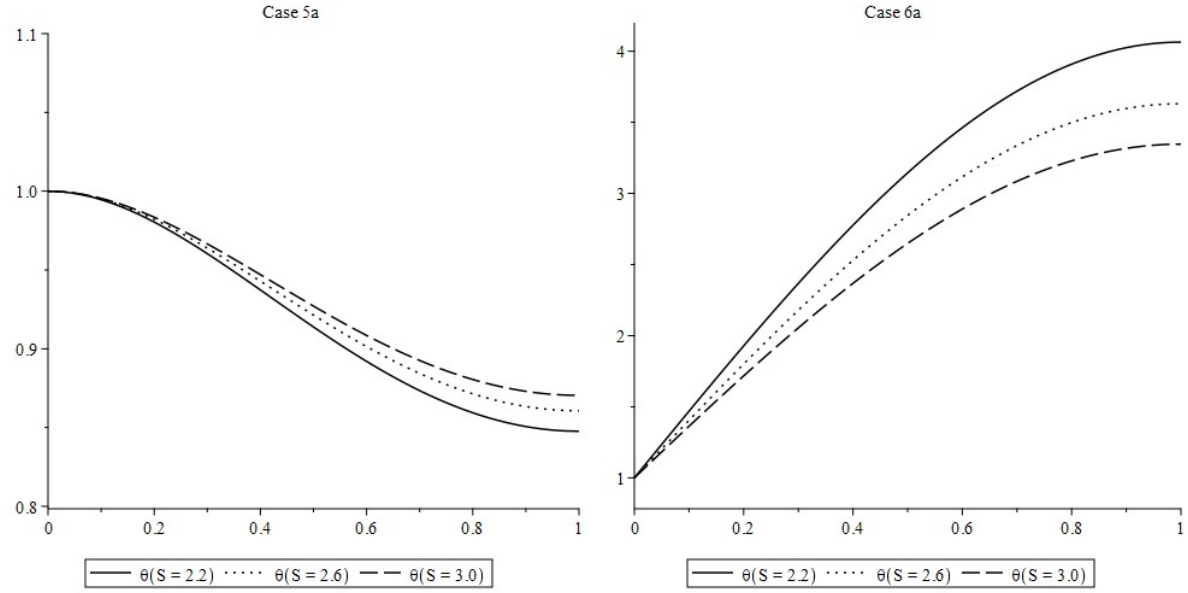

Figure 5.7: Case (5,6)a plots of θ(η) for S (2.2,2.6,3.0) at Pr=1, B=0.5, R=0.5

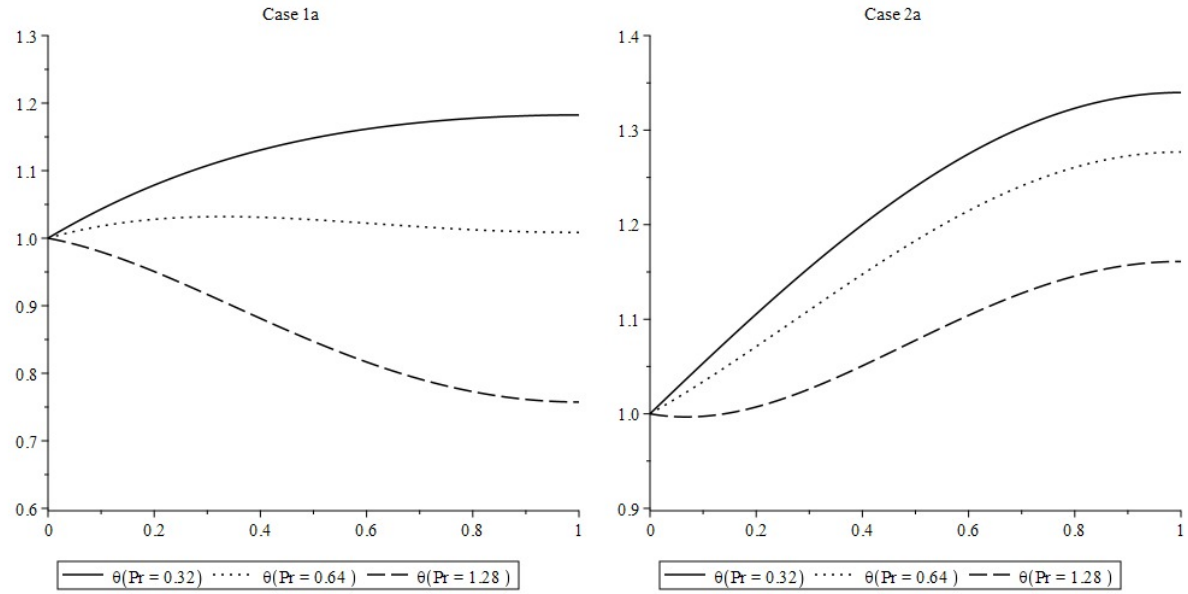

Figure 5.8: Case (1,2)a plots of θ(η) for Pr (0.32,0.64,1.28) at S=2.4, B=0.5, R=0.5

Figure 5.7 depicts the effect of the unsteadiness parameter S on $\theta(\eta)$ for cases 5a and 6a. It is evident from the figures that the value of $\theta(1)$ varies directly with the unsteadiness parameter for case 5a, while for case 6a, the value of $\theta(1)$ varies inversely with the

unsteadiness parameter. Similarly, Figure 5.8 demonstrates the impact of varying Prandtl number on $\theta(\eta)$ for cases 1a and 2a. The figures reveal that the value of $\theta(1)$ is inversely proportional to the Prandtl number for cases 1a and 2a. The effect of varying the Prandtl number on the θ(η) curve is analyzed for internal heating, radiation, and unsteadiness parameter, with the parameter values of 0.5, 0.5, and 2.4, respectively.

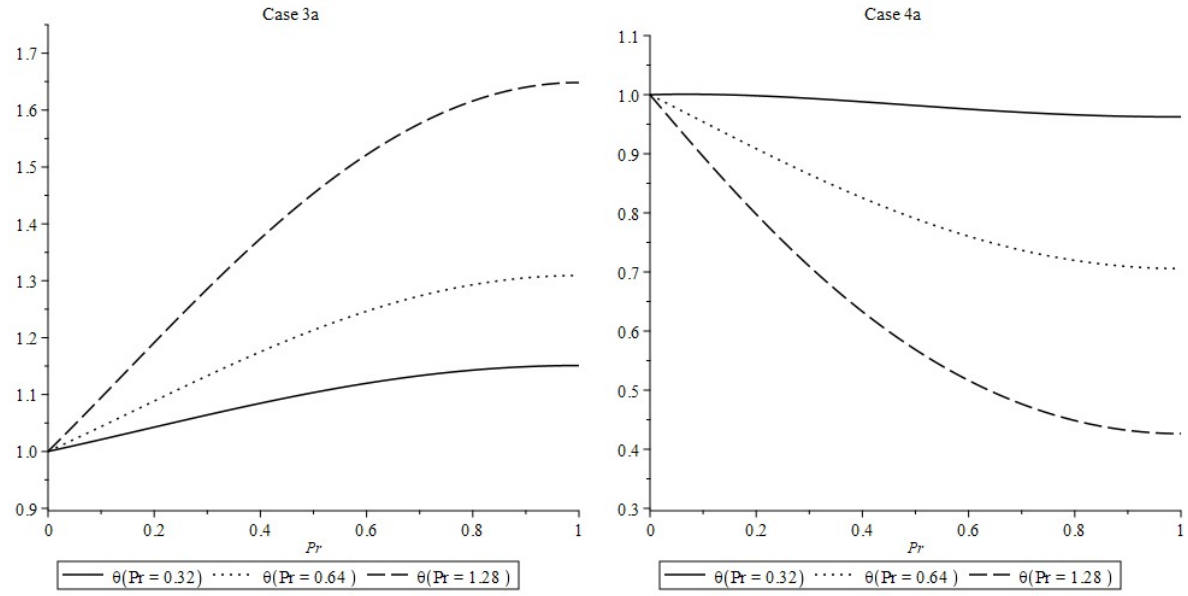

Figure 5.9: Case (3,4)a plots of θ(η) for Pr (0.32,0.64,1.28) at S=2.4, B=0.5, R=0.5

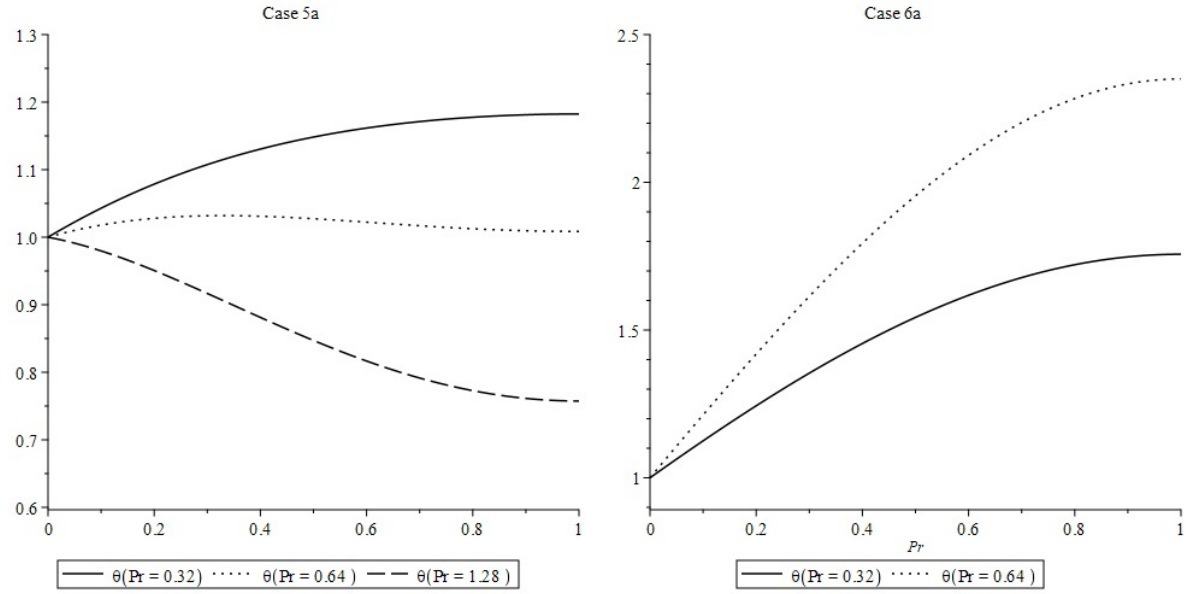

Figure 5.10: Case (5,6)a plots of θ(η) for Pr (0.32,0.64,1.28) at S=2.4, B=0.5, R=0.5

Figure 5.9 shows the impact of varying the Prandtl number on $\theta(\eta)$ for cases 3a and 4a. From the above figures, it is obvious that the value of $\theta(1)$ is directly proportional to the

Prandtl number for case 3a while the value of $\theta(1)$ is inversely proportional to the Prandtl number for case 4a. Whereas, Figure 5.10 shows the impact of varying the Prandtl number on $\theta(\eta)$ for cases 5a and 6a. From the above figures, it is obvious that the value of $\theta(1)$ is inversely proportional to the Prandtl number for case 5a. However, the value of $\theta(1)$ is directly proportional to the Prandtl number for case 6a. HAM could not generate the $\theta(\eta)$-curve for the case 6a at 1.28, as no valid h_θ-curve exists for this value.

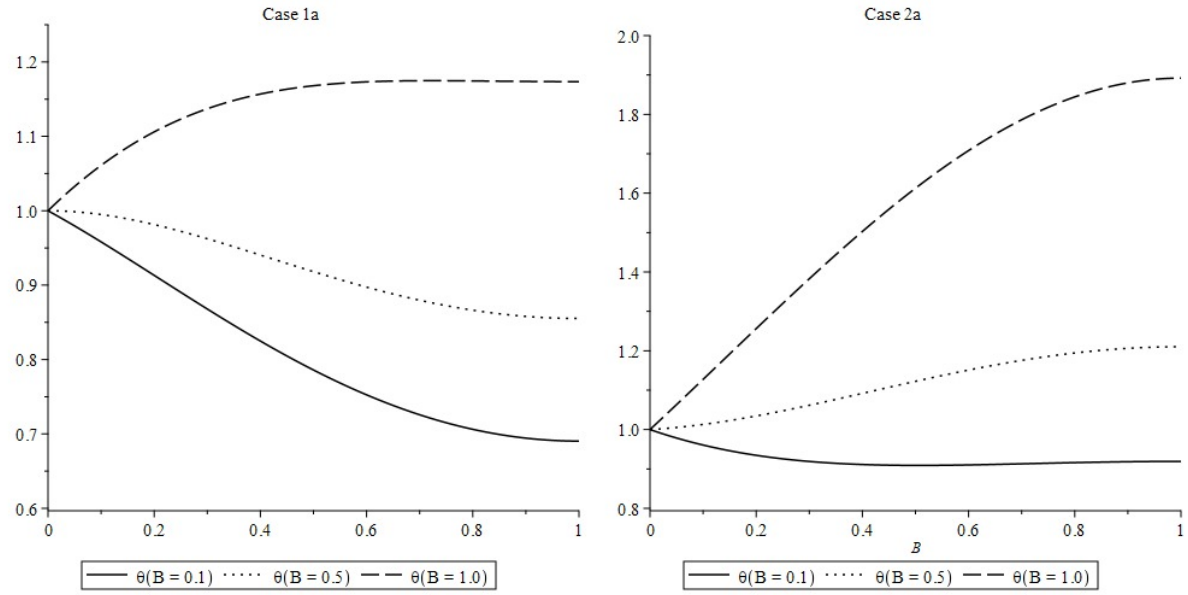

Figure 5.11: Case (1,2)a plots of θ(η) for B (0.1,0.5,1.0) at S=2.4, Pr=1, R=0.5

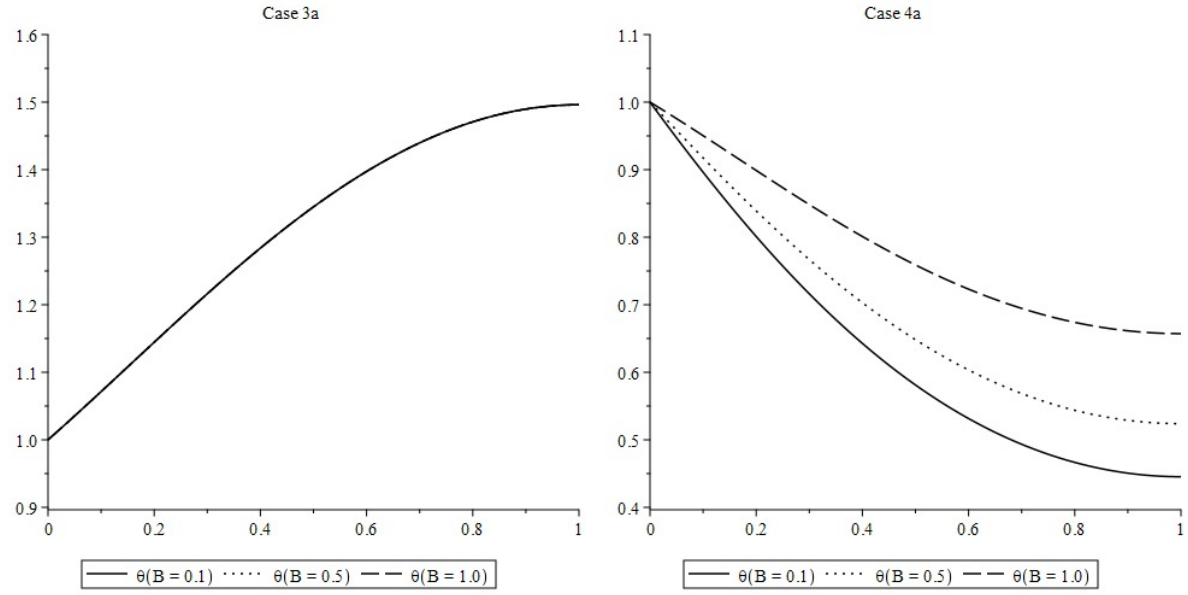

Figure 5.12: Case (3,4)a plots of θ(η) for B (0.1,0.5,1.0) at S=2.4, Pr=1, R=0.5

The impact of the internal heat generation parameter on $\theta(\eta)$ for cases 1a and 2a is illustrated in Figure 5.11. It is evident from the aforementioned figures that the value of $\theta(1)$ is directly proportional to the internal heating parameter for both cases 1a and 2a. On the other hand, Figure 5.12 portrays the effect of varying the internal heating parameter on $\theta(\eta)$ in cases 3a and 4a. The figure demonstrates that the value of $\theta(1)$ remains constant for different values of the internal heating parameter in case 3a, this is attributed to the absence of the internal heating parameter. However, in case 4a, the value of $\theta(1)$ is directly proportional to B.

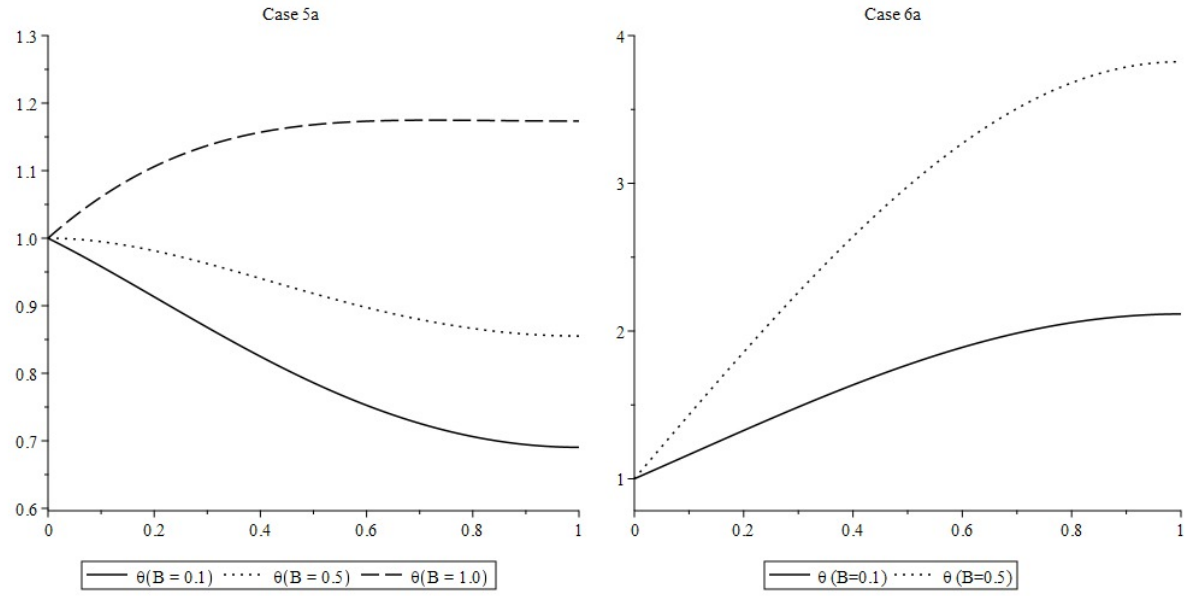

Figure 5.13: Case (5,6)a plots of θ(η) for B (0.1,0.5,1.0) at S=2.4, Pr=1, R=0.5

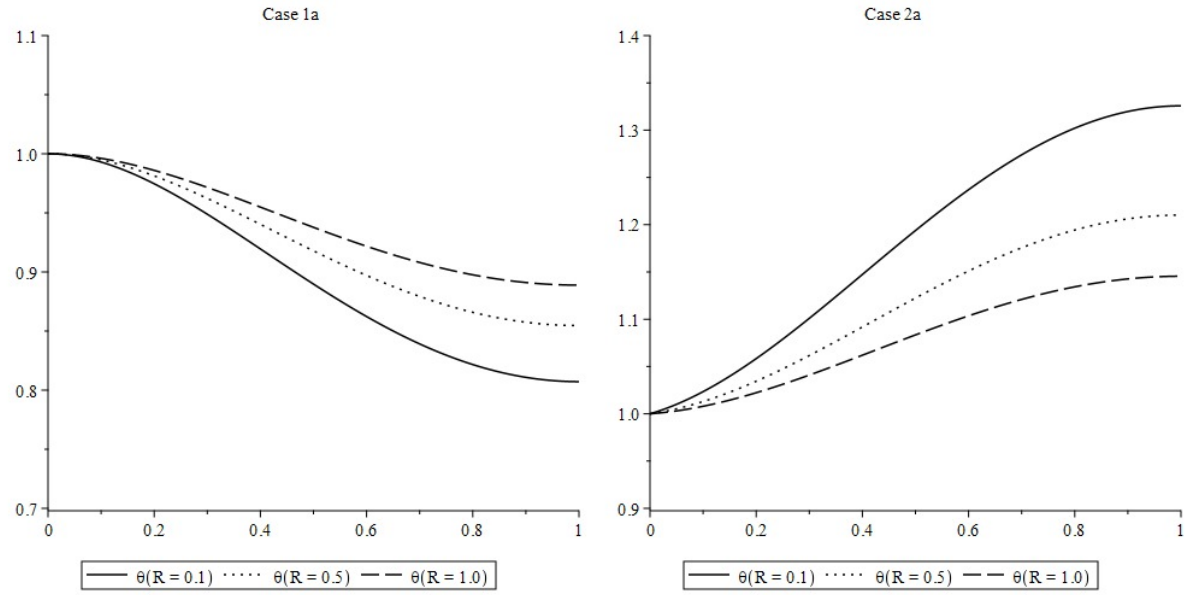

Figure 5.14: Case (1,2)a plots of θ(η) for R (0.1,0.5,1.0) at S=2.4, Pr=1, B=0.5

The impact of varying the internal heat generation parameter B on $\theta(\eta)$ for cases 5a and 6a is demonstrated in Figure 5.13. It is evident from the figures that the value of $\theta(1)$ is directly proportional to the internal heating parameter for both cases 5a and 6a. However, the $\theta(\eta)$ curve for case 6a at 1.0 could not be generated as no valid h_θ-curve exists for 1.0. Furthermore, Figure 5.14 illustrates the impact of varying the thermal radiation parameter on $\theta(\eta)$ for cases 1a and 2a. The figure reveals that the value of $\theta(1)$ is directly proportional to the thermal radiation parameter R for case 1a. However, in case 2a, the value of $\theta(1)$ is inversely proportional to R.

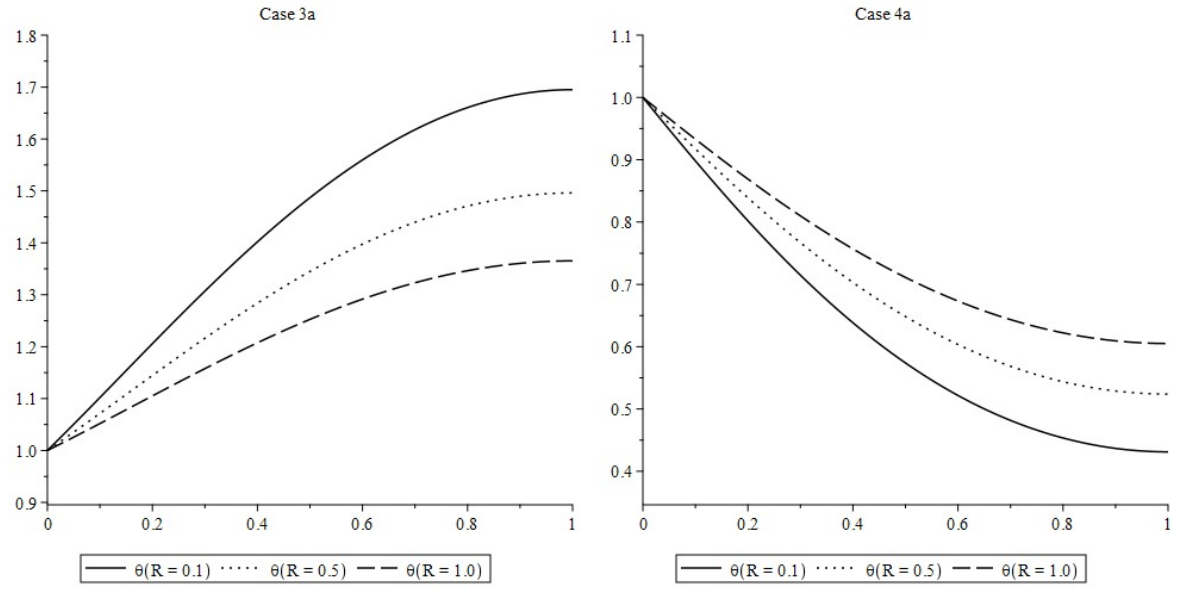

Figure 5.15: Case (3,4)a plots of θ(η) for R (0.1,0.5,1.0) at S=2.4, Pr=1, B=0.5

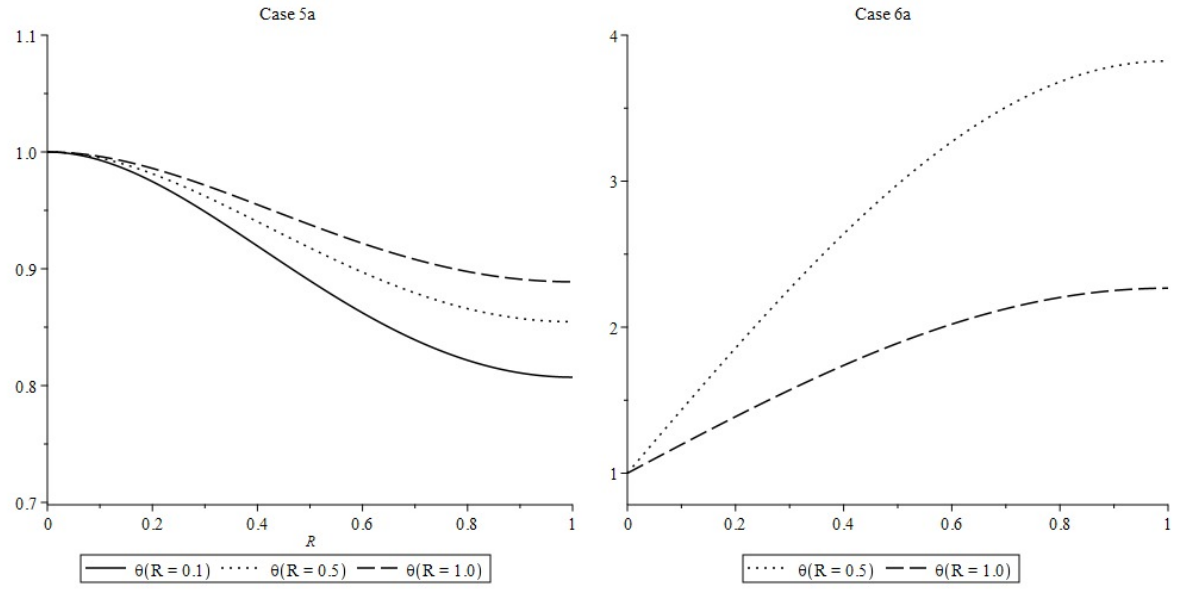

Figure 5.16: Case (5,6)a plots of θ(η) for R (0.1,0.5,1.0) at S=2.4, Pr=1, B=0.5

Figure 5.15 shows the impact of varying the thermal radiation parameter R on $\theta(\eta)$ for cases 3a and 4a. From the above figures, it is obvious that the value of $\theta(1)$ is inversely proportional to the thermal radiation parameter for case 3a. However, the value of $\theta(1)$ increased with an increase in the thermal radiation parameter for case 4a. Figure 5.16 depicts the effect of varying thermal radiation parameters on $\theta(\eta)$ in cases 5a and 6a. From the above figures, it is obvious that the value of $\theta(1)$ is directly proportional to the value of the thermal radiation parameter R for case 5a. However, the value of $\theta(1)$ decreased with an increase in the thermal radiation parameter in case 6a. HAM could not generate the $\theta(\eta)$-curve for the case 6a at 0.1, as no valid h_θ-curve exists for this value.

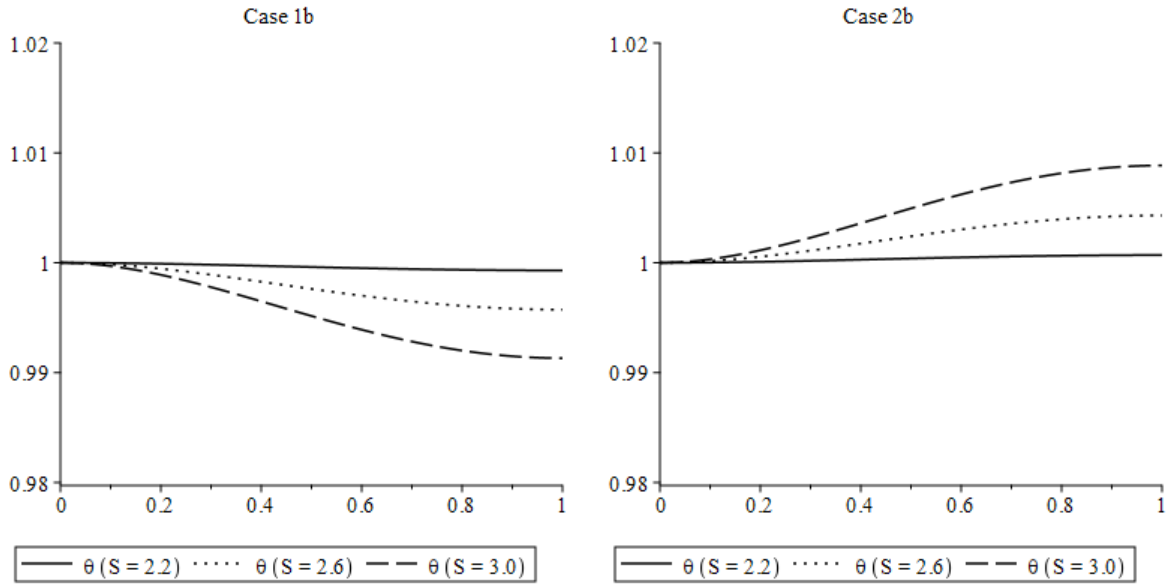

Figure 5.17: Case (1,2)b plots of θ(η) for S (2.2,2.6,3.0) at Pr=1, B=0.5, R=0.5

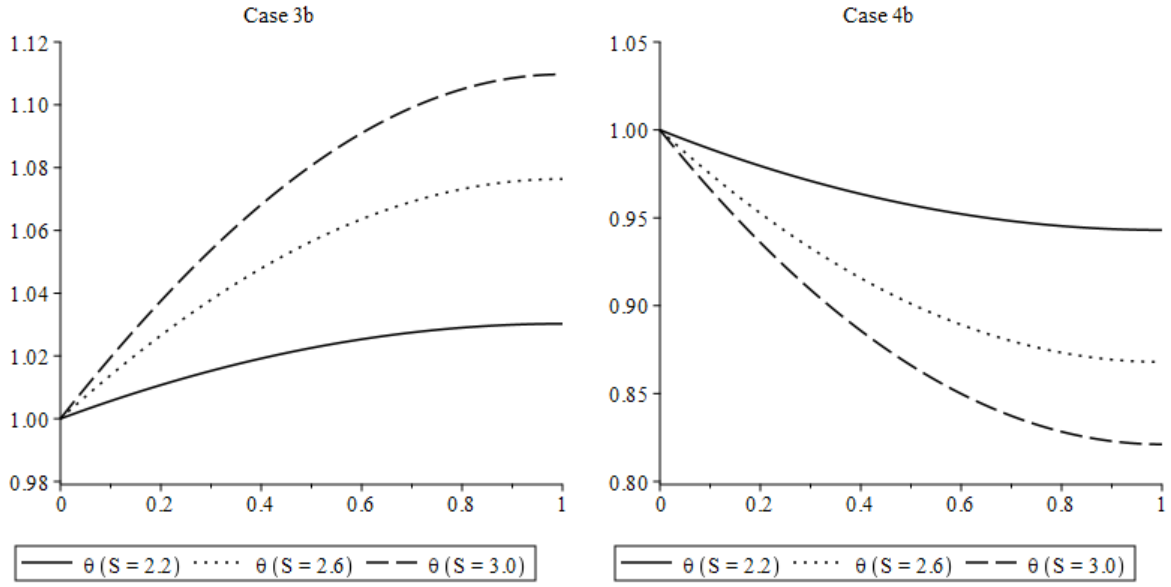

Figure 5.18: Case (3,4)b plots of θ(η) for S (2.2,2.6,3.0) at Pr=1, B=0.5, R=0.5

Figure 5.17 exhibits the effect of changing the unsteadiness parameter on $\theta(\eta)$ curve for cases 1b and 2b. As per the figures presented, it is apparent that, for case 1b, the value of $\theta(1)$ exhibits a slight reduction with an increase in the unsteadiness parameter, whereas, for case 2b, the value of $\theta(1)$ displays a slight increase with an increase in the unsteadiness parameter. On the other hand, Figure 5.18 showcases the influence of the unsteadiness parameter on $\theta(\eta)$ for cases 3b and 4b. The above figures illustrate that, in case 3b, the value of $\theta(1)$ is directly proportional to the unsteadiness parameter S, whereas, in case 4b, the value of $\theta(1)$ is inversely proportional to S.

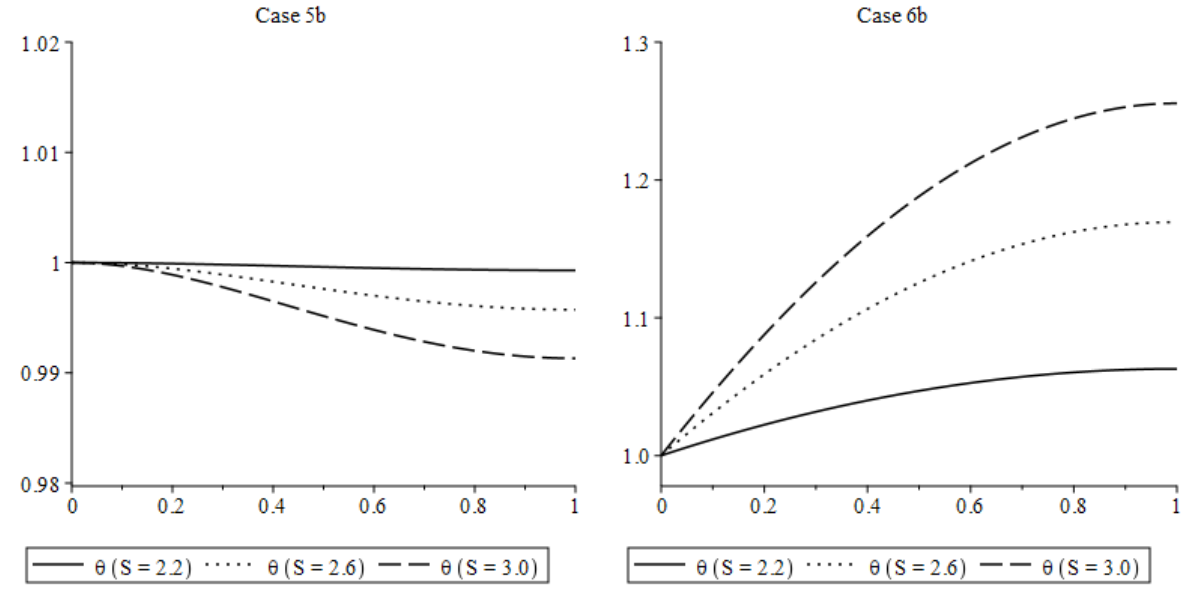

Figure 5.19: Case (5,6)b plots of θ(η) for S (2.2,2.6,3.0) at Pr=1, B=0.5, R=0.5

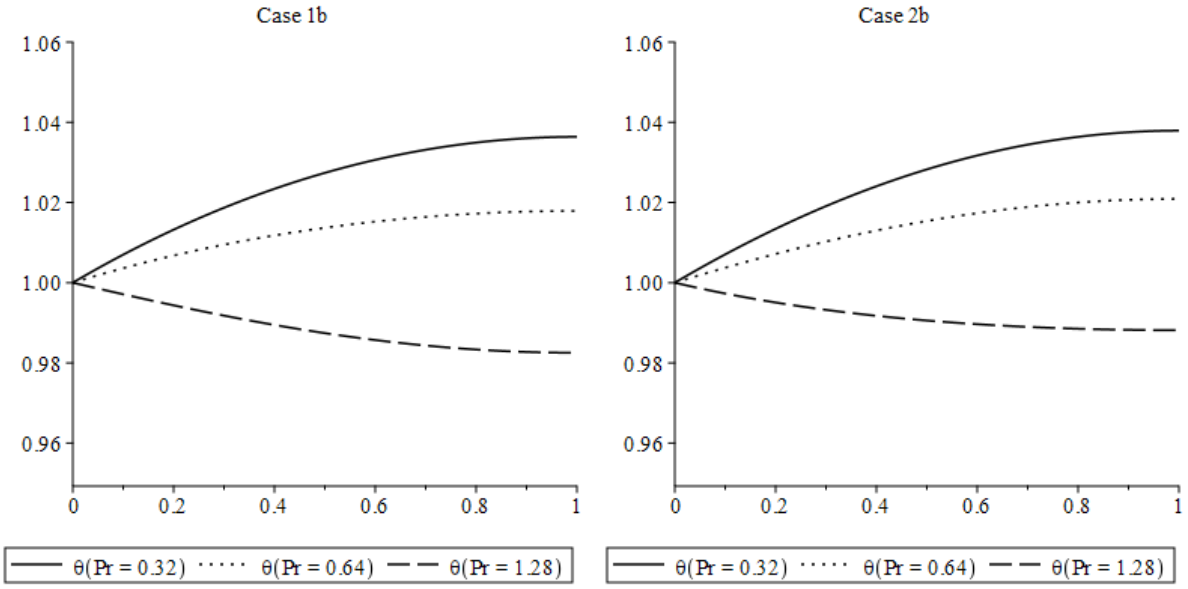

Figure 5.20: Case (1,2)b plots of θ(η) for Pr (0.32,0.64,1.28) at S=2.4, B=0.5, R=0.5

Figure 5.19 shows the impact of varying the unsteadiness parameter on $\theta(\eta)$ for cases 5b and 6b. From the above figures, it is obvious that the value of $\theta(1)$ decreased slightly with an increase in the unsteadiness parameter for case 5b. However, the value of $\theta(1)$ is directly proportional to the unsteadiness parameter for case 6b. Whereas Figure 5.20 shows the impact of varying the Prandtl number on $\theta(\eta)$ for cases 1b and 2b. From the above figures, it is obvious that varying the Prandtl number affects the value of $\theta(1)$ in the same manner in both cases. The value of $\theta(1)$ decreases with an increase in the Prandtl number for cases 1b and 2b.

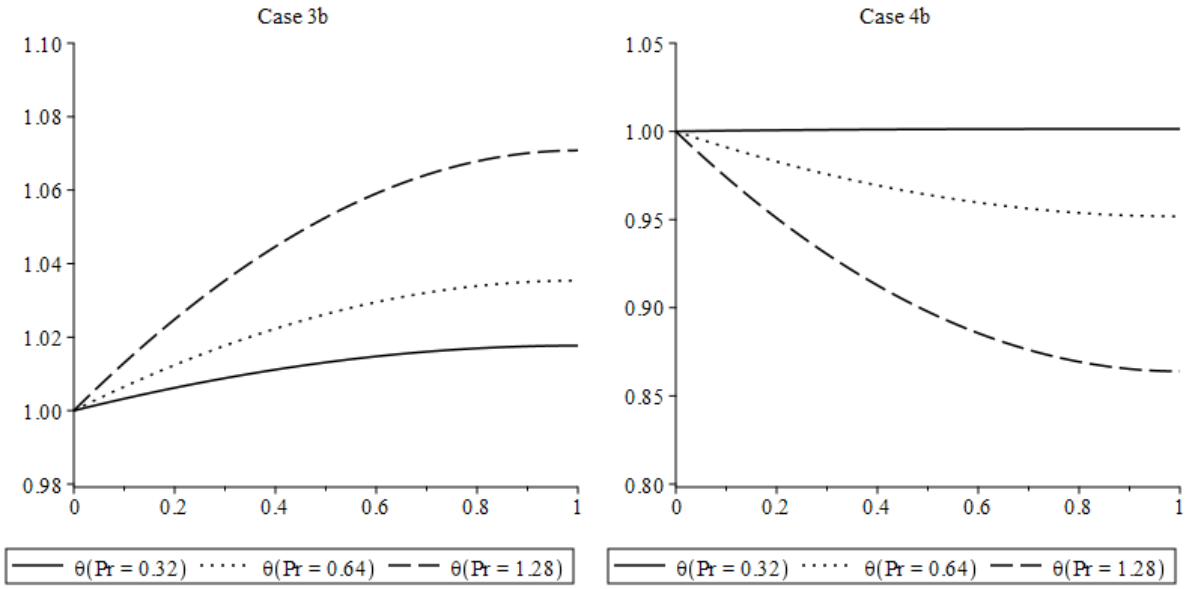

Figure 5.21: Case (3,4)b plots of θ(η) for Pr (0.32,0.64,1.28) at S=2.4, B=0.5, R=0.5

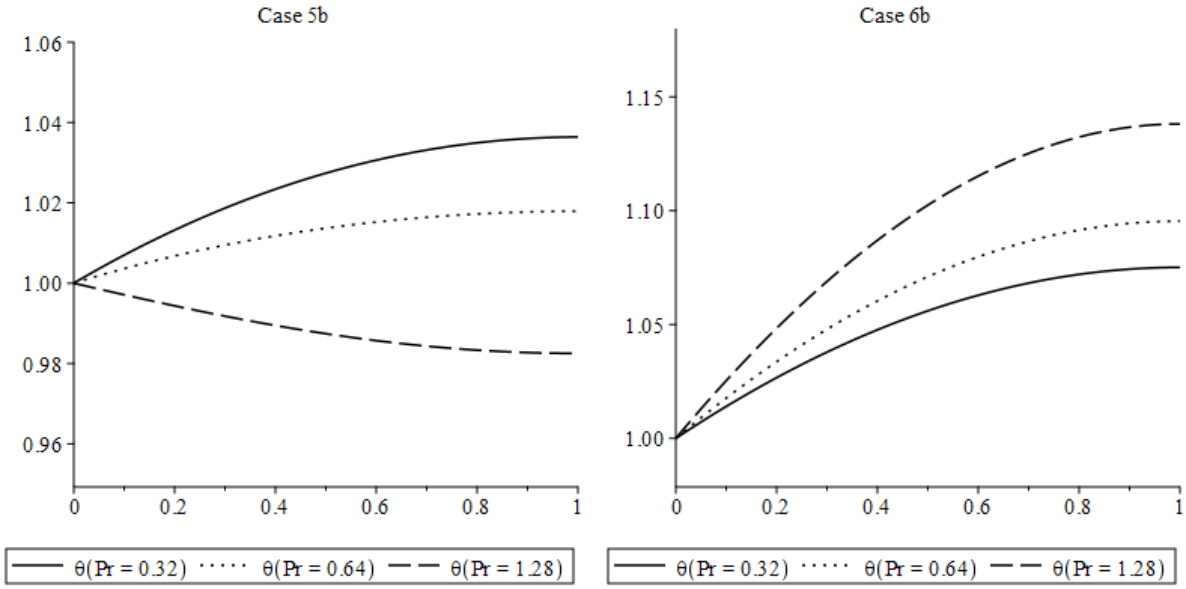

Figure 5.22: Case (5,6)b plots of θ(η) for Pr (0.32,0.64,1.28) at S=2.4, B=0.5, R=0.5

Figure 5.21 portrays the influence of varying the Prandtl number Pr on $\theta(\eta)$ for cases 3b and 4b. The above figures reveal that, in case 3b, the value of $\theta(1)$ is directly proportional to the value of the Prandtl number. On the contrary, in case 4b, the value of $\theta(1)$ is inversely proportional to the Prandtl number. Furthermore, Figure 5.22 uncovers the impact of altering the Prandtl number on $\theta(\eta)$ for cases 5b and 6b. The figures presented above indicate that, for case 5b, the value of $\theta(1)$ exhibited a slight decrease with an increase in the Prandtl number. However, in case 6b, the value of $\theta(1)$ is directly proportional to the Prandtl number.

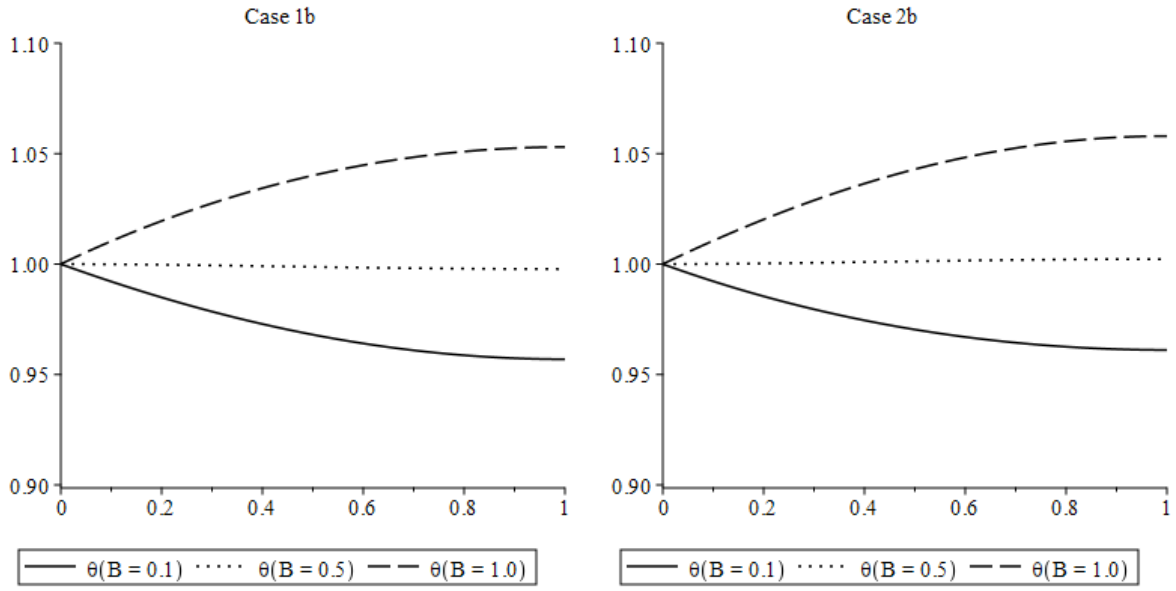

Figure 5.23: Case (1,2)b plots of θ(η) for B (0.1,0.5,1.0) at S=2.4, Pr=1, R=0.5

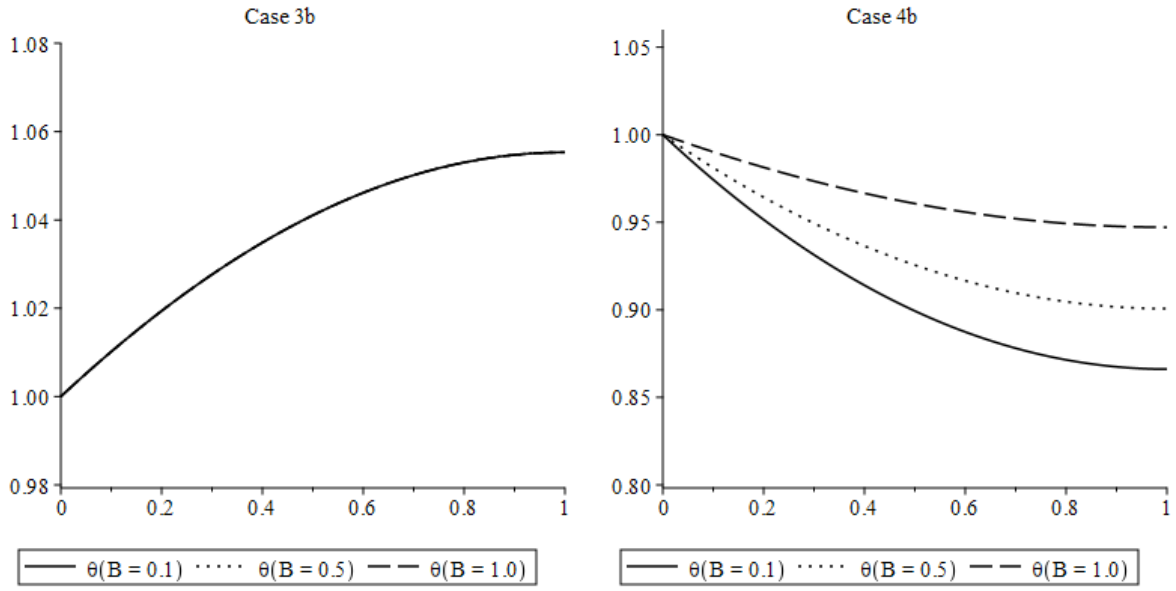

Figure 5.24: Case (3,4)b plots of θ(η) for B (0.1,0.5,1.0) at S=2.4, Pr=1, R=0.5

The effect of varying the internal heat generation parameter B on $\theta(\eta)$ for cases 1b and 2b is shown in Figure 5.23. It is conspicuous from the above figures that the value of $\theta(1)$ is unequivocally linked to the internal heat generation parameter for both cases 1b and 2b. On the other hand, Figure 5.24 showcases the effect of varying the internal heat generation parameter on $\theta(\eta)$ for cases 3b and 4b. It is perceptible from the above figures that the value of $\theta(1)$ remains invariant when the internal heat generation parameter is changed in case 3b, which can be attributed to the absence of the internal heat generation parameter in the equations for case 3b. However, for case 4b, the value of $\theta(1)$ is directly proportional to the internal heat generation parameter.

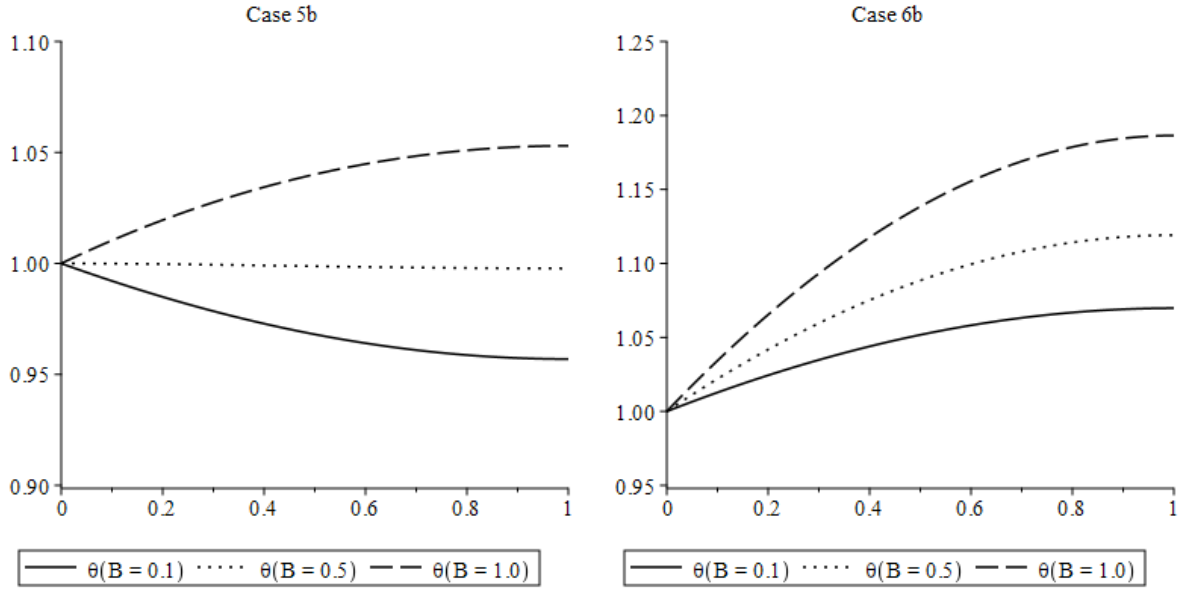

Figure 5.25: Case (5,6)b plots of θ(η) for B (0.1,0.5,1.0) at S=2.4, Pr=1, R=0.5

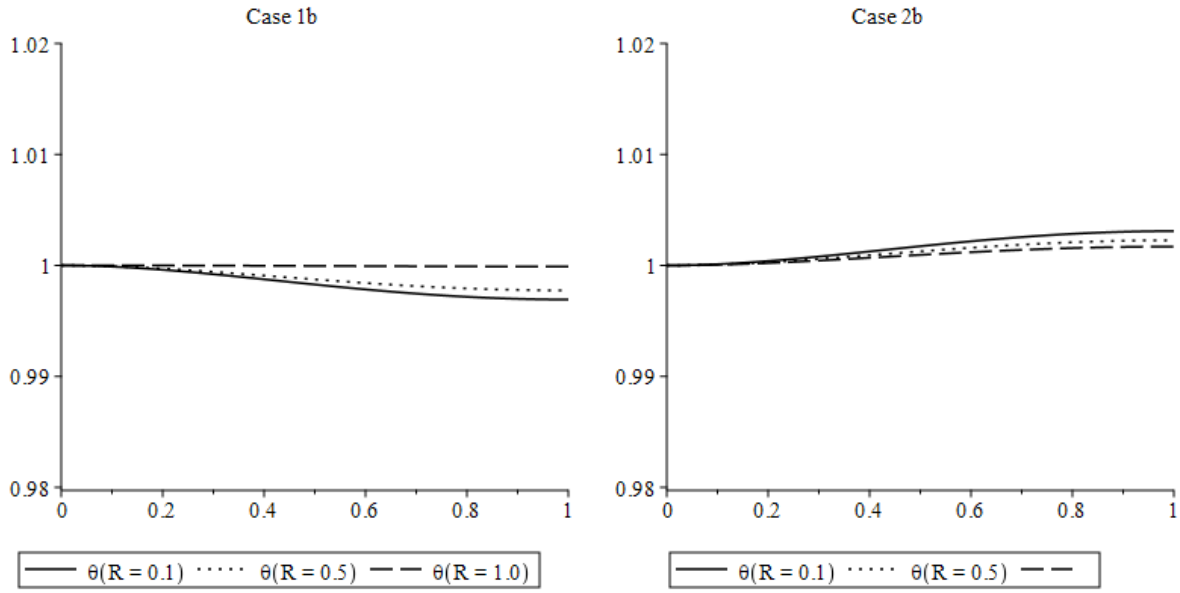

Figure 5.26: Case (1,2)b plots of θ(η) for R (0.1,0.5,1.0) at S=2.4, Pr=1, B=0.5

Figure 5.25 shows the impact of varying the internal heat generation parameter B on $\theta(\eta)$ for cases 5b and 6b. From the above figures, it is obvious that the value of $\theta(1)$ is directly proportional to the internal heat generation parameter for both cases 5b and 6b. Whereas Figure 5.26 shows the impact of varying the thermal radiation parameter on $\theta(\eta)$ for cases 1b and 2b. From the above figures, it is obvious that the value of $\theta(1)$ increased with an increase in the thermal radiation parameter for case 1b. However, the value of $\theta(1)$ decreased with an increase in the thermal radiation parameter for case 2b.

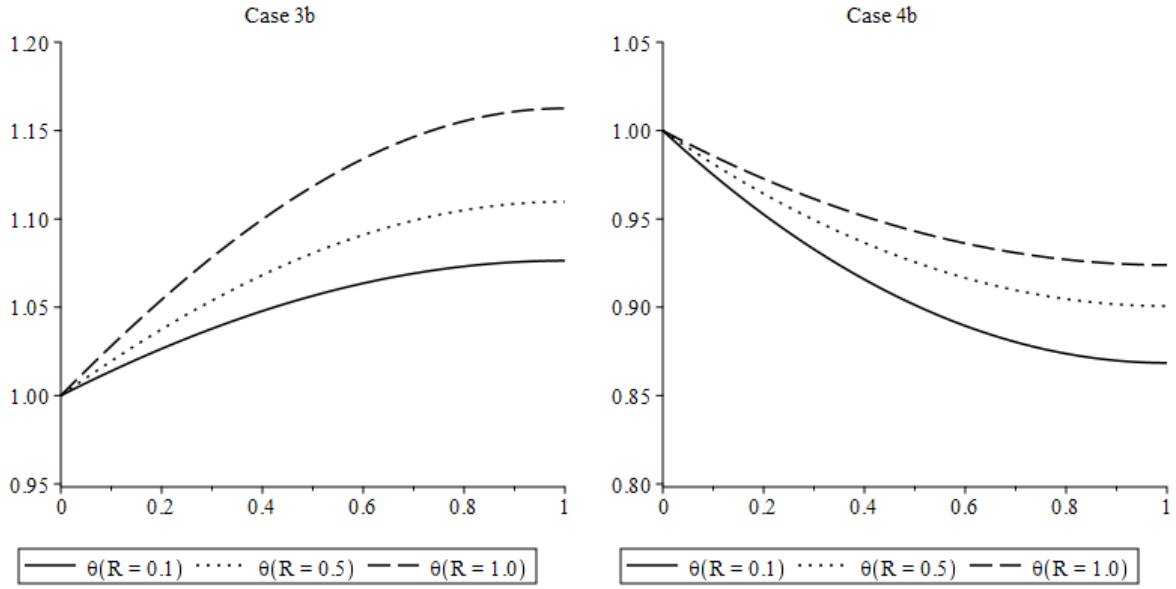

Figure 5.27: Case (3,4)b plots of θ(η) for R (0.1,0.5,1.0) at S=2.4, Pr=1, B=0.5

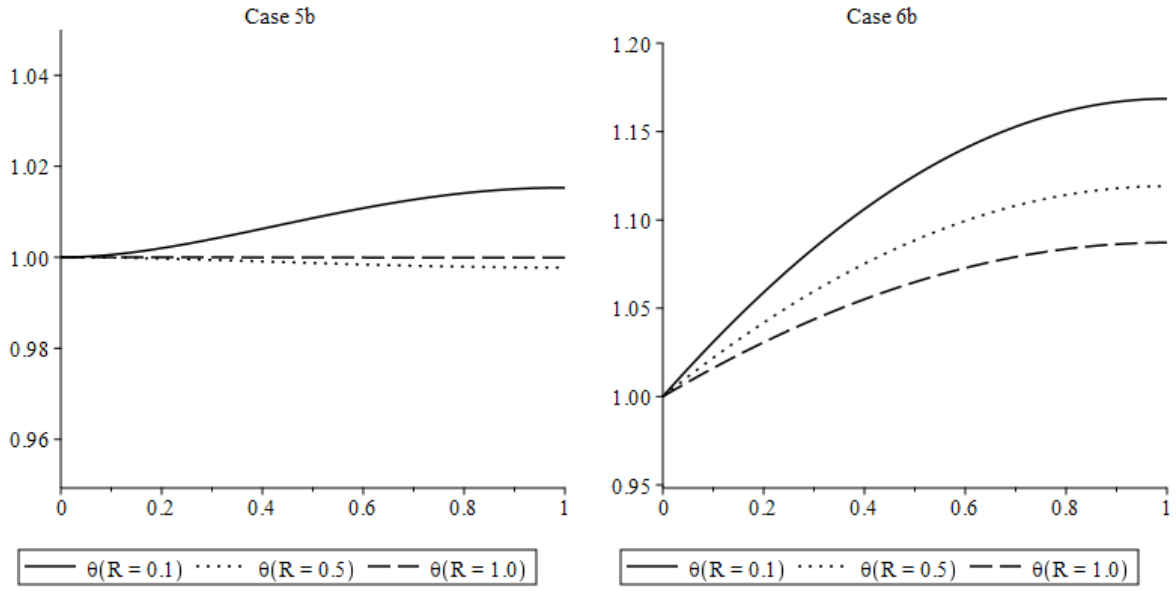

Figure 5.28: Case (5,6)b plots of θ(η) for R (0.1,0.5,1.0) at S=2.4, Pr=1, B=0.5

Figure 5.27 shows the impact of varying the thermal radiation parameter R on $\theta(\eta)$ for cases 3b and 4b. From the above figures, it is obvious that the value of $\theta(1)$ is directly proportional to the thermal radiation parameter in cases 3b and 4b. Whereas Figure 5.28 shows the impact of varying the thermal radiation parameter on $\theta(\eta)$ for cases 5b and 6b. From the above figures, it is obvious that the value of $\theta(1)$ decreased and then increased slightly with an increase in the thermal radiation parameter in case 5b. However, the value of $\theta(1)$ is inversely proportional to the thermal radiation parameter in case 6b.

Table 5-3: Effect of varying physical parameters on θ(1) for systems with positive stretching velocity (1-6)a

S	**System 1a**	**System 2a**	**System 3a**	**System 4a**	**System 5a**	**System 6a**
2.2	0.847677	1.225033	1.510145	0.518169	0.847677	4.063591
2.6	0.860642	1.197883	1.483815	0.529119	0.860642	3.630457
3.0	0.870447	1.178702	1.463496	0.538141	0.870447	3.346323
4.0	0.886848	1.148947	1.428529	0.554918	0.886848	2.942074
B						
0.1	0.690381	0.919115	1.496075	0.445332	0.690381	2.115318
0.5	0.855194	1.210188	1.496075	0.523922	0.855194	3.823053
1.0	1.173441	1.892081	1.496075	0.657223	1.173441	-
Pr						
0.32	1.182462	1.339788	1.151011	0.962426	1.182462	1.756623
0.64	1.008510	1.276887	1.309166	0.705733	1.008510	2.349885
1.28	0.757446	1.161093	1.648355	0.426413	0.757446	-
2.56	0.464966	0.963898	2.429459	0.196971	0.464966	-
R						
0.1	0.807191	1.325722	1.695057	0.431141	0.807191	-
0.5	0.854639	1.210188	1.496075	0.523920	0.854639	3.823053
1.0	0.888867	1.145503	1.365245	0.605044	0.888867	2.267011

Figures 5.5-5.16 show the impact of varying physical parameters like the unsteadiness parameter, Prandtl number, internal heat generation parameter, and thermal radiation parameter on the $\theta(\eta)$ curves of systems of ODEs due to positive stretching velocity. The same result can be visualized in tabulated form through Table 5-3. Similarly, Figure 5.17-5.28 show the impact of varying physical parameters like the unsteadiness parameter, Prandtl number, internal heat generation parameter, and thermal radiation parameter on the $\theta(\eta)$ curves of systems of ODEs due to negative stretching velocity. The same result can be visualized in tabulated form through Table 5-4.

Table 5-4: Effect of varying physical parameters on θ(1) for systems with negative stretching velocity (1-6)b

S	System 1b	System 2b	System 3b	System 4b	System 5b	System 6b
2.2	0.999303	1.000698	1.030241	0.943050	0.999303	1.062936
2.6	0.995738	1.004303	1.076361	0.868016	0.995738	1.169442
3.0	0.991318	1.008853	1.109689	0.821139	0.991318	1.255630
4.0	0.981331	1.019457	1.162580	0.756958	0.981313	1.411783
B						
0.1	0.956927	0.961116	1.055301	0.866135	0.956927	1.069758
0.5	0.997747	1.002264	1.055301	0.900675	0.997747	1.119113
1.0	1.053010	1.057989	1.055301	0.947154	1.053010	1.186441
Pr						
0.32	1.036392	1.037934	1.017685	1.001400	1.036392	1.075122
0.64	1.017904	1.020896	1.035381	0.951801	1.017904	1.095445
1.28	0.982519	0.988151	1.070803	0.863949	0.982519	1.138140
2.56	0.917516	0.927540	1.141773	0.723340	0.917516	1.232748
R						
0.1	0.996929	1.003091	1.075436	0.868508	1.015292	1.168565
0.5	0.997748	1.002264	1.055301	0.900675	0.997748	1.119113
1.0	0.999899	1.001696	1.041466	0.923936	0.999899	1.087151

All the results shown in this thesis are found using the 10^{th} order HAM. I-Chung found the solution to thin film flow over unsteady stretching sheet with internal heat generation, thermal radiation and variable heat flux, the solution to the said flow model can be found in [12]. However, I-Chung considered a single set of transformation equations which produced a single system of ODEs. I-Chung showed in his study that the value of free surface dimensionless temperature gets high when the unsteadiness parameter, the internal heat generation parameter and the thermal radiation parameter are increased, while it starts to decrease when Prandtl number is increased. However, these observations hold true until the transformation equations mentioned in his study are used. As new transformation equations are used in the present study to solve the existing flow model for different physical conditions, so the results and trends are destined to differ from the existing ones.

CHAPTER 6: CONCLUSION:

Lie Symmetry method has been used to successfully generate the Lie point symmetries for a system of PDEs describing unsteady thin film flow over stretching surface with internal heat generation and thermal radiation. Seven symmetry generators exist for the said flow model. Combination of these symmetry generators are used to construct invariants and similarity transformations. The system of PDEs is reduced to the system of ordinary differential equation using the deduced transformations. System of differential equations for the considered flow are reduced to the system of ODEs using twelve different sets of similarity transformations. However, the similarity transformation in case 1a and 5a, and 1b and 5b produce same system of ODEs respectively. So, the total number of distinct systems of ODEs reduces to ten.

The value of unsteadiness parameter must be greater than 2.0 for the solution to exist and this statement is valid only for the cases with negative stretching velocity. Moreover, the solution of flow equation for the cases due to positive stretching velocity exist even at low characteristic values of unsteadiness parameter. However, the upper limit of unsteadiness parameter is different for most of the cases.

The flow velocity $f'(\eta)$, value of dimensionless film thickness β and the reduced skin friction coefficient increase with an increase in the unsteadiness parameter for all cases of negative stretching velocity. The value of dimensionless film thickness β gets stable, and the phenomenon of gain in its value gets slow when unsteadiness parameter is increased beyond 3.0. However, the $f'(\eta)$ curves exist in two quadrants for positive stretching velocity cases, which hints toward the change in direction of fluid, and the inverse relation exist between the dimensionless boundary layer thickness and the unsteadiness parameter for these cases. Most of the results produced by the 10^{th} and 20^{th} order HAM match up to 5 decimal places which support the fact that the solutions given in this study are stable.

The value of free surface temperature $\theta(1)$ increases with an increase in the internal heat generation parameter for all cases except case 3a and 3b, and this happened due to the non-existence of internal heat generation parameter in the odes of said cases. As new transformation equations are used in this study to solve the existing fluid flow model for different physical conditions, so the results and trends of θ-curves differed from those found in literature.

REFERENCES:

1. Prandtl, L., *On fluid motions with very small friction.* Verhldg, 1904. **3**: p. 484-491.
2. Wang, C., *Liquid film on an unsteady stretching surface.* Quarterly of applied Mathematics, 1990. **48**(4): p. 601-610.
3. Andersson, H.I., J.B. Aarseth, and B.S. Dandapat, *Heat transfer in a liquid film on an unsteady stretching surface.* International Journal of Heat and Mass Transfer, 2000. **43**(1): p. 69-74.
4. Wang, C., *Analytic solutions for a liquid film on an unsteady stretching surface.* Heat and Mass Transfer, 2006. **42**(8): p. 759-766.
5. Liu, I.C. and H.I. Andersson, *Heat transfer in a liquid film on an unsteady stretching sheet.* International Journal of Thermal Sciences, 2008. **47**(6): p. 766-772.
6. Dandapat, B., B. Santra, and K. Vajravelu, *The effects of variable fluid properties and thermocapillarity on the flow of a thin film on an unsteady stretching sheet.* International Journal of Heat and Mass Transfer, 2007. **50**(5-6): p. 991-996.
7. Aziz, R.C. and I. Hashim, *Liquid film on unsteady stretching sheet with general surface temperature and viscous dissipation.* Chinese Physics Letters, 2010. **27**(11): p. 110202.
8. Noor, N. and I. Hashim, *Thermocapillarity and magnetic field effects in a thin liquid film on an unsteady stretching surface.* International Journal of Heat and Mass Transfer, 2010. **53**(9-10): p. 2044-2051.
9. Aziz, R.C., I. Hashim, and A. Alomari, *Thin film flow and heat transfer on an unsteady stretching sheet with internal heating.* Meccanica, 2011. **46**(2): p. 349-357.
10. Megahed, A.M., *HPM for the slip velocity effect on a liquid film over an unsteady stretching surface with variable heat flux.* The European Physical Journal Plus, 2011. **126**(9): p. 1-8.
11. Liu, I. and A. Megahed, *Numerical study for the flow and heat transfer in a thin liquid film over an unsteady stretching sheet with variable fluid properties in the presence of thermal radiation.* Journal of Mechanics, 2012. **28**(2): p. 291-297.
12. Liu, I. and A.M. Megahed, *Homotopy perturbation method for thin film flow and heat transfer over an unsteady stretching sheet with internal heating and variable heat flux.* Journal of Applied Mathematics, 2012. **2012**.
13. Mahmoud, M.A. and A.M. Megahed, *MHD flow and heat transfer in a non-Newtonian liquid film over an unsteady stretching sheet with variable fluid properties.* Canadian Journal of Physics, 2009. **87**(10): p. 1065-1071.
14. Idrees, M., et al., *A similarity solution of time dependent MHD liquid film flow over stretching sheet with variable physical properties.* Results in physics, 2018. **8**: p. 194-205.
15. Rehman, A., Z. Salleh, and T. Gul, *Heat transfer of thin film flow over an unsteady stretching sheet with dynamic viscosity.* Journal of Advanced Research in Fluid Mechanics and Thermal Sciences, 2021. **81**(2): p. 67-81.
16. Safdar, M., et al., *Construction of similarity transformations and analytic solutions for a liquid film on an unsteady stretching sheet using lie point symmetries.* Chaos, Solitons & Fractals, 2021. **150**: p. 111115.
17. Wulfman, C. and B. Wybourne, *The Lie group of Newton's and Lagrange's equations for the harmonic oscillator.* Journal of Physics A: Mathematical and General, 1976. **9**(4): p. 507.
18. Siriwat, P., C. Kaewmanee, and S.V. Meleshko, *Symmetries of the hyperbolic shallow water equations and the Green–Naghdi model in Lagrangian coordinates.* International Journal of Non-Linear Mechanics, 2016. **86**: p. 185-195.

19. Ibragimov, N.K. and N.K. Ibragimov, *Elementary Lie group analysis and ordinary differential equations*. Vol. 197. 1999: Wiley New York.
20. Olver, P.J., *Applications of Lie groups to differential equations*. Vol. 107. 2000: Springer Science & Business Media.
21. Yaseen, M.H., et al., *Reduction of systems of two nonlinear parabolic type partial differential equations to solvable forms using differential invariants.* Chaos, Solitons & Fractals, 2021. **150**: p. 111107.
22. Safdar, M., et al., *Analytic solutions for the MHD flow and heat transfer in a thin liquid film over an unsteady stretching surface with Lie symmetry and homotopy analysis method.* Waves in Random and Complex Media, 2022: p. 1-19.
23. Taj, S., et al., *Lie symmetry analysis of heat transfer in a liquid film over an unsteady stretching surface with viscous dissipation and external magnetic field.* Waves in Random and Complex Media, 2022: p. 1-16.
24. Raptis, A., *Flow of a micropolar fluid past a continuously moving plate by the presence of radiation.* International Journal of Heat and Mass Transfer, 1998. **41**(18): p. 2865-2866.
25. Miller, W., *Symmetry groups and their applications*. 1973: Academic Press.
26. Liao, S.J., *The proposed homotopy analysis technique for the solution of nonlinear problems*. 1992, PhD thesis, Shanghai Jiao Tong University.
27. Shijun, L., *Homotopy analysis method: A new analytic method for nonlinear problems.* Applied Mathematics and Mechanics, 1998. **19**(10): p. 957-962.
28. Liao, S., *Beyond perturbation: introduction to the homotopy analysis method*. 2003: Chapman and Hall/CRC.
29. Liao, S., *An optimal homotopy-analysis approach for strongly nonlinear differential equations.* Communications in Nonlinear Science and Numerical Simulation, 2010. **15**(8): p. 2003-2016.

APPENDIX A

This section contains the MAPLE codes that are written specifically for this study. The MAPLE codes used for generating similarity transformations, finding suitable ranges of convergence control parameters, and plotting dimensionless velocity and temperature profiles are given in this section.

```
> restart:with(PDEtools):declare(u(t,x,y),v(t,x,y),T(t,x,y),
  quiet):
> System_of_PDEs:={diff(u(t,x,y),x)+diff(v(t,x,y),y)=0,diff(u
  (t,x,y),t)+u(t,x,y)*diff(u(t,x,y),x)+v(t,x,y)*diff(u(t,x,y),y)
  -nu*diff(u(t,x,y),y,y)=0,rho*C[p]*(diff(T(t,x,y),t)+u(t,x,y)*
  diff(T(t,x,y),x)+v(t,x,y)*diff(T(t,x,y),y))-kappa*diff(T(t,x,
  y),y,y)-(4*sigma[1]/(3*kappa[1])*4*a[0]^3*diff(T(t,x,y),y,y))-
  (kappa*rho)/(mu*t)*B*(T(t,x,y)-a[0])=0};
```

$$System\_of\_PDEs := \left\{ u_x + v_y = 0,\ \rho\, C_p \left(T_t + u\left(T_x\right) + v\left(T_y\right)\right) - \kappa\left(T_{y,y}\right) - \frac{16\,\sigma_1\, a_0^3\left(T_{y,y}\right)}{3\,\kappa_1} - \frac{\kappa\,\rho\, B\left(T - a_0\right)}{\mu\, t} = 0,\ u_t + u\left(u_x\right) + v\left(u_y\right) - \nu\left(u_{y,y}\right) = 0 \right\} \tag{1}$$

```
> Infinitesimals(System_of_PDEs):nops(%):
> with(PDEtools,SymmetryTransformation,ChangeSymmetry,
  InfinitesimalGenerator):declare(u(t,x,y),v(t,x,y),T(t,x,y),L(m
  [1],m[2],m[3]),M(m[1],m[2],m[3]),N(m[1],m[2],m[3]),quiet):
> S[1]:=[0,1,0,0,0,0];S[2]:=[0,t,0,1,0,0];S[3]:=[0,x,0,u,0,0];S
  [4]:=[0,0,0,0,0,T-a[0]];S[5]:=[0,0,0,0,0,t^(B*kappa/(mu*C[p]))
  ];S[6]:=[t,0,y/2,-u,-v/2,0];S[7]:=[1,0,0,0,0,kappa*B*(T-a[0])/
  (mu*t*C[p])];
```

$$S_1 := [0, 1, 0, 0, 0, 0]$$

$$S_2 := [0, t, 0, 1, 0, 0]$$

$$S_3 := [0, x, 0, u, 0, 0]$$

$$S_4 := \left[0, 0, 0, 0, 0, T - a_0\right]$$

$$S_5 := \left[0, 0, 0, 0, 0, t^{\frac{B\,\kappa}{\mu\, C_p}}\right]$$

$$S_6 := \left[t, 0, \frac{y}{2}, -u, -\frac{v}{2}, 0\right]$$

$$S_7 := \left[1, 0, 0, 0, 0, \frac{\left(T - a_0\right) B\,\kappa}{\mu\, C_p\, t}\right] \tag{2}$$

```
> for i from 1 to 7 do G[i]:=InfinitesimalGenerator(S[i],([u(t,
  x,y),v(t,x,y),T(t,x,y)]));SymmetryTransformation(G[i],([u(t,x,
  y),v(t,x,y),T(t,x,y)]),([L(m[1],m[2],m[3]),M(m[1],m[2],m[3]),N
  (m[1],m[2],m[3])])) end do;
```

$$G_1 := f \to \frac{\partial}{\partial x} f$$

$$\left\{m_1 = t, m_2 = x + \_\epsilon, m_3 = y, L = u, M = v, N = T\right\}$$

$$G_2 := f \to t\left(\frac{\partial}{\partial x} f\right) + \frac{\partial}{\partial u} f$$

$$\left\{m_1 = t, m_2 = t\_\epsilon + x, m_3 = y, L = u + \_\epsilon, M = v, N = T\right\}$$

$$G_3 := f \to x\left(\frac{\partial}{\partial x} f\right) + u\left(\frac{\partial}{\partial u} f\right)$$

$$\left\{m_1 = t, m_2 = x\, e^{-\epsilon}, m_3 = y, L = e^{-\epsilon} u, M = v, N = T\right\}$$

$$G_4 := f \to \left(T - a_0\right)\left(\frac{\partial}{\partial T} f\right)$$

$$\left\{m_1 = t, m_2 = x, m_3 = y, L = u, M = v, N = T\, e^{-\epsilon} - a_0\, e^{-\epsilon} + a_0\right\}$$

$$G_5 := f \to t^{\frac{B\kappa}{\mu C_p}}\left(\frac{\partial}{\partial T} f\right)$$

$$\left\{m_1 = t, m_2 = x, m_3 = y, L = u, M = v, N = \_\epsilon\, t^{\frac{B\kappa}{\mu C_p}} + T\right\}$$

$$G_6 := f \to t\left(\frac{\partial}{\partial t} f\right) + \frac{1}{2} y\left(\frac{\partial}{\partial y} f\right) - u\left(\frac{\partial}{\partial u} f\right) - \frac{1}{2} v\left(\frac{\partial}{\partial v} f\right)$$

$$\left\{m_1 = t\, e^{-\epsilon}, m_2 = x, m_3 = \frac{y\sqrt{t\, e^{-\epsilon}}}{\sqrt{t}}, L = e^{-\epsilon} u, M = \frac{v\sqrt{t}}{\sqrt{t\, e^{-\epsilon}}}, N = T\right\}$$

$$G_7 := f \to \frac{\partial}{\partial t} f + \frac{\left(T - a_0\right) B\kappa\left(\frac{\partial}{\partial T} f\right)}{\mu C_p\, t}$$

$$\left\{m_1 = t + \_\epsilon, m_2 = x, m_3 = y, L = u, M = v, N = t^{-\frac{B\kappa}{\mu C_p}}\left(T - a_0\right)\left(t + \_\epsilon\right)^{\frac{B\kappa}{\mu C_p}} + a_0\right\} \qquad \textbf{(3)}$$

>

```
> restart:with(PDEtools):declare(f(eta),theta(eta),quiet):x[0]:=
  0:S:=2.2:
> for m from 1 to 10 do eq[m]:=diff(f[m-1](eta),eta,eta,eta)+sum(g
  [m-1-n]*sum(f[i](eta)*diff(f[n-i](eta),eta,eta)-diff(f[i](eta),
  eta)*diff(f[n-i](eta),eta),i=0..n),n=0..m-1)+(eta*S/2)*sum(g[n]*
  diff(f[m-1-n](eta),eta,eta),n=0..m-1)+S*sum(g[n]*diff(f[m-1-n]
  (eta),eta),n=0..m-1) end do:
> f[0](eta):=eta-((3*S+6)/4)*eta^(2)+((2+S)*eta^(3))/4:
> for n from 1 to 10 by 1 do x[n]:=(n/n):
  sys[(2*n)-1]:=h[1]*(int(int(int(eq[n],eta),eta),eta))+(C[(5*n)
  -4]*eta^2+C[(5*n)-3]*eta+C[(5*n)-2])+(x[n-1]*(f[n-1](eta))):
  subs(eta=0,sys[(2*n)-1])=0:solve(%,C[(5*n)-2]):C[(5*n)-2]:=%:
  subs(eta=0,diff(sys[(2*n)-1],eta))=0:solve(%,C[(5*n)-3]):C[(5*n)
  -3]:=%:
  subs(eta=1,sys[(2*n)-1])=0:solve(%,C[(5*n)-4]):C[(5*n)-4]:=%:
  subs(eta=1,diff(sys[(2*n)-1],eta,eta))=0:solve(%,g[n-1]):g[n-1]
  :=%:
  f[n](eta):=simplify(sys[(2*n)-1],size):
  end do:Gamma:=sum(g[i],i=0..9):aa:=subs(eta=0,Gamma):
> plot(aa,h[1]=-3..0.5,0.5..1.2,linestyle=[solid],legend=[s=S],
  legendstyle=[font=["Times New Roman",12],location=left])
```

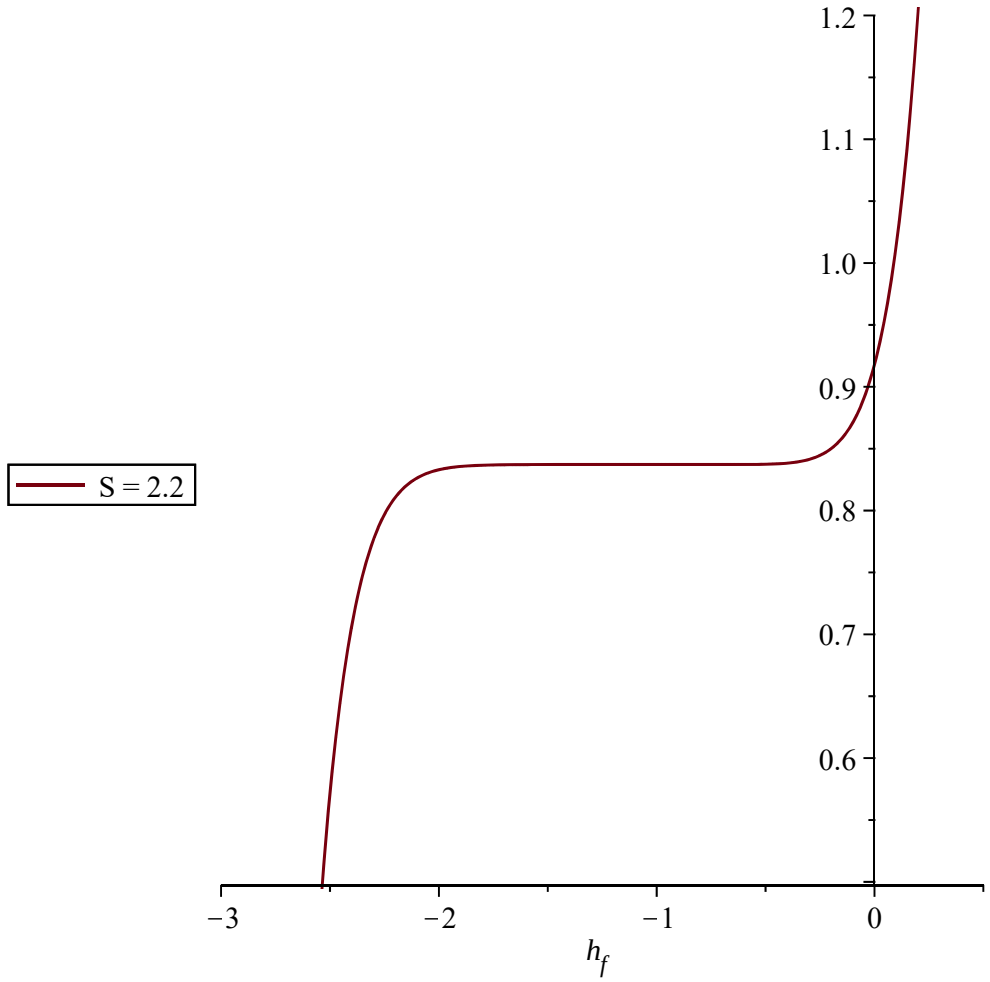


```
> |
```

```
> restart:with(PDEtools):declare(f(eta),theta(eta),quiet):x[0]
  :=0:S:=2.2:Pr:=1:R:=0.5:B:=0.5:h[1]:=-1.25:
> for m from 1 to 10 do eq[m]:=diff(f[m-1](eta),eta,eta,eta)+
  sum(g[m-1-n]*sum(f[i](eta)*diff(f[n-i](eta),eta,eta)-diff(f[i]
  (eta),eta)*diff(f[n-i](eta),eta),i=0..n),n=0..m-1)+(eta*S/2)*
  sum(g[n]*diff(f[m-1-n](eta),eta,eta),n=0..m-1)+S*sum(g[n]*diff
  (f[m-1-n](eta),eta),n=0..m-1):eqn[m]:=((1+R)*Pr^(-1))*diff
  (theta[m-1](eta),eta,eta)+sum(g[m-1-n]*sum(f[i](eta)*diff
  (theta[n-i](eta),eta)+theta[i](eta)*diff(f[n-i](eta),eta),i=0.
  .n),n=0..m-1)+(eta*S/2)*sum(g[n]*diff(theta[m-1-n](eta),eta),
  n=0..m-1)+S*sum(g[n]*B*(Pr^(-1))*theta[m-1-n](eta),n=0..m-1)
  end do:
> theta[0](eta):=1:f[0](eta):=eta-((3*S+6)/4)*eta^(2)+((2+S)*
  eta^3)/4:
> for n from 1 to 10 by 1 do x[n]:=(n/n):
  sys[(2*n)-1]:=h[1]*(int(int(int(eq[n],eta),eta),eta))+(C[(5*n)
  -4]*eta^2+C[(5*n)-3]*eta+C[(5*n)-2])+(x[n-1]*(f[n-1](eta))):
  sys[(2*n)]:=h[2]*(int(int(eqn[n],eta),eta))+(C[(5*n)-1]*eta+C[
  (5*n)])+(x[n-1]*(theta[n-1](eta))):
  subs(eta=0,sys[(2*n)-1])=0:solve(%,C[(5*n)-2]):C[(5*n)-2]:=%:
  subs(eta=0,diff(sys[(2*n)-1],eta))=0:solve(%,C[(5*n)-3]):C[(5*
  n)-3]:=%:
  subs(eta=1,sys[(2*n)-1])=0:solve(%,C[(5*n)-4]):C[(5*n)-4]:=%:
  subs(eta=1,diff(sys[(2*n)-1],eta,eta))=0:solve(%,g[n-1]):g
  [n-1]:=%:
  subs(eta=0,sys[(2*n)])=0:solve(%,C[(5*n)]):C[(5*n)]:=%:
  subs(eta=1,diff(sys[(2*n)],eta))=0:solve(%,C[(5*n)-1]):C[(5*n)
  -1]:=%:
  f[n](eta):=simplify(sys[(2*n)-1],size):theta[n](eta):=simplify
  (sys[(2*n)],size): end do:Gamma:=sum(g[i],i=0..9);beta:=sqrt
  (Gamma);
```

$$\Gamma := 0.8372079939$$

$$\beta := 0.9149907070 \qquad (1)$$

```
> aa:=sum(f[i](eta),i=0..10):Skin_friction_Coeff:=subs(eta=0,
  diff(aa,eta,eta))
```

$$Skin\_friction\_Coeff := -4.86391595058503 \qquad (2)$$

```
> bb:=sum(theta[i](eta),i=0..10):cc:=subs(eta=0,diff(bb,eta))
  :plot(cc,h[2]=-2.5..0,-0.02..0.02)
```

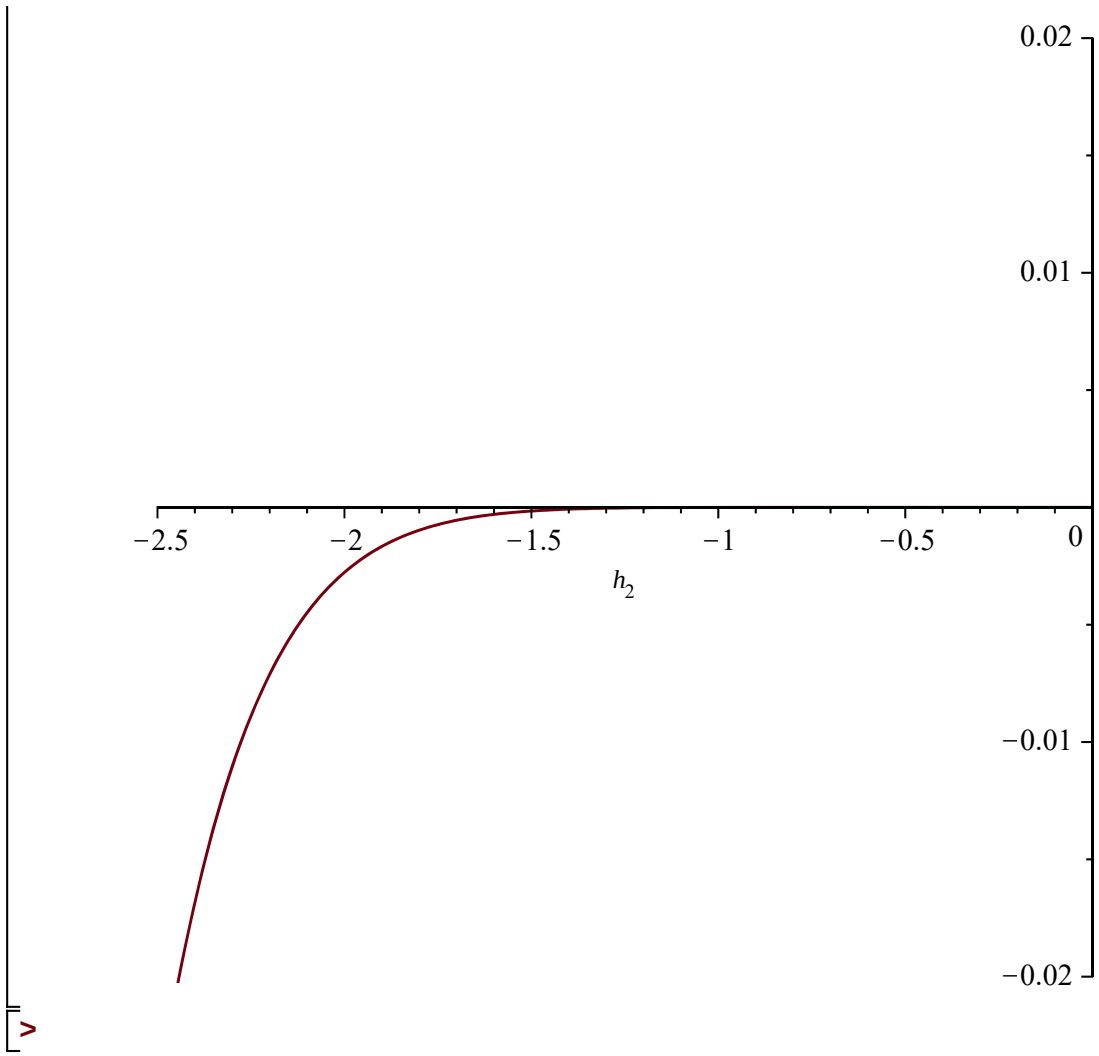
0.02
0.01
−0.01
−0.02
−2.5
−2
−1.5
−1
−0.5
0
h_2
V

```
> restart:with(PDEtools):declare(f(eta),theta(eta),quiet):x[0]:=
  0:S:=2.2:h[1]:=-1.25:
> for m from 1 to 10 do eq[m]:=diff(f[m-1](eta),eta,eta,eta)+sum(g
  [m-1-n]*sum(f[i](eta)*diff(f[n-i](eta),eta,eta)-diff(f[i](eta),
  eta)*diff(f[n-i](eta),eta),i=0..n),n=0..m-1)+(eta*S/2)*sum(g[n]*
  diff(f[m-1-n](eta),eta,eta),n=0..m-1)+S*sum(g[n]*diff(f[m-1-n]
  (eta),eta),n=0..m-1): end do:
> f[0](eta):=eta-((3*S+6)/4)*eta^(2)+((2+S)*eta^(3))/4:
> for n from 1 to 10 by 1 do x[n]:=(n/n):
  sys[(2*n)-1]:=h[1]*(int(int(int(eq[n],eta),eta),eta))+(C[(5*n)
  -4]*eta^2+C[(5*n)-3]*eta+C[(5*n)-2])+(x[n-1]*(f[n-1](eta))):
  subs(eta=0,sys[(2*n)-1])=0:solve(%,C[(5*n)-2]):C[(5*n)-2]:=%:
  subs(eta=0,diff(sys[(2*n)-1],eta))=0:solve(%,C[(5*n)-3]):C[(5*n)
  -3]:=%:
  subs(eta=1,sys[(2*n)-1])=0:solve(%,C[(5*n)-4]):C[(5*n)-4]:=%:
  subs(eta=1,diff(sys[(2*n)-1],eta,eta))=0:solve(%,g[n-1]):g[n-1]
  :=%:
  f[n](eta):=simplify(sys[(2*n)-1],size):
  end do:Gamma:=sum(g[i],i=0..9):beta:=sqrt(Gamma);
```

$$\beta := 0.9149907070 \qquad (1)$$

```
> aa:=sum(f[i](eta),i=0..10):
> plot((diff(aa,eta)),eta=0..1,-2.5..1,linestyle=[solid],
  legendstyle=[font=["Times New Roman",9],location=bottom]);
```

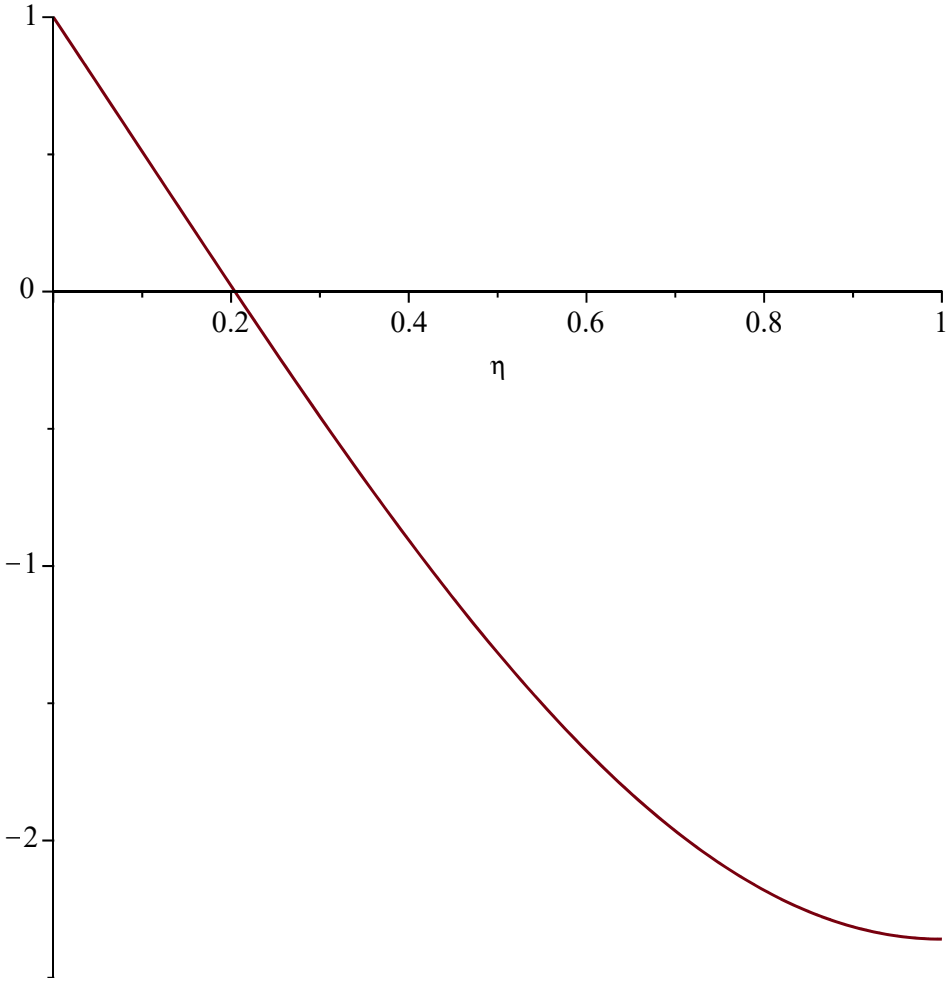


```
>
```

```
> restart:with(PDEtools):declare(f(eta),theta(eta),quiet):x[0]
  :=0:S:=2.2:Pr:=1:R:=0.5:B:=0.5:h[1]:=-1.25:h[2]:=-0.75:
> for m from 1 to 10 do eq[m]:=diff(f[m-1](eta),eta,eta,eta)+
  sum(g[m-1-n]*sum(f[i](eta)*diff(f[n-i](eta),eta,eta)-diff(f[i]
  (eta),eta)*diff(f[n-i](eta),eta),i=0..n),n=0..m-1)+(eta*S/2)*
  sum(g[n]*diff(f[m-1-n](eta),eta,eta),n=0..m-1)+S*sum(g[n]*diff
  (f[m-1-n](eta),eta),n=0..m-1):eqn[m]:=((1+R)*Pr^(-1))*diff
  (theta[m-1](eta),eta,eta)+sum(g[m-1-n]*sum(f[i](eta)*diff
  (theta[n-i](eta),eta)+theta[i](eta)*diff(f[n-i](eta),eta),i=0.
  .n),n=0..m-1)+(eta*S/2)*sum(g[n]*diff(theta[m-1-n](eta),eta),
  n=0..m-1)+S*sum(g[n]*B*(Pr^(-1))*theta[m-1-n](eta),n=0..m-1)
  end do:
> theta[0](eta):=1:f[0](eta):=eta-((3*S+6)/4)*eta^(2)+((2+S)*
  eta^(3))/4:
> for n from 1 to 10 by 1 do x[n]:=(n/n):
  sys[(2*n)-1]:=h[1]*(int(int(int(eq[n],eta),eta),eta))+(C[(5*n)
  -4]*eta^2+C[(5*n)-3]*eta+C[(5*n)-2])+(x[n-1]*(f[n-1](eta))):
  sys[(2*n)]:=h[2]*(int(int(eqn[n],eta),eta))+(C[(5*n)-1]*eta+C[
  (5*n)])+(x[n-1]*(theta[n-1](eta))):
  subs(eta=0,sys[(2*n)-1])=0:solve(%,C[(5*n)-2]):C[(5*n)-2]:=%:
  subs(eta=0,diff(sys[(2*n)-1],eta))=0:solve(%,C[(5*n)-3]):C[(5*
  n)-3]:=%:
  subs(eta=1,sys[(2*n)-1])=0:solve(%,C[(5*n)-4]):C[(5*n)-4]:=%:
  subs(eta=1,diff(sys[(2*n)-1],eta,eta))=0:solve(%,g[n-1]):g
  [n-1]:=%:
  subs(eta=0,sys[(2*n)])=0:solve(%,C[(5*n)]):C[(5*n)]:=%:
  subs(eta=1,diff(sys[(2*n)],eta))=0:solve(%,C[(5*n)-1]):C[(5*n)
  -1]:=%:
  f[n](eta):=simplify(sys[(2*n)-1],size):theta[n](eta):=simplify
  (sys[(2*n)],size):end do:Gamma:=sum(g[i],i=0..9);beta:=sqrt
  (Gamma);
```

$$\Gamma := 0.8372079937$$

$$\beta := 0.9149907069 \qquad (1)$$

```
> bb:=sum(theta[i](eta),i=0..10):plot(bb,eta=0..1,0..2,
  linestyle=[solid],legend=["Theta(eta)@S"=S],legendstyle=[font=
  ["HELVETICA",9],location=bottom]);free_surface_temp:=subs(eta=
  1,bb);heat_flux:=(-1)*(subs(eta=0,diff(bb,eta)));
```

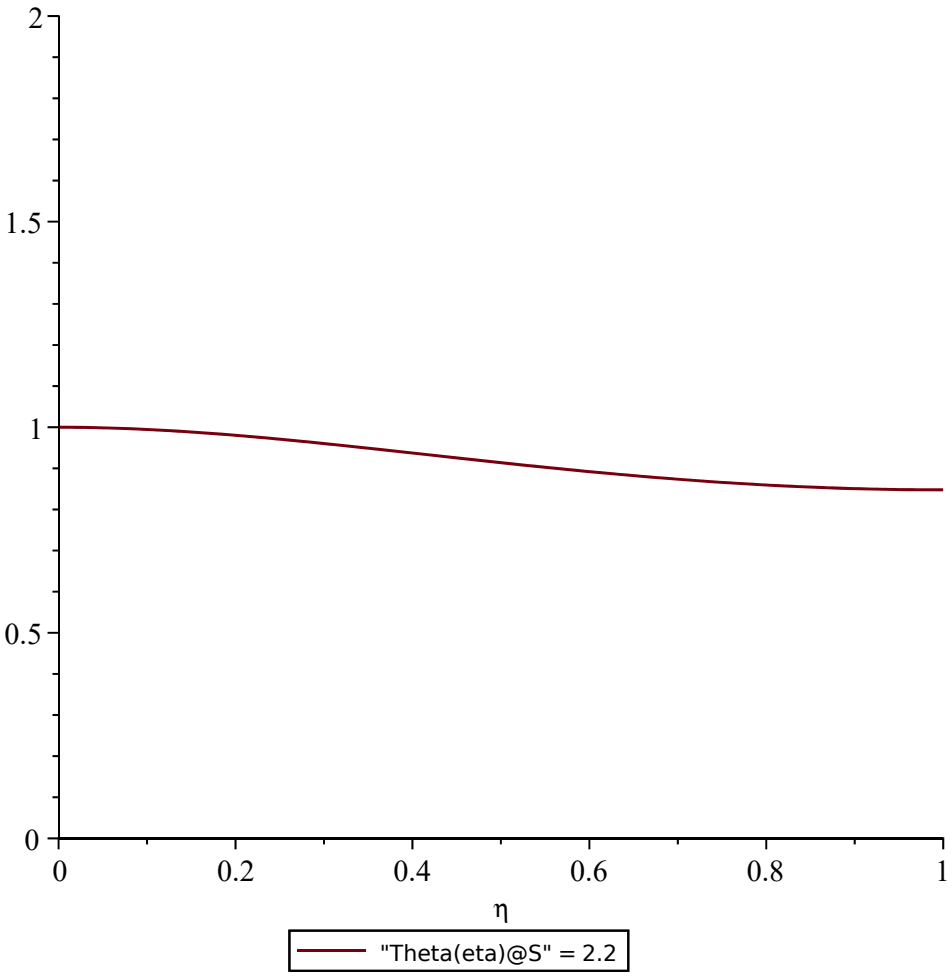

$$free\_surface\_temp := 0.847677260678459$$

$$heat\_flux := 7.69656011068847 \times 10^{-9} \quad \textbf{(2)}$$

>

Ahsan Thesis Complete

by Muhammad Safdar

Submission date: 23-May-2023 05:23PM (UTC+0500)
Submission ID: 2100020451
File name: Thesis1_Final_complete.pdf (2.06M)
Word count: 20642
Character count: 100409

Ahsan Thesis Complete

ORIGINALITY REPORT

9%	6%	10%	3%
SIMILARITY INDEX	INTERNET SOURCES	PUBLICATIONS	STUDENT PAPERS

PRIMARY SOURCES

1	Ahsan Ali Naseer, Muhammad Safdar, Safia Taj, Muhammad Umair Ali, Amad Zafar, Kwang Su Kim, Jong Hyuk Byun. "Analytical Solutions for Unsteady Thin Film Flow with Internal Heating and Radiation", Journal of Mathematics, 2023 Publication	4%
2	www.hindawi.com Internet Source	2%
3	Submitted to Higher Education Commission Pakistan Student Paper	2%
4	Nevzat Onur. "Introduction to Convective Heat Transfer", Wiley, 2023 Publication	1%

Exclude quotes	On	Exclude matches	< 1%
Exclude bibliography	On		